EFFECTIVE STRESS DEVELOPMENT IN KAOLIN AND BENTONITE CLAYS DURING THE HYDRO-MECHANICAL LOADING

A

Report

Submitted in partial fulfillment of the requirements

of the degree of

DOCTOR OF PHILOSOPHY

by

Chinumani Choudhury

Roll No. 136104006

Indian Institute of Technology Guwahati

Department of Civil Engineering

April 2019

INDIAN INSTITUTE OF TECHNOLOGY GUWAHATI, ASSAM, INDIA

Department of Civil Engineering

CERTIFICATE

This is to certify that the thesis entitled **"Effective stress development in kaolin and bentonite clays during the hydro-mechanical loading"** submitted by **Chinumani Choudhury** to the Indian Institute of Technology Guwahati, for the award of the degree of Doctor of Philosophy in Civil Engineering is a record of bonafide research work carried out by her under my supervision and guidance. The thesis work, in my opinion, has reached the requisite standard fulfilling the requirement for the degree of Doctor of Philosophy. The results contained in this thesis have not been submitted in part or full to any other University or Institute for the award of any degree or diploma.

Dr. T.V Bharat
Associate Professor
Department of Civil Engineering
IIT, Guwahati
Guwahati - 781039, India

Date:

INDIAN INSTITUTE OF TECHNOLOGY GUWAHATI, ASSAM, INDIA

Department of Civil Engineering

STATEMENT

I do hereby declare that the matter embodied in this thesis is the result of investigations carried out by me in the Department of Civil Engineering, Indian Institute of Technology Guwahati, Guwahati, Assam, India.

In keeping with the general practice of reporting scientific observations, due acknowledgements have been made wherever the work described is based on the findings of other investigators.

Date: Chinumani Choudhury

IIT Guwahati

In sweet memory of my beloved mother

After all the hard works and efforts, I would like to dedicate this study to my heavenly mother.

ABSTRACT

The knowledge of hydro-mechanical response of the two extreme clays namely, kaolin and bentonite are important due to their presence in many parts of the world and these clays are subjected to wetting cycles under external loads during the monsoon. Bentonite clays are further subjected to combined hydraulic and mechanical loading from the surrounding saturated rock mass or ground water during the placement in nuclear waste repositories and landfills, respectively. In this work, it will be shown that kaolin is a collapsible soil similar to the loess soil. The collapse mechanism in kaolin is, however, due to changes in particle association (fabric) with the interaction with different pore-fluids. Collapsible soils are known to withstand high normal stresses without undergoing a significant volume change in air-dry state. The soil is, however, susceptible to a large volume change upon wetting. Several physicochemical parameters strongly influenced the particle association in kaolin by altering the charges on the particle surfaces and edges due to interaction with different pore-fluids. The collapse nature of the kaolin is investigated with great detail in this work. Wetting induced collapse behavior of kaolin was studied under the influence of pore-fluid chemistry using a multi-scale approach. The influence of pH, salt concentration, and dielectric pore-fluid environment on the clay behavior was analyzed using sedimentation and collapse tests. The collapse test results were well corroborated with the sedimentation test data, SEM images of lyophilized specimens, and edge isoelectric point (IEP_{edge}). The influence of inundation fluid and inundation pressure on the fabric changes and collapse potential was elucidated.

In contrast, bentonite clays swell due to wetting. These clays exert swelling pressure on the surroundings in isochoric conditions due to wetting. Swelling pressure evolution curve (SPEC) for different quality Indian bentonites was established under different compaction density. The effect of compaction density and bentonite quality on the pore-size distributions (PSDs) and clay fabric were analyzed for understanding the influence on SPEC behavior. The evolution of PSD and fabric during the water uptake process was analyzed for understanding the microstructural influence on the SPEC behavior. Swelling pressure of the bentonites is influenced by the initial compaction density and plasticity. The knowledge of swelling pressure variation with initial

compaction density for bentonites of different plasticity is important for the design of the repository. Theoretical models on establishing the swelling pressure vs. dry density relationship are gaining attention as the laboratory estimation of swelling pressure over a wide range of dry densities is highly time-consuming and expensive. Current theoretical models based on the surface properties of the bentonites using the diffuse double layer theory and using the water adsorption isotherm are associated with several limitations. A predictive model based on the linearization of the swelling pressure data using normalization dry density was proposed in this work. Influence of the bentonite plasticity and swelling mechanisms were well studied for establishing the appropriate model parameter and for choosing the normalization factor. The proposed model required a single experimentally measured swelling pressure data point in the dry density range varying between 1.45 – 1.7 Mg/m^3 for accurately establishing the swelling pressure curves over a wide range of dry densities. The model does not require the knowledge of surface properties and pore–fluid parameters, unlike the previous models.

The effective stress variation in clays of different mineralogy under hydro-mechanical loads was studied. Three series of suction-controlled tests were considered for understanding the effective stress development using the suction stress approach. In the first series of tests, the drying behavior of slurried kaolin and mixtures of kaolin – bentonite clays were considered. Two clay mixtures were used in these tests. The Volumetric Shrinkage Curve (VSC) and drying Soil Water Characteristics Curve (SWCC) of initially slurried clays were established by conducting a series of volumetric shrinkage and suction controlled tests for understanding the effective stress development due to drying using suction stress concept. The second series of experiments consisted of suction controlled swelling pressure and SWCC tests for ascertaining wetting SWCCs in isochoric conditions. The last series consisted of suction-controlled, wetting induced collapse tests on compacted kaolin under different inundation pressures. The suction stresses and effective stresses in kaolin, bentonite, and kaolin – bentonite mixtures were analyzed under the studied hydro-mechanical conditions. The study concludes that the suction stress approach does not explain the effective stresses correctly in the collapsible and swelling clays under hydro-mechanical loading and for the studied conditions.

Keyword: Kaolin, bentonite, hydro-mechanical load, nuclear waste repository, collapse, swell pressure, effective stress.

ACKNOWLEDGMENT

At the very beginning, I offer my sincere gratitude to the almighty for his blessings. God has always been with me. My all the ups and down are taken care of by the supreme power. He always showers his blessings on me and because of his blessings, my life has got value.

I am sincerely grateful to my supervisor Dr. T V Bharat, Associate Professor, Department of Civil Engineering, IIT Guwahati, without whom the whole thing would not have been possible to accomplish. I also offer my sincere thanks to him for his tireless and continuous effort towards my research works during this whole journey. He is having immense knowledge that helps me to clear each doubt I raised in front of him. He is a very generous person and always tolerated me in every pros and con I am having. He is very student friendly and because of this quality, I could share my problems with him. I have become someone from no one because of his efforts only. Big thanks to him.

I take this opportunity to pay my heartiest thanks to all the wonderful Doctoral Committee members, Prof. Gautam Baruah, Prof. Rajan Choudhary, and Sukanya Sharma. I am lucky to have their guidance in the right direction. Their continuous and relentless help will always be recognized.

I convey my warm thanks to my parents, Khagendra Nath Choudhury and Abanti Kalita Choudhury for their perseverance during my journey in Ph. D. They were always beside me for any kind of assistance. Though my family had to face severe hurdles, they never allowed feeling me these situations. During my research work, I have lost my mother who was a mentor to me yet my parent and other family members support me like anything. Thanks to my mother who is heavenly abode now, father, sister, brother-in-law and little niece for your all round support and blessings.

I shall always be grateful to all the faculties and the staff of the Department of Civil Engineering, IIT Guwahati. I am especially thankful to all the technicians, staff and labors of Geotechnical Laboratory for their unconditional help. I particularly offer thanks to Mr. Hariram Upadhya for his untiring help to fulfill my goal.

It is my privilege to say thanks to the Centre for Environment, Centre for Instruments Facility, Mechanical Workshop, Biotech Park, and Department of Chemical

Engineering IIT Guwahati. I have got uncountable help from all of them. Without their support, it would not be possible to finish my thesis works.

I am thankful to have an excellent library in IIT Guwahati. I am happy to avail of all the facilities provided in the library. It is a place of ultimate silence so that the thoughts can flow in any direction and eventually a good result come up.

I offer my gratitude to Guwahati University SAIF, Guwahati, Assam, and IIT Madras for their help. They had allowed me to carry out some of the experiments.

I also take this opportunity to pay thanks from the core of my heart to the entire amazing lab mate, colleagues, and my friends. I was able to learn many new things and ideas from them. They had always been very helpful and kind to me. It was very nice to have their company. I got relaxed while I talked to them over tea, in cores or in hostels. All these memories will remain to save in my heart forever. I would like to mention the names of some of my friends because of whose support and motivation I am able to finish the work. I pay my thanks to Biswajyoti for his unconditional help and support. I pay my big thanks to Chiranjib, Partha, Dhanesh, Doordarshi, Rana, Purabi, Sudheer, Avishek, Ankit, Bedabrata and Gopi without whom my journey would not have been possible. I got all round of help from their side.

I am also thankful to Dr. Malaya Chetia, Department of Civil Engineering, Assam Engineering College, Jalukbari. Because she had recognized my ability and inspired me to go for research.

I also appreciate the help received from the staff present in different bookshop and food stall at IIT Guwahati. I offer my gratitude to Tapan for serving me with food and beverages during my seminars and all.

The last but not least I would like to offer my heartiest thanks to the Director of IIT Guwahati for facilitating me with all kinds of support to carry out my works. I also pay thanks to the IIT Guwahati fraternity for including me in the nice greenery beautiful campus. I have spent the best time in my life in the midst of mesmerizing scenery of IIT Guwahati. IIT Guwahati is very beautiful and I wish to enrich its beauty every day.

TABLE OF CONTENT

LIST OF FIGURES

LIST OF TABLES

ABBREVIATIONS

S_r	Degree of saturation
Gs	Specific gravity
ρ_d	Dry density
ξ	Zeta potential
ψ	Matric suction
ρ_d^*	Normalization dry density
$P_{\rho_d^*}$	Swelling pressure at normalization dry density

CHAPTER 1
INTRODUCTION

1.1 GENERAL

The clay minerals are very important in engineering applications and found naturally in many parts of the world. Kaolinite and montmorillonite are two important minerals having extreme activity. The kaolinite is abundantly available in many parts of India, such as Andhra Pradesh, Jammu, and Kashmir, Jharkhand, Kerala, Madhya Pradesh, Orissa, Rajasthan, and Northeast. Kaolin clay contains primarily the kaolinite mineral. The kaolin is a non-active clay. There is no such engineering application of kaolin. Nevertheless, kaolin is used in pottery industries. Bentonite is an active clay and is available in many parts of India, such as Karnataka, Maharashtra, Andra Pradesh, Madhya Pradesh, Gujarat, and Tamil Nadu. The dominant mineral of bentonite is montmorillonite. Soils, high in montmorillonite content exhibit high swell potential due to wetting or high swelling pressures under the applied mechanical loading. The bentonite is considered as a problematic soil due to its swelling characteristics. The swelling characteristics of these clay soils often cause problem leading to structural damage and loss of property. On the other hand, studies have shown that due to its swelling and self-sealing characteristics, bentonite is used for various engineering applications such as the construction of landfills, drilling mud, and nuclear waste repositories. The wetting induced behavior of these two clays soil is observed to be very interesting. The wetting induced behavior of these two clay under mechanical loading is becoming an important research topic. Both the clay have extreme behavior and completely opposite from each other. Kaolin clay has collapsible nature and considered as collapsible soil (Wheeler and Sivakumar, 1995). However, the causes of collapsibility of the kaolin are not fully understood yet. The failure of many engineering structures in many places is due to the occurrence of collapsible soil underneath the foundation. The heaving of the structures and development of stresses in radioactive waste repositories from the buffer material are associated with the swelling characteristics of bentonite. The potential to change the

volume upon wetting depends on many factors such as the initial compaction state, pore-fluid characteristics, the degree of wetting, and the external load.

The study of the hydro-mechanical behavior of clay soil has gain importance since the last few decades by the researchers and field practitioners around the world. Literature shows that effective stress development is completely different in these clays. The effective stress in bentonite reduces due to wetting whereas the effective stress gets increase in kaolin. Karl Terzaghi, 1936 first proposed the effective stress concept do describe the behavior of saturated soil. He explained that the effective stress concept could explain the mechanical behavior of soil. But later on, the principle as suggested Terzaghi fails to explain the behavior compacted and natural soil. One of the major loopholes in Terzaghi's effective stress concept is that it does not consider the forces in the soil, which produce a measurable effect in controlling the behavior of both saturated and unsaturated soil (Lu and Likos, 2006). Nevertheless, the concept was not found to be application based. Terzaghi's effective stress concept was modified many times over the years to explain the behavior of unsaturated soil. However, it was observed that none of the models gives a satisfactory result when used for practical application. A new approach by Lu and Likos (2006) to define effective stress using suction stress characteristics curve is gaining importance. Suction stress is defined as the force that tends to pull the soil grains towards each other. Suction stress depends on the degree of saturation, water content, and matric suction of the soil. The variation of suction stress with volumetric water content is known as the suction stress characteristics curve (SSCC). Literature shows that SSCC gives a simple and efficient solution to understand the behavior of unsaturated soil.

1.2 Motivation for the study

To have a better understanding of the hydro-mechanical behavior of collapsible and expansive clays, a systematic study revealing the influence of critical soil parameters is required. A clear understanding of the mechanism of collapse and swelling is necessary for a sound understanding of the soil behavior under different stress conditions. A detailed study conducted on the two clay soils that exhibit extreme behavior due to the presence of distinct minerals namely, kaolinite and montmorillonite. The collapse behavior of

kaolin under mechanical loading and in the presence of different pore fluids was studied for understanding the micromechanical nature. Swelling pressure development under the isochoric conditions was observed due to wetting. The bimodal behavior of swelling pressure with time and the swelling nature of different bentonites with initial compaction density was well addressed in this work. The effective stress concept based on suction stress characteristic curve was verified by considering different suction controlled test. The development of effective stress during drying and wetting of the above-mentioned soil and understanding their behavior motivated the present study.

Outline of the thesis

The research work undertaken was presented in the thesis in the following manner**.**

Chapter 1: Chapter 1 introduces the topic of research and a brief structure of the thesis.

Chapter 2: Chapter 2 provides a review of literature relevant to the present area of research. The main objectives and detailed scope of work were selected from the critical appraisal of the literature review.

Chapter 3: Chapter 3 describes the materials selected for the study, their basic characterization, and surface properties. The testing methods for measuring collapse potential and swelling pressure kaolin and bentonite respectively were detailed to meet the objective of the paper. The theoretical estimation of swelling pressure was discussed. The measurement of VSC and SWCC for slurried soil presented. The method of suction controlled collapse test and swelling pressure were presented.

Chapter 4: Chapter 4 presents the results of the sediment volume test and one-dimensional collapse potential test of kaolin. The settlement behavior of kaolin described using isoelectric point of kaolin, which measured using NaCl solution for different pH value. Collapse potential under different inundation pressure was measured for different electrolyte solution under different pH environment and dielectric constant. The fabric of compacted sample under different load and electrolyte solution were studied under Field Emission Scanning Electron Microscope.

Chapter 5: This chapter presents the swelling pressure characteristic curve for different quality Indian bentonites was established under different compaction density. The effect of compaction density and bentonite quality on the pore-size distributions (PSDs) and clay fabric were analyzed for understanding the influence on SPCC behavior. The evolution of PSD and fabric during the water uptake process was analyzed for understanding the microstructural influence on SPCC behavior.

Chapter 6: Chapter 6 presents a new theory to estimate swelling pressure based on Bharat and Sridharan (2016) work. The theory was verified with the literature data and the present data.

Chapter 7: Chapter 7 presents the results of suction control collapse potential test and swelling pressure test. The effect of suction on collapse potential under different inundation pressure was discussed in this chapter. The relation between collapse potential and suction for kaolin; swelling pressure and suction for bentonites; SWCC for both kaolin and bentonite for the compacted state were established from the experimental data. The suction stress characteristics curve was estimated from the measured SWCC data of compacted kaolin and bentonite. The concept of effective stress was explained for collapsible and expansive soils under various loading conditions. The suction stress and suction follow a 1:1 line up to a certain suction value and beyond that suction stress deviates and it decreased. On the other hand, the effective stress of compacted bentonite shows a slight increase with swelling pressure and after that effective stress become constant which is physically not possible.

Chapter 8: This chapter presents a summary, conclusions, and major research contribution, of the study.

CHAPTER 2
LITERATURE REVIEW

2.1 General

The wetting induced soil behavior under mechanical load is received great interest. Terzaghi in 1936 proposed the effective stress concept for the first time to describe the behavior of saturated soil. He explained that the effective stress concept could explain the mechanical behavior of soil. The effective stress was defined as the difference between total stress and pore-water pressure. The basic assumption in Terzaghi's effective soil concept was that both the soil grain and liquid are incompressible. Thus, effective stress concept describe nothing but the strength of solid soil particles. Soon it was observed that the Terzaghi's effective stress concept has several limitations when applying to natural and engineered soil where the soil is partially saturated. Partial saturation of soil is that condition where the voids are filled with more than one fluids (water and air) i.e., a three-phase system. Apart from this, the effective stress concept did not consider the physicochemical forces, which play an important role in controlling the behavior of clays. The physicochemical forces in clays are governed by the van der Waals attraction and electrical double-layer repulsion. Therefore, effective stress concept was modified several times to incorporate the missing forces to define the behavior of soil. Bishop (1959) first proposed the modified effective stress equation by incorporating the concept of matric suction in soil behavior. Bishop's effective stress equation involves an effective stress parameter, which depends on the degree of saturation of the soil. However, the practical applicability of Bishops modified form of effective stress equation became limited. Since then, there were several models available in literature, which were proposed to understand unsaturated soil behavior (Skempton 1960; Alonso et al. 1990, 1999; Gens and Alonso 1992; Nuth and Laloui 2008; Laloui and Nuth 2009; Khalili et al. 2004; Gallipoli et al. 2003; Lu and Likos 2006; Alonso et al. 2010). The practical application of this approach for describing the behavior of unsaturated soil is uncertain and remain as a huge scope of research. The effective stress concept proposed

by Lu and Likos (2006) is gaining importance nowadays. The effective stress for any soil can be estimated from the suction stress, which is again related to the SWCC of the soil. The suction stress is the results of the combined effects of negative pore water pressure and surface tension. The estimation of suction stress required the knowledge of SWCC of the soil in terms of degree of saturation. The relation between suction stress and volumetric water content is known as the suction stress characteristics curve (SSCC). It was observed that the effective degree of saturation plays an important role in controlling parameter for unsaturated soil property functions. Baille et al. (2016) showed that the concept of suction stress could use successfully to predict the behavior of unsaturated soil. It was also observed that the effective stress based on SSCC could clearly explain both swelling and collapse behavior under hydro-mechanical load.

The understanding of collapse and swelling behavior of clay due to wetting under mechanical loading is a highly active area of research. The next part will discuss a detailed review of collapsible behavior of low active/plastic soil and behavior of kaolin in the presence of different solvents. The next part will also focus on the swelling characteristics of expansive clay.

2.2 Characteristics of low active clay

The past studies have shown that the low active clay soils such as red soil are prone to volume reduction due to wetting (Alonso et al. 1990; Rao and Revanasiddappa 2002; Liu et al. 2015). These clays are described as collapsible soil. These soils pose high strength and stiffness at the air-dry state and can withstand a very high normal pressure. Particles of loess soil form metastable, open structures with the interstitial clay-sized particles congregating at the quartz particle contacts (Zourmpakis et al. 2005). The open structure is maintained by a process of bonding and withstands overburden stresses to a certain degree, but exhibits volumetric collapse with additional loading or wetting (Derbyshire et al. 1995). A few studies have shown that kaolin exhibit collapsible behaviour but under certain stress state condition (Wheeler and Sivakumar 1995; Sun et al. 2007). The behaviour of kaolin at natural air-dry state under hydro-mechanical load was not reported in any single study.

Collapsible soils possess high strength and stiffness at their dry and natural state but exhibit a significant decrease in volume upon wetting. Collapsible soils are also called "hydro compactive soils" because they compact after water is added. The existence of collapsible soils has long been recognized since World War II. Collapsible soils are distributed in most parts of the world. These soils are particularly available in arid and semi-arid regions. Collapsible soils are considered as one of the problematic soils for foundation material. These soils pose a potential threat to structures built on them when wetted. Foundation of a structure constructed on collapsible soil may experience a sudden and huge amount of settlement. The amount of settlement depends on how loosely the particles are packed initially and the thickness of the soil that becomes wetted. Collapse may be initiated by water alone or by wetting and mechanical loads acting together. Many researchers defined collapsible soils in many different ways. Dudley (1970) defined collapsible soil as any unsaturated soil that goes through an excessive loss of volume upon wetting due to a major rearrangement of particles with or without additional loading. Jennings and Knight (1975) defined collapsible soil as an unsaturated soil that exhibits additional settlement due to wetting, without any increase in vertical pressure.

2.3 Criteria for the collapse

Different criteria were proposed for recognizing the collapsible soils. A soil is said to be a collapsible soil if it undergoes an appreciable amount of volume change due to hydraulic load, mechanical load, or a combination of both (Sultan 1969). The geotechnical earthen structure may collapse if compacted at dry of optimum (Fredlund and Gan 1995; Pereira and Fredlund 2000). Soils, which are potentially unstable, and needs sufficient suction pressure to maintain the structure with temporary rigidity, and high-applied stress necessary to develop the potential instability, may develop a collapsible soil (Barden et al. 1969). The possibility of collapse also depends on the percentage of clay content present in the soil (Handy 1973). If clay content is less than 16 %, there is a high possibility of collapse; 16-24 %, possibility of collapse; 25-32 %, possibility of the collapse of less than 50 percent; and more than 32 %, no collapse (Handy 1973). Loess with natural moisture content less than 6 % was potentially unstable, whereas if it exceeds 19 % the loess could be regarded as stable (Grabowska-olszewsla 1988). Collapsible soil is

generally metastable soil (Peck et al. 1974). Metastable soil includes extra-sensitive clays such as quick clays, loose saturated sands susceptible to liquefaction, unsaturated primarily granular soils in which a loose state is maintained by apparent cohesion, and some saprolites (Peck et al. 1974).

2.4 Collapse mechanism

Casagrande (1932) first demonstrated the collapse mechanism. According to him, the portion of the fine grain fraction of the soil acts as a bonding material for the larger grained particle. These bonds undergo local compression between the adjacent grains due to application of load resulting in the development of strength. At their natural water content, these soils compress slightly resulting in increased overburden pressure. When water is added to the loaded soil, and certain critical moisture content is exceeded, those bonding or cementation provided by the fine fraction become soften, weaken and/or dissolve to some extent. Finally, the binders reach a stage where they no longer resist any stress and the structure collapses. The characterization and understanding of collapsible soil depend on the collapse potential of the soil.

Pereira and Fredlund (2000) divide the entire collapse process into three phases, namely pre-collapse, collapse, and post-collapse phase. The pre-collapse phase, take place at a relatively high matric suctions. In this phase, soil does not collapse and only small deformations occur in response to a decrease in matric suction. The second phase is called the collapse phase and takes place at intermediate matric suctions. In the collapse phase, large deformations were observed in response to a decrease in matric suction. In the third phase, phase, at low matric suctions, there is an absence of deformations as the matric suction is reduced to zero. This phase is termed as “post-collapse” phase.

2.5 Measurement of Collapse potential

The characterization of collapsible soil was done based on the value of collapse potential (P_c) which is the amount of deformation that would occur at any stress level at which the soil get saturated. The role of collapse potential for collapsible soil in geotechnical engineering was well recognized in the past (Jennings and Knight 1957,

Jennings and Burland 1962, Houston et al. 1988). The collapse potential of compacted soil can be measured by three different techniques in the laboratory. (i) Double-oedometer test (Jennings and Knight 1957) (ii) Single-oedometer test (Houston et al. 1988) and ASTM D5333, 2003 and (iii) Single point, multiple specimen tests (Noorany 1992). Based on the collapse potential, the severity of the collapse of collapsible soil can found out, which is given below.

Table 2.1. Collapse potential (P_c) and severity of collapse (Jennings and Burland 1962; Bell and Culshaw 2001)

Collapse Potential, P_c (%)	**Severity of Collapse**
0–1	No-Problem
1–5	Moderate Trouble
5–10	Trouble
10–20	Severe Trouble
>20	Very Severe Trouble

2.6 Parameters influencing Collapse Potential

There are various opinions found in the literature related to the parameters influencing collapse potential. The roles of initial dry density, compaction moisture content, clay content, inundation stress (the external stress at which a laboratory specimen is inundated), matric suction, in determining the collapse potential of compacted soils are well recognized in the past (Lefebvre and Belfadhel 1989; Lawton et al. 1989, 1992; Houston 1993; Pereira and Fredlund 2000; Estabragh et al. 2004). The next part will discuss the different parameter/factors influencing the collapse potential of the soil.

2.6.1 *Effect of inundation stress*

The collapse potential is maximum at some critical value of inundation pressure corresponding to a given compaction moisture content and dry unit weight (Lawton et al. 1989; Basma and Tuncer 1992). Beyond that, collapse potential decreased with increasing inundation pressure. There is a certain pressure level at which the maximum compaction

takes places due to collapse and there is no change or very minute change is observed after the maximum degree is reached (Basma and Tuncer 1992).

2.6.2 *Effect of compaction pressure, compaction water content, and compaction procedure*

The compaction pressure, compaction water content, and compaction procedure have a significant effect on the mechanical behavior of compacted fine-grained soils (Lambe 1958; Seed and Chan 1959). The changes in compaction water content have an effect on the fabric in fine-grained soil. The influence of compaction procedure on the mechanical behavior of soil is due to the occurrence of the flocculated structure when compacted at dry of the optimum and dispersed structure when compacted at wet of optimum (Lambe 1958; Seed and Chan 1959). Barden and Sides (1970); Delage et al. (1996) demonstrated that samples compacted at dry of optimum produce a double-structure fabric, with a macro-fabric consisting of large clay packets or macropods separated by interpacket voids, whereas samples compacted wet of optimum have a more uniform fabric. This difference in fabric was observed by Garcia-Bengochea et al. (1979); Juang and Holtz (1986); Delage et al. (1996). Alonso et al., (1987) suggested that the double-structure type of fabric would be more susceptible to collapse on wetting than would a uniform fabric. Lawton et al. (1989) observed that when compaction moisture content reaches the value of optimum moisture content, the collapse potential reduces.

2.6.3 *Effect of net confining pressure and matric suction*

The net confining pressure, matric suction and degree of saturation of soil influence the collapse potential. (Pereira and Fredlund 2000). At high net confining pressure, the wetting induced volumetric collapse would be more for a collapsible soil than a low net confining pressure (Pereira and Fredlund 2000). According to Pereira and Fredlund (2000), a higher matric suction present corresponding to a higher net confining pressure at the starting phase of collapse and lower matric suction where collapse phase ends. Pereira and Fredlund (2000) observed that wetting-induced collapse produces two opposite and different effect when an unsaturated metastable soil structure is tested. The first effect is related to the reduction of the void ratio and second is the reduction in the

water flow into the soil structure. Due to a reduction in void ratio, the degree of saturation gets increases and due to the increasing amount of trapped air within the microstructure of the metastable-structured soil results in a reduction in the water flow into the soil structure. Collapse potential decreased with the increasing degree of saturation.

Commonly known collapsible soils such as loess and silty clay had studied extensively to understand the collapse mechanism under mechanical loading and the influence of inundation pressure using both natural and artificially prepared laboratory specimens (Jennings and Burland 1962; Houston et al., 1993; Lawton et al., 1989; 1992; Pereira and Fredlund 2000; Zourmpakis et al. 2005; Li et al. 2016). Kaolin, on the other hand, is a lesser−known collapsible soil. Sridharan et al. (1985) observed that the free swell index (FSI) of kaolin is negative, indicating a higher equilibrium volume of kaolin in kerosene compared to its volume in distilled water. However, the negative value of FSI was reported to be due to complex formation between clay platelets and a nonpolar solvent (Sivapullaiah et al. 1987). Further, the volume change behavior of kaolin in different solvents attributed to the dipole moment of the adsorbed solvent molecules and hydrogen bonding between the clay platelets (Rao and Sridharan 1985). The role of surface forces between the platelets of kaolin in the presence of different pore fluids downplayed in these studies (Sridharan et al. 1988). However, several careful laboratory studies (Schofield and Samson 1954; Van Olphen 1963; Rand and Melton 1977; Zhou and Gunter 1992; Lyklema 1995; Schroth and Sposito 1997; Ma and Pierre 1999) in combination with the studies related to physical examination of the platelet arrangements using advanced imaging tools in science literature (Zbik and Smart 1998; Miller et al. 2007; Gupta 2011; Liu et al. 2014) reveal that the fabric of the kaolin is sensitive to the pH and electrolyte concentration. A fabric map, depicting the fabric changes with pH and pore-fluid concentration, is developed based on this knowledge and controlled equilibrium sediment volume test data (in a no-stress condition) (Santamarina et al. 2002; Palomino and Santamarina 2005). Similar observations were made using the sediment volume test data by Palomino et al. (2008), but these studies conclude that the fabric changes due to pore-fluid interactions is not applicable at a higher solid/liquid ratio (ϕ). In contrast to these observations, the compressibility and dynamic properties of the kaolin

(at very high ϕ) are found to be strongly influenced by the surface forces (Wang and Siu 2006a, 2006b; Di Matteo et al. 2011). The kaolin behavior under the influence of mechanical stresses is inconclusive due to very limited studies. Wheeler and Sivakumar (1995) conducted a series of triaxial tests on speswhite kaolin for validating critical state framework for collapse behavior of kaolin. Sun et al. (2007) studied the wetting-induced collapse behaviour of compacted Pearl clay, which contained some percentage of kaolin mineral, in triaxial tests under different initial suction conditions. The collapse in these studies was attribute to changes in the mean net stress. However, no study is available on the nature and mechanism of collapse in kaolin. The knowledge of wetting-induced collapse behaviour and the collapse mechanism of kaolin is lacking due to poor understanding of the physicochemical dependency on fabric changes.

2.7 BEHAVIOR OF KAOLIN

The kaolin is a low plastic soil. The volume change behavior of kaolin in different solvents attributed to the dipole moment of the adsorbed solvent molecules and hydrogen bonding between the clay platelets (Rao and Sridharan 1985). The role of surface forces between the platelets of kaolin in the presence of different pore fluids downplayed in the previous studies (Sridharan et al. 1988). However, several careful laboratory studies (Schofield and Samson 1954; Van Olphen 1963; Rand and Melton 1977; Zhou and Gunter 1992; Lyklema 1995; Schroth and Sposito 1997; Ma and Pierre 1999) in combination with the studies related to physical examination of the platelet arrangements using advanced imaging tools in science literature (Zbik and Smart 1998; Miller et al. 2007; Gupta 2011; Liu et al. 2014) reveal that the fabric of the kaolin is sensitive to the pH and electrolyte concentration. A fabric map, depicting the fabric changes with pH and pore-fluid concentration, is developed based on this knowledge and controlled equilibrium sediment volume test data (in a no-stress condition) (Santamarina et al. 2002; Palomino and Santamarina 2005). Similar observations are made using the sediment volume test data by Palomino et al. (2008), but these studies conclude that the fabric changes due to pore-fluid interactions is not applicable at a higher solid/liquid ratio (ϕ). In contrast to these observations, the compressibility and dynamic properties of the kaolin (at very high ϕ) are found to be strongly influenced by the surface forces (Wang and Siu,

2006a, 2006b; Di Matteo et al., 2011). The kaolin behavior under the influence of mechanical stresses is inconclusive due to very limited studies. Wheeler and Sivakumar (1995) conducted a series of triaxial tests on speswhite kaolin for validating critical state framework for collapse behavior of kaolin. Sun et al. (2007) studied the wetting-induced collapse behavior of compacted Pearl clay, which contained some percentage of kaolin mineral, in triaxial tests under different initial suction conditions. The collapse in these studies is attributed to changes in the mean net stress. However, no study is available on the nature and mechanism of collapse in kaolin. The knowledge of wetting-induced collapse behavior and the collapse mechanism of kaolin is lacking due to poor understanding of the physicochemical dependency on fabric changes. The knowledge of volume change behavior of kaolin due to the influence of pore-fluid chemistry is, however, very important to address the subsidence problems in alluvial marine deposits due to pore-fluid alterations during saltwater intrusions (Torrance and Ohtsubo 1995; Melloul and Goldenberg 1997; Ohtsubo et al. 2002). In this study, the collapse nature was studied in detail for the first time and was found to be physicochemical in nature. Compacted kaolin specimens were able to withstand large mechanical loads in the air-dry state, but a significant collapse was noticed on wetting, similar to the loess soil. The collapse behavior of kaolin, however, was observed to be due to physicochemical interaction between the particle and pore fluids. The collapse potential of the compacted kaolin specimens due to fabric changes under the application of mechanical loading was analyzed. The rate of volumetric collapse and collapse potential in the presence of different pore fluids was investigated.

2.8 Interparticle association in kaolin

Kaolin is a 1:1 layer silicate formed by the building blocks of the tetrahedral siloxane layer (silica sheet) and dioctahedral layer (alumina–gibbsite sheet) as shown in Fig. 2.1. Silica sheet consisted of Si^{4+} at the center of a tetrahedron with O^{2-} at the vertices and the gibbsite sheet consisted of Al^{3+} at the center with OH^- at the vertices, rendering different termination sites on the faces and edges. Kaolin has OH^- termination sites on the gibbsite face, O^{2-} termination sites on the silica face, and both OH^- and O^{2-} termination sites on the edges (Fig. 2.2a). The kaolin basal surface (face) carries a net

negative, permanent charge ascribed to the isomorphous substitution of Si^{4+} with Al^{3+} in the tetrahedral layer. The structural charge on the tetrahedral basal plane is, however, insignificant (Brady et al. 1996) due to very small (1–5 meq/100 g) cation exchange capacity (Conley and Althoff 1971; Ma and Eggleton1999). Kaolin consists of pH-dependent charges (Celik 2004), apart from the permanent (i.e., pH-independent) charge, due to the presence of reactive termination sites on the edges and alumina basal surface. The pH-dependent charges in kaolin come from (i) protonation and deprotonation of the alumina sheet on the edge; (ii) deprotonation of the silica sheet on the edge; and (iii) protonation and deprotonation of the alumina basal surface. Protonation is the adsorption of H^+ ions onto the surface at low pH values, which adds positive charge to the surface while deprotonation is the removal of protons from the particle surface when OH^- ions are abundantly available. Therefore, the charge on the edges or basal surface becomes negative in the presence of the pore fluid with high pH value. Changes in the pH-dependent charges are often analyzed using the particle isoelectric point (IEP). The IEP is the pH value of a pore fluid at which the electrophoretic mobility of the clay particle is zero, i.e., the particle ξ-potential is zero. The ξ-potential is defined as the electric potential at the shear plane between the bulk solution and an envelope of water that moves with the particle under an electric field (Van Olphen 1963). The IEP of the basal surface (IEP_{face}) is different from the one at the edges (IEP_{edge}), rendering complex alterations of the surface charges and different particle arrangements due to changes in the pore-fluid chemistry in kaolin. The IEP_{face} is found to vary in the range of 2–4 and IEP_{edge} in the range of 7–10 based on the electrophoresis and potentiometric titrations (Carty 1999; Palomino and Santamarina 2005). However, the IEP determination based on electrophoresis is questionable due to the limitations associated with the ξ-potential measurement, as the Smoluchowski equation is applicable only for spherical particles (Gupta 2011).

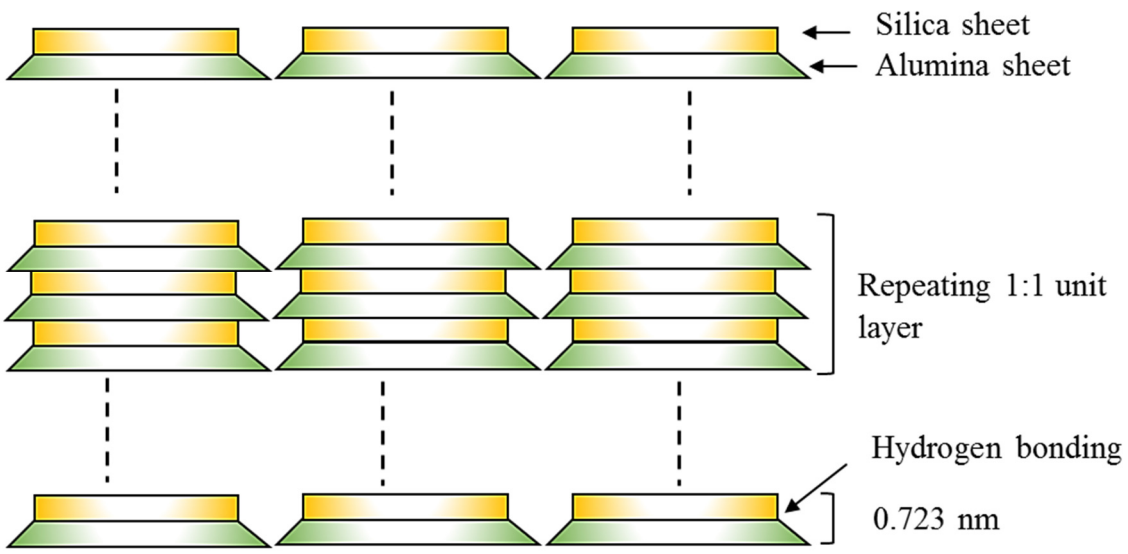

Fig. 2.1 Staking of 1:1 unit layers of kaolin

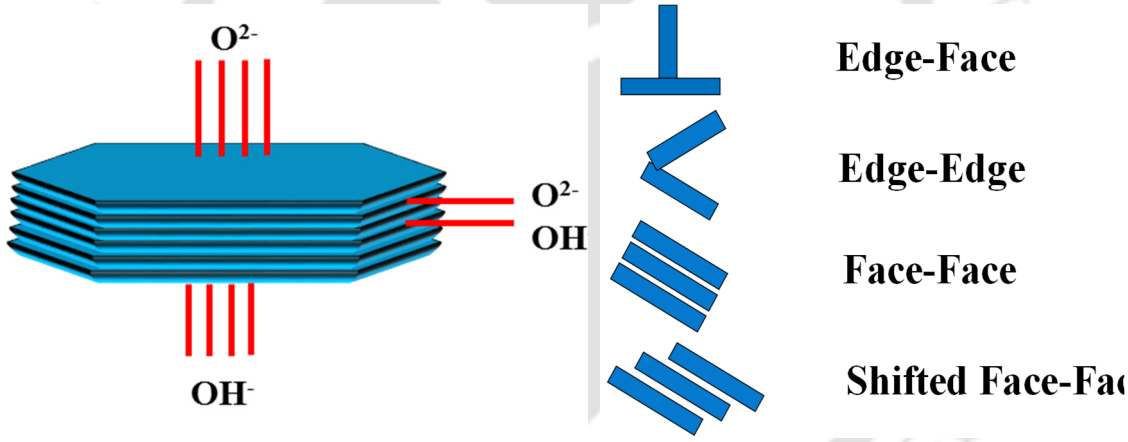

Fig. 2.2 (a) Termination sites and Iso Electric Point (b) The mode of particle association

Moreover, the IEP_{edge} is found to be in the range of 5–6, which is an average of the IEP of silica (i.e., 2.2) and gibbsite (i.e., 9.2) and is based on the pure mineral colloid behavior (Kim 2008; Gupta 2011). The IEP from the mineralogical consideration is smaller than the reported values from the electrophoresis technique. The estimated IEP_{edge} value using sediment volume tests, therefore, provides an accurate analysis of particle association in different pH environments (Wang and Siu, 2006a). Characteristics of the pore fluid may also promote dissolution of the mineral. Several modes of particle associations—such as edge–face (EF) flocculation, edge–edge (EE) flocculation, shifted face–face (FF)

aggregation, and "dispersed" (Michaels and Bolger 1962; Van Olphen 1963; Palomino and Santamarina 2005) — are observed due to changes to dissolution and surface charge modification (Fig. 2.2b). The mode of particle association when pH < IEP_{edge} is observed to be EF due to Coulombic attraction between the negative face and positive edge, but the arrangement is dispersed when pH > IEP_{edge} due to the presence of negative charge on all the surfaces (Wang and Siu 2006a). In acidic environments, alumina dissociates preferentially which generates positive charge (Wieland and Stumm 1992). Alumina dissociation promotes EF flocculation due to the attraction between the edges and faces. On the other hand, silica dissociation under alkaline conditions and low electrolyte concentrations promotes FF aggregation due to negative charges on both edges and face. At high electrolyte concentrations (n > 0.1 mol/L NaCl), however, the kaolin fabric is pH independent and FF aggregation is promoted due to van der Waals attractive forces (Rand and Melton 1977). Apart from pH and electrolyte concentration, the kaolin behavior is also strongly influenced by the dielectric medium (Rao and Sridharan 1985; Chen and Anandarajah 1998; Anandarajah and Zhao 2000; Chen et al. 2000; Di Matteo et al. 2011; Sloane and Kell 2013).

2.9 STRUCTURE OF BENTONITE AND ITS SWELLING CHARACTERISTICS

Bentonite is considered to be the potential buffer material in high-level nuclear waste (HLNW) repositories of many countries (Pusch and Yong 2006; Zheng et al. 2011; Gapak and Bharat 2018). Bentonite clay consisting mostly of montmorillonite. The structure of montmorillonite is a unit made of an alumina octahedrala sandwitched between two silica tetrahedral sheets. Bentonite powder is compacted to the design density at air-dried state; placed between the waste canisters and surrounding saturated rock mass for creating an impermeable zone. The stress state of the repository is appropriately maintained from the swelling pressure development of the compacted bentonite blocks during the saturation process apart from sealing the construction joints (Grindrod et al. 1999; Gens et al. 2002; Ye et al. 2010). Water-entry into the compacted bentonite blocks from the surrounding rock masses results in the development of swelling pressure due to particle repulsion (Verwey and Overbeek 1948) during the hydration of the interlamellar layers of the montmorillonite mineral, hydration of exchangeable

cations, and external surface of the aggregates. The evolution of swelling pressure with time, termed as swelling pressure evolution curve (SPEC) in this work, is important for understanding the stress development in the repository during the bentonite saturation process. A distinct SPEC is often observed with different bentonites and different initial compaction effort during water uptake under isochoric conditions when the swelling pressures are continuously monitored using digital load cells (Pusch 1982). The magnitude of swelling pressure increased during the initial water uptake before a decrease in the pressure and followed by increase in the swelling pressure to a final equilibrium value (Pusch 1982; Imbert and Villar 2006; Schanz and Tripathy 2009; Zhu et al. 2013; Chen et al. 2018; He et al., 2019). A decrease in swelling pressure after initial water uptake is attributed to the loss of shear strength at the aggregate level, whereas a further increase in the swelling pressure attributed to the redistribution of clay particles to a more homogenous and dispersed state (Pusch 1982). The drop in swelling pressure after the initial phase of water uptake is found to be significant in French FoCa bentonite and the qualitative behavior is similar for all different studied initial compaction densities (Imbert and Villar 2006). However, the decrease in swelling pressure after reaching the first peak is insignificant to zero with a flat SPEC behavior before the increase in the swelling pressure to final equilibrium value for GMZ bentonite (Chen et al. 2018; Zhu et al. 2013; He et al. 2019). Further, the decreasing tendency of swelling pressure after the initial phase of water uptake is observed to be dependent on the initial compaction bentonite for German bentonite and GMZ (Schanz and Tripathy 2009; Chen et al. 2018; He et al. 2019) in contrary to French FoCa clay. The SPEC behavior is thus strongly influenced by the bentonite quality (i.e., plasticity) and initial compaction density. Albeit the dominant swelling mechanisms viz. crystalline and osmotic swelling (van Olphen, 1977) are well cited and accepted in the literature (Bradbury and Baeyens 2003; Savage 2005; Massat et al. 2016), the variable nature of SPEC with compaction density and bentonite is not understood.

2.10 Measurement of swelling Pressure

Swelling pressure is defined as the pressure exerted by a clayey soil when is exposed to water in a confined space. The swelling pressure of compacted clay is of great

engineering interest. There are many laboratory measurement techniques as well as analytical methods to calculate swelling pressure of compacted clay. The measurement of swelling pressure of compacted bentonites was attempted in the past by several researchers (Pusch 1982; Dixon and Gray 1985; Bucher and Muller-Vonmoos 1989; Komine and Ogata 1994; Villar and Lloret 2007; Karnland et al 2007; Schanz and Tripathy 2009). There are three distinct methods for the measurement of swelling pressure in the laboratory (Brackley 1973). These are (1) free swell and load method, (2) swell under load method, and (3) No swell or constant volume method.

Constant volume swell pressure test received a wide acceptance over swell – consolidation and swell under load methods (Pusch 1980b; Muller-Vonmoos and Kahr 1982; Pusch 1982; Gray et al. 1984; Swedish Nuclear Fuel and Waste Management Company 1983; Dixon and Gray 1985; Sridharan et al. 1986; Kanno and Wakamatsu 1992; Komine and Ogata 1996; Japan Nuclear Cycle Development Institute, 1999; ENRESA 2000; Herbert and Moog 2002) due to large variability in the swelling pressures to the tune of 0.027 – 40 MPa at high compaction density, for different bentonites based on their quality. Moreover, constant volume swelling pressure test simulates the in–situ conditions, estimates more accurate swelling pressures, and widely used (Zhang et al. 2019). However, establishing the entire swelling pressure – dry density relationship over wide density range is highly expensive and time-consuming.

2.11 Theoretical estimation of swelling pressure

Several attempts are made, in the past, therefore, for the theoretical estimation of swelling pressure data at a given compaction density. Swelling pressures of the compacted bentonites are predicted based on the sorption isotherm by Agus and Schanz (2008). The laboratory estimation of total suction data of the compacted bentonite in the lower suction range limits the accurate prediction of swelling pressures using this approach. Swelling – pressure vs. dry density relationship of the compacted bentonites are often predicted based on the diffuse double layer (DDL) theory. Empirical relationships between mid–plane potential and interplate distance based on the empirical estimation of equation coefficients to match the observed data are proposed by several researchers for specific bentonites (Sridharan and Choudhury 2002; Tripathy et al. 2004;

Schanz and Tripathy 2009; Baille et al. 2010) and bentonite-sand mixtures (Wang et al. 1996; Komine and Ogata 1999; Xu et al. 2003; Sun et al. 2009; Cui et al. 2012). Reduction factor to the swelling pressures is incorporated based on the percentage presence of different coarse fractions in the bentonite-sand mixtures in these studies. The applicability of such expressions, however, is not guaranteed for a wide range of bentonites and bentonite-sand mixtures. Normalization approach based on the linearization model is recently introduced for predicting the compressibility data of highly plastic clays (Bharat and Sridharan 2015a). Normalization approach is found to be advantageous due to the requirement of no knowledge of clay surface and pore-fluid characteristics, or the computation of midway potentials to relate with the distance between clay platelets. The applicability of this model for predicting the swelling pressure – dry density data is yet to be explored.

2.12 Parameters influencing the swelling pressure of compacted soil

This section deals with the review of different parameters influencing swelling pressure of compacted soil. There are various conflicting observations found in the literature related to the parameters influencing swelling pressure. This review would be quite helpful to understand the behavior of clayey soil. Since the swelling pressure is used as the basis for the understanding of mechanical behavior of clay, it is important to have an accurate determination of the swelling pressure. Therefore, it is necessary to gain an in-depth knowledge of the various factors influencing the swelling pressure for compacted soil. some of the important parameters that influence the swelling pressure of clay are, clay content and plasticity, initial dry density and water content, clay fabric, hydration path, suction, and initial vertical loading.

2.12.1 Influence of clay content and plasticity

The swelling pressure of clay is influenced by the percentage of clay content present (Seed et al. 1962). The swelling pressure can best be related to the water plasticity ratio which is defined as the ratio of water content minus plastic limit to plasticity index (Sowers and Kennedy 1967). The swelling pressure for a high plastic clay is more than a low plastic clay for any given dry density.

2.12.2 *Influence of Dry Density and Water Content*

The swelling pressure is a function of the initial density of the sample and there exist an exponential relation between initial density and the swelling pressure of clay (Komine and Ogata 1994; Villar and Lloret 2008; Baille et al. 2010; Wang et al. 2012; Lee et al. 2012; Djedid and Quadah 2012). However swelling pressure doesnot affected by initial water content (Sridharan et al., 1986; Komine and Ogata 1994; Villar and Lloret 2008; Baille et al. 2010; Wang et al. 2012; Djedid and Quadah 2012).

2.12.3 *Influence of soil fabric*

The fabric of the compacted clay plays an important role in development of swelling pressure of compacted clays. Pusch (1982), observed a double structure in compacted soil. The same double structure was also recognized in several compacted clays (Atabek et al. 1991; Alonso et al. 1999; Cui et al. 2002; Gens and Alonso 1992; Romero et al. 1999; Pusch and Moreno 2001; Lloret et al. 2003 ; Sanchez et al. 2005).

2.12.4 *Influence of hydration path*

Swelling characteristics of clay is dependent on hydration path and hydration process (Tang et al. 2011). Hydration of clay minerals is proceeded by the adsorption of water molecule into the interlayers of the montmorillonite mineral and hydration of exchangeable cations (Saiyouri et al. 2000). The number of water molecule layers penetrate into the inter layers varies up to four in the fully hydrated state (Mooney et al. 1952a).

2.12.5 *Influence of suction*

Suction plays an important role in the development of swelling pressure of compacted clay. Wang et al. (2012), observed an exponential relation between swelling pressure and the applied suction. When the clay samples were exposed to moist water vapor, water molecules first migrate into the open channels and adsorbed on the exposed mineral surface (Pusch 2001b; Arifin 2008), then move to elementary clay layers. The number of water molecules absorbed by the clay layers depends on the relative humidity

or suction applied (Chipera et al. 1997; Likos 2004; Pusch 2001b; Saiyouri et al. 2004; Delage 2006), which defines the swelling pressure of the sample.

2.12.6 *Influence of initial vertical loading*

Swelling pressure of compacted clays depends on the initial applied vertical loading (Komine and Ogata, 1999; Lloret et al., 2003; Tang et al., 2011). Wetting induced an increase of swelling pressure when the initial vertical pressure is low and a decrease in swelling pressure when the initial vertical pressure is high. Tang et al. (2011) concluded this observed phenomenon based on the double-structure model described by Gens and Alonso (1992), Alonso et al. (1999), Sanchez et al. (2005), and Tang and Cui (2009). The interlayer distance between the clay sheets is increased due to wetting resulting in clay aggregates swelling, and subsequently weakens the resistance of the macropores. When the soil is wetted under low vertical pressure, the first mechanism prevails over the second and an increase in swelling pressure is observed. However, when the soil is wetted under high vertical pressure, the second mechanism prevails: wetting induces collapse of macro-pores and thus decreases the swelling pressure.

2.13 Critical appraisal of the literature review

The kaolin and bentonite are two important clays pose challenges to geotechnical engineers and are found naturally in many parts of India and elsewhere. Kaolin contains kaolinite mineral and bentonite contains montmorillonite as a dominant mineral. These two clays exhibit extreme characteristics due to their mineralogy. Kaolin in low active and bentonite is highly active clay.

The low active soils are generally prone to volumetric collapse due to wetting and considered as collapsible soil. Soils such as red-soil and loess are fall in this category. These soils pose high strength and stiffness at the air-dry state and can withstand a very high normal pressure. The collapse in these soils mainly depends on the hydro-mechanical loading. Kaolin clay also shows collapsible behavior under certain stress state condition. The behavior of kaolin at natural condition under hydro-mechanical load was not known. There was no study available in the literature to explain the nature and mechanism of collapse in the natural state under hydro-mechanical loading. Studies have

shown that the behavior of kaolin influenced by the pore fluid environment under no stress condition. Kaolin behavior strongly depends on the pH environment and electrolyte concentration. There are several modes of particle associations in kaolin due to changes to dissolution and surface charge modification in different pH environment. Apart from pH and electrolyte concentration, kaolin behavior is also strongly influenced by the dielectric medium. The knowledge of hydro-mechanical behavior of kaolin is lacking due to poor understanding of the physicochemical dependency in different pore fluid environment. The behavior of the compacted kaolin specimens in the different pore-fluid environment under the application of mechanical loading needs to be understood to address the behavior.

Bentonite exerts swelling pressure on the surroundings, due to wetting, when the volumetric swelling is restricted. Different techniques were available in the literature for the measurement of swelling pressure of compacted bentonite. Out of which constant volume swell pressure test received wide acceptance as the test simulates the in–situ conditions, estimates more accurate swelling pressures. Swelling pressure of bentonites depends on the bentonite plasticity and initial compaction state. The evolution of swelling pressure with time show a distinct behavior with different bentonites and different initial compaction condition during water uptake under constant volume conditions when the swelling pressures are continuously monitored using digital load cells. The magnitude of swelling pressure increased during the initial water uptake before a decrease in the pressure and followed by an increase in the swelling pressure to a final equilibrium value. However, the drop in swelling pressure after the initial phase of water uptake is found to be insignificant in many clays. The variable nature of swelling pressure with time for different compaction density and bentonite is not understood.

The measurement of entire swelling pressure – dry density relationship over wide density range is highly expensive and time-consuming. The theoretical estimation of swelling pressure data at a given compaction density was attempted by several researches in the past. Swelling pressures of the compacted bentonites are predicted based on the sorption isotherm but limited to the only lower suction range. The diffuse double layer (DDL) theory is used to predict Swelling – pressure vs. dry density relationship of the

compacted bentonites. There are many approaches to estimate swelling pressure of compacted bentonite based on DDL theory. Several empirical relationships were proposed by several researchers for specific bentonites and bentonite-sand mixtures. The applicability of such expressions, however, is not guaranteed for a wide range of bentonites and bentonite-sand mixtures. A new estimation model is necessary for predicting the swelling pressure variation over a wide range of dry densities with minimal cost and time. Normalization approach based on the linearization model is recently introduced for predicting the compressibility data of highly plastic clays (Bharat and Sridharan 2015a). the approach was found to be advantageous due to the requirement of a single measured point to estimate the entire curve. The applicability of this model for predicting the swelling pressure – dry density data is yet to be explored.

The development of effective stress due to wetting is opposite in kaolin and bentonite. Several constitutive relations were proposed to understand the development of effective stress in clays during wetting. However, the practical applications of these models became limited due to the difficulty associated with the several parameters which are difficult to obtain experimentally. There is no such approach, which can clearly explain effective stress development during collapse and swelling in clay due to wetting. The Lu and Likos (2006) approach of estimating effective stress based on SSCC was found to be a new promising approach. However, the models need to be validated with the new laboratory measured data for application in the field situation.

2.14 Objective of the study

The critical appraisal of the reviewed literature clearly highlights that there is a need for a systematic study to understand the volume change (swelling and shrinkage, and collapse) behavior of unsaturated soil. There are several methodologies and theory available for the measurement of swelling for unsaturated soil. At the same time, there are several anomalies associated with these methodologies and theories. The influence of several factors related to the measurement methodologies and theories still need to be studied in detail. There is no theory available in the literature to explain the collapsible behavior of unsaturated soils. The experimental techniques available for collapsible soil

are dependent on several factors. With this in view, the broad scope of this research work was written below:

1. To study the behavior of compacted kaolin at air-dry state under hydro-mechanical loading. The effect of pore fluid characteristics on kaolin behavior under mechanical loading will be studied to analyze the behavior of kaolin under hydro-mechanical loading.
2. To study the temporal variation of swelling pressure with time for different plasticity and different compaction state. The effect of clay fabric, initial density, and surface property on the variation of swelling pressure of compacted will be address in the study.
3. To propose a model to estimate swelling pressure of compacted clay and clay-sand mixture using linearization model.
4. To find the effect of suction on the collapse of kaolin under mechanical loading and the effect of suction on swelling pressure of clay.
5. To understand the effective stress development in kaolin and bentonite clays using the suction stress approach, during wetting under hydro-mechanical load.

Chapter 3
MATERIALS AND METHODS

3.1 General

This chapter describes the materials and their properties and details of the laboratory experiments carried out for this study. A wide-range of laboratory tests were performed to explore the collapse phenomena of kaolin and swelling phenomena of bentonite. The experimental procedures used in subsequent chapters were also described. Parameters measured in this chapter were used to support the analysis of volume change behavior of clays under mechanical loading.

3.2 Material used in the current study

Indian bentonites of two different plasticity indices (quality), namely B1 and B2, and one nonplastic clay, namely Kaolin were used in this study as shown in Table 3.1. These are commercially available soils. The bentonites were procured from Barmer district of Rajasthan and Kucth region of Gujarat. The origin of Kaolin in not known. The bentonites provided as a fine, granular powder, predominately grey-yellow in color. While the kaolin provided as a fine, granular powder and completely white in color. The soils were stored at room temperature prior to testing in a sealed environment. Apart from these soils, seventeen bentonites and bentonite-sand mixtures of different plasticity indices, considered in the literature for the potential application in high-level nuclear waste repositories as buffer and backfill material in different countries, were considered in this study (Table 3.2). The quality of these bentonites varied over a wide range due to the variations in their surface properties

Table 3.1. Details of clays used in the present study

Sl. No.	Soil	Designation	Remarks
1	Indian kaolin	-	Commercially Procured

2	Indian bentonite1	B1	Commercially Procured
3	Indian bentonite2	B2	Commercially Procured

Table 3.2: Details of clays from literature used in the present study

Clay type	References
MX80	Bucher and Muller-Vonmoos (1989)
K-1	Schanz et al. 2010
K-3	Komine and Ogata (1996)
Montigel	Bucher and Muller-Vonmoos (1989)
SB1	Komine and Ogata (2003)
SB2	Komine and Ogata (2003)
SB3	Komine and Ogata (2003)
SB4	Komine and Ogata (2003)
SB5	Komine and Ogata (2003)
S1	Schanz and tripathy (2009)
K-2	Japan Nuclear Cycle Development Institute (2000)
GMZ-EXE	Schanz and Badran (2014)
GMZ-1	Zhang et al. (2012)
Volclay	Komine and Ogata (2004)
Kunibond	Komine and Ogata (2004)
GMZ-Na	Sun et al. (2014)
GMZ-Ca	Sun et al. (2014)

The percentage of bentonite in the sand-bentonite mixture for SB1, SB2, SB3, SB4, SB5 are 100%, 90%, 80%, 70%, and 60% respectively.

3.3 Clay properties

The kaolin and the bentonites were subjected to different physical, chemical, mineralogical and geotechnical characterization. The soils were classified at the civil engineering laboratories of IIT Guwahati following the ASTM standards described below.

3.3.1 *Particle size distribution*

The particle size distribution of the bentonite, samples were obtained by using the standard test method of ASTM D422-63 (2007). The particle size distribution for particles below 75μm was obtained by the standard test method for fine-grained soils using the sedimentation (hydrometer) analysis, ASTM D7928-17 (ASTM 2017). The particle-size distribution of the kaolin was obtained by using the Hydrometer analysis, standard test method D7928-17 (ASTM 2017) as it contains only fine particle. The soils were dominant by the percentage of clay content. The kaolin has a clay content of 72% whereas the bentonites B1 and B2 have 68 to 80% respectively.

3.3.2 *Specific Gravity*

The specific gravity (G_s) of soil solids were obtained by density bottle method following the procedure of ASTM D854–92 (1994). The specific gravity of all the three clays i.e., kaolin, B1 and B2 were 2.6, 2.76, and 2.77 respectively.

3.3.3 *Atterberg Limits*

The consistency limits of the plastic clay samples were determined as per the guidelines provided by ASTM D4318, 2010; IS: 2720 (Part V) for liquid limit, plastic limit. The test results of liquid limit and plastic limit were listed in Table 3.3. The liquid limit was determined using liquid limit apparatus of ASTM D4318 (2010a). The plastic limit was carried out using the method of ASTM D4318 (2010a). Based on the value of plastic limit and plasticity index, the kaolin was classified as low plastic clay (CL) and bentonite B1 and B2 were classified as high plastic clay (CH).

The kaolin is a low plasticity soil with very low surface properties. The bentonite B1 is low-quality bentonite and B2 is high-quality bentonite, distinguished based on the percentage montmorillonite content in these clays. The quality of the bentonites also reflected in their surface and index properties. The details of these clays were listed in Table 3.3.

3.3.4 *Mineral identification*

The mineralogy of the kaolin was determined by using x-ray diffraction technique. The XRD data were presented in Fig. 3.1. The XRD phase identification was performed in accordance with Mosser-Ruck et al. (2005). The XRD data of kaolin

showed the presence of only kaolinite mineral, i.e., the soil is pure kaolin. The XRD data of the studied bentonites showed montmorillonite as the dominant mineral with multiple peaks and available in Gapak et al. (2017). Other important minerals such as kaolin, illite, and quartz were also present in both the bentonites.

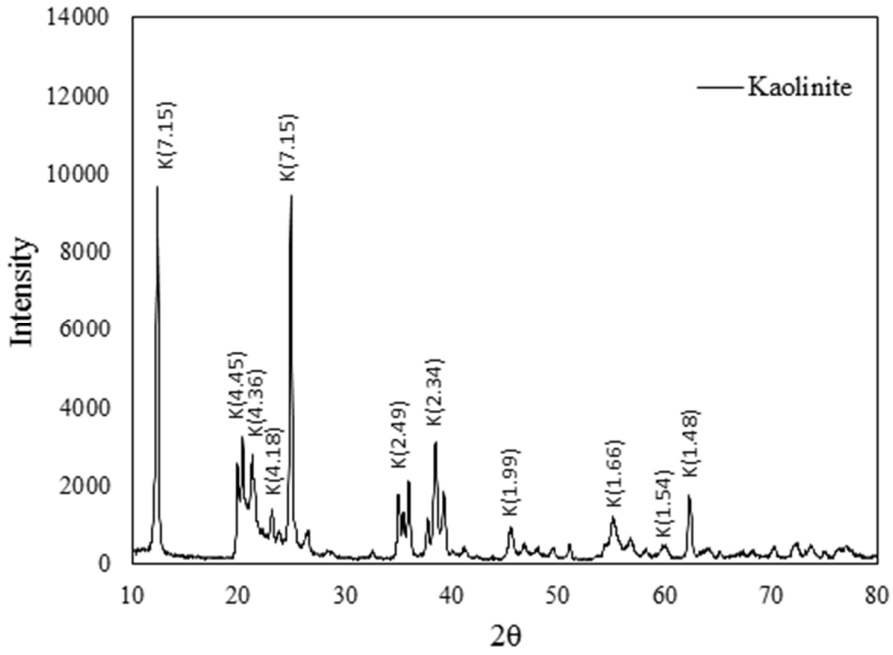

Fig. 3.1. XRD pattern of the studied kaolin

3.3.5 *Specific Surface Area and Cation Exchange Capacity*

Specific surface areas (SSA) of the soil specimens passing through 425-µm sieve were determined using ethylene glycol mono-ethyl ether (EGME) retention procedure (Cerato and Lutenegger 2002) on four duplicate samples. The average values were reported in Table 3.3 (Yagom et al. 2017). The cation exchange capacity (CEC) of the soils were determined using the standard procedure (Chapman 1965; Ross 1995). A 25 g of oven dried samples, 425-micron passing was washed thoroughly with 250 mL of 1 M ammonium acetate solution at pH 7.0 (Chapman 1965). The Washing was done in an orbital shaker (Borg lab shaker) for four hours and allow to stand for overnight. The supernatant solution was extracted by centrifugation for 3–4 min at 1000 rpm for the determination of individual exchangeable cation concentration. The individual exchangeable cation concentration in the extracted solution was determined the major cations (i.e., Na^+, Ca^{2+}, K^+, and

Mg^{2+}) using the flame photometer and atomic adsorption spectroscopy. The total CEC was used from the summation of all the individual cations. The average data obtained from three trials were reported in Table 3.3 (Yagom et al. 2017).

Table 3.3. Details of soils used in the present study

Property	Kaolin	B1	B2
Particle size distribution (%)			
Fine Sand (%)	-	3.79	1.39
Silt size (%)	28	27.48	20.18
Clay size (%)	72	68.73	78.43
Specific Gravity, (G_s)	2.6	2.76	2.77
Consistency limits (%)			
Liquid limit, w_{LL}	40	296	393
Plastic limit, w_{PL}	32	46	50
Shrinkage limit, w_{SL}	28	14	18
Specific Surface Area (m^2/g)	11.69	376	495
Total Cation Exchange Capacity (meq/100 g)	5	55.2	71.7
Classification	ML	CH	CH
Montmorillonite content	-	42	55

Table 3.4. Properties of the bentonites from literature

Sl. No.	Soil type	Sp. Gravity	Liquid limit (%)	Plastic Limit (%)	SSA (m^2/g)	CEC (meq/100 g)
1	MX80	2.76	411±10	47, 70	562	110.4
2	K-1	2.79	-	-	810[#]	73.2
3	K-3	2.8	-	-	-	-
4	Montigel	2.85	130±3	50	493	62
5	S1	2.8	178.0	56.1	650.0	74.0
6	Calcigel-2	2.78	-	-	-	-
7	GMZ-EXE	2.78	-	-	-	-

8	GMZ-1	2.71	276	37	570	78.3
9	Volclay	2.84	-	-	-	100.7
10	Kunibond	2.71	-	-	810[#]	79.6
11	GMZ-Na	2.71	276	37	-	76
12	GMZ-Ca	2.725	99	41	-	83
13	SB1	2.79	-	-	-	-
14	SB2	2.79	-	-	-	-
15	SB3	2.78	-	-	-	-
16	SB4	2.78	-	-	-	-
17	SB5	2.75	-	-	-	-

[#] *Specific surface area of montmorillonite mineral*

The most important aspect of studies related to the volume change behavior of unsaturated clays is the measurement of collapse potential, swelling pressure, swell potential, and suction of clay sample. With this in view, this chapter deals with a concise overview, working principle, and testing methodology of the instruments used in the present study for collapse potential, swelling pressure, and suction measurement of the clayey soils.

The behavior of kaolin was studied by conducting sedimentation test and collapse potential test according to section 3.4 and 3.5. Sedimentation test was conducted to study the settling behavior of kaolin in different pore fluid medium and the mode of particle association. The collapse potential test was carried in compacted sample to understand the collapse nature. The details of the testing methodlogy was described in the following sections.

3.4 Sedimentation test

The IS 2720-40 (IS 1977) test methodology was used to conduct sedimentation tests in this work. A 10 g specimen of an oven-dry soil fraction passing through a 425 μm sieve size was thoroughly mixed with water in a 100 mL measuring jar to create a clay suspension for the sedimentation tests (Bharat and Das 2017). The clay-solution suspension in the jar was stirred thoroughly and the clay particles were allowed to settle under the influence of gravity without any disturbance. The sediment volume (cm^3 or mL) was monitored regularly until an equilibrium volume was achieved. The sediment volume was read on the measuring cylinder using the grading divisions

against the soil–water interface. The equilibrium time varied from a few hours to several days depending on the electrolyte properties. The room temperature varied between 24 and 28 °C during the test. The final sediment volume was visually recorded to an accuracy of 0.5 mL. Three independent tests using duplicate samples for each test showed that the reported equilibrium sediment volume data were reproducible. The equilibrium sediment volume (cm^3/g or mL/g) was finally reported in terms of sediment volume per initial dry mass (i.e., 10 g). The ASTM D5890 (ASTM 2003) methodology for swell index of clay mineral component of geosynthetic clay liners is similar to the adopted procedure. This ASTM methodology suggests adding a 2 g specimen of minimum 65% passing through a 75 μm sieve and 100% passing through a 150 μm sieve to the distilled water and allowing it to reach equilibrium for 16 h. However, 10 g of kaolin was used in this work (where 100% of the soil fraction was passing through a 75 μm sieve) for accurate measurement of sediment volume as kaolin is a nonexpansive clay.

3.5 Collapse test

Kaolin specimens were statically compacted at air-dry state in consolidation rings to an initial dry density of 1.25 Mg/m^3. The air-dry (hygroscopic) water content of the kaolin was 3%. A collar was placed on top of the ring and a plunger was inserted after placing a pre-calculated amount of specimen for the static compaction. A proving ring was attached to the plunger to estimate the compaction-induced stresses in the specimen. The static compaction load was measured to be 3.6 MPa to achieve a dry density of 1.25 Mg/m^3. The ring with the compacted specimen was placed in the oedometer to carry out single-oedometer testing (ASTM 2003, 2014) for estimating the collapse potential under different inundation pressures (IPs). The procedure is similar to the standard test procedure followed for studying the wetting induced collapse behavior of soils (Jennings and Knight 1957; Clemence and Finbarr 1981; ASTM 2003 2014). The test method consisted of compressing the clay specimen at hygroscopic moisture content in a consolidometer by subjecting the specimen to incremental loads and inundating the specimen using different solvents at a predefined vertical stress to induce the collapse. The collapse estimation of wetting-induced collapsible soils in the single oedometer test set-up is illustrated in Fig. 3.2. The compression of an air-dry specimen under different normal pressures is represented by line a–b. The collapse strain resulting from the inundation at a normal pressure of

400 kPa is shown by line b–c. The consolidation behavior of an inundated (saturated) specimen is represented by line c–d. As the collapse behavior of kaolin was the subject of the present interest, only the volume change due to inundation (line b–c) was estimated in terms of collapse potential using different inundation fluids and analyzed. The collapse potential under a given inundation pressure was estimated by (ASTM 2003; Medero et al. 2003)

$$Pc = \frac{\Delta e}{1+e_0} \times 100 \qquad (3.1)$$

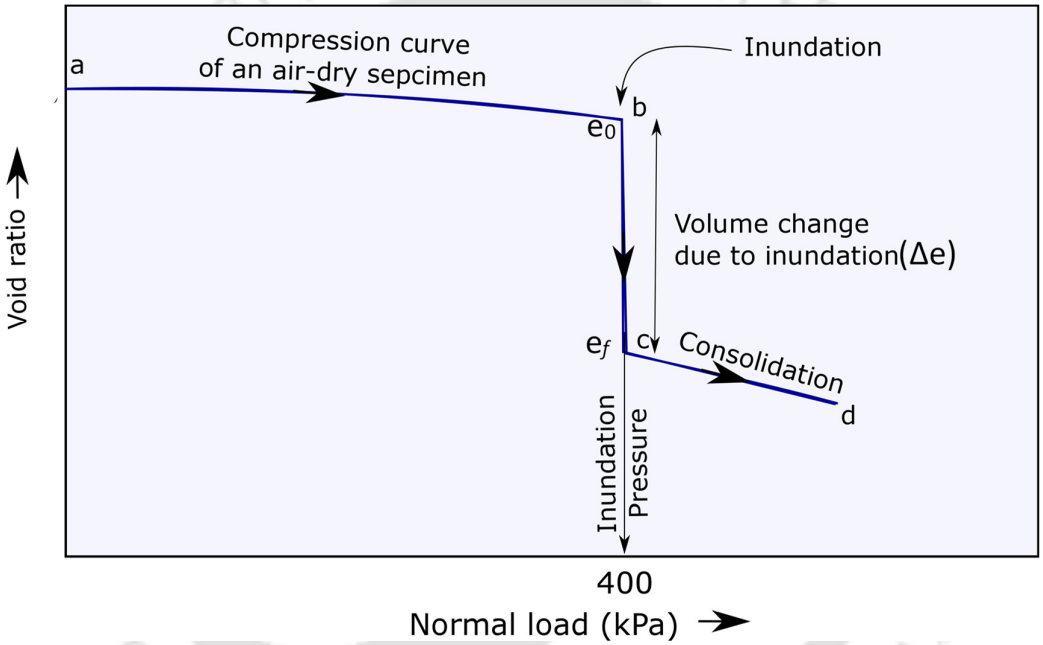

Fig. 3.2 Illustration of collapse potential determination in single oedometer test

3.6 Swelling behavior of bentonite

The swelling behavior of bentonite was studied by conducting swelling pressure test on compacted bentonite sample. The swelling pressure was measure by modifying the conventional consolidation mould into smaller size to reduce the time of the experiments. The consolidation mould reduced to 38 mm diameter, therefore reducing the area of the sample specimen. The new mould can be used for measuring higher swelling pressure in less amount of time. The sample preparation and measurement methodology was discussed in detailed in the next section.

3.6.1 Measurement of swelling pressure

The swelling characteristics with time at five different initial compaction densities viz., 1.2, 1.45, 1.65, 1.8, and 2.0 Mg/m^3 were measured for these bentonites using isochoric swelling pressure test. The air–dry bentonite powder was compacted using the displacement–controlled uniaxial compaction method by raising the specimen in oedometer ring against firmly placed proving ring at a constant speed to the desired dry density. The compacted specimens with final thickness of 15 mm and 38 mm diameter were placed in oedometer rings by placing two oven-dried filter papers and porous stones on bottom and top of the compacted specimen. A cover plate was placed on top of the porous stone for the uniform load distribution. A reservoir was connected to the specimen for wetting the bentonite specimen and for the development of swelling pressure. The swelling pressure of the bentonite specimen was continuously recorded by the data logger attached to the load cell. The temporal variation of swelling pressure for different bentonites and initial compaction densities were reported for understanding the swelling characteristics.

The influence of compaction density and bentonite plasticity on the development of swelling pressure was analyzed by understanding the changes to the pore size distribution (PSD) and the clay fabric during the swelling pressure development. The PSDs and fabric of the bentonite specimens under the influence of different hydro-mechanical loads were obtained by Mercury Intrusion Porosimetry (MIP) and Field Emission Scanning Electron Microscope (FESEM).

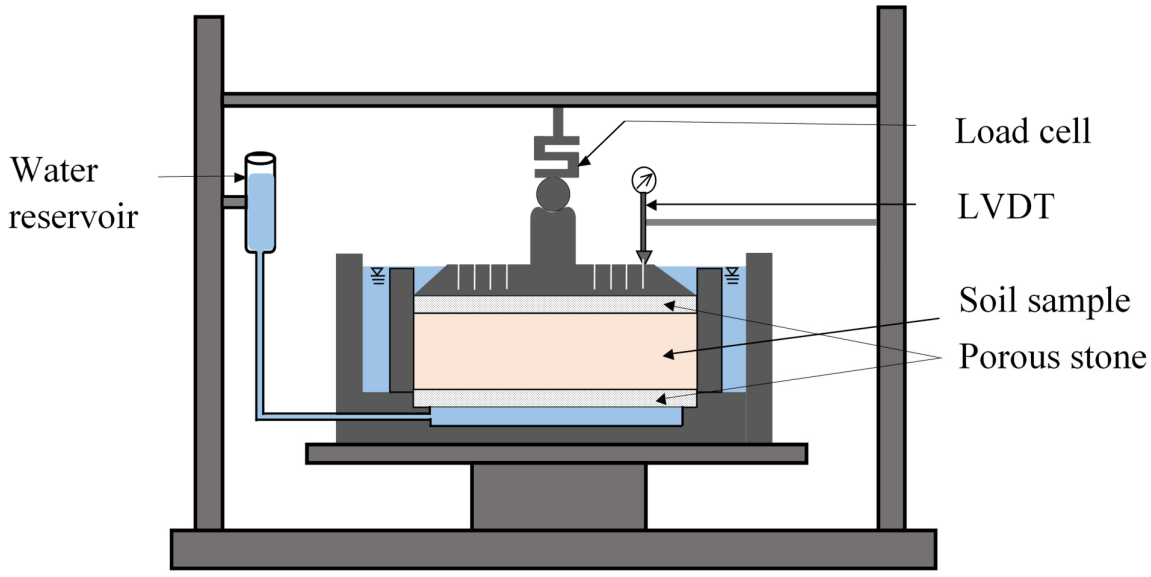

Fig. 3.3 Illustration of constant volume swelling pressure test set-up

3.7 Theoretical estimation of swelling pressure

The theoretical swelling pressure–dry density curves for the studied bentonites were obtained in this study using GC theory. The theoretical estimation is very essential as it reduces the time and effort of the experimental work. The GC theory is described in the following section.

3.7.1 Estimation of swelling pressure by GC theory

Gouy – Chapman (GC) DDL theory (Guoy 1910; Chapman 1913) is most widely used model for the estimation of compressibility and swelling behavior of expansive clays such as bentonites (Bolt 1956; Komine and Ogata 1996; Komine and Ogata 2003; Tripathy et al. 2004; Schanz and Tripathy 2009; Bharat et al. 2013; Bharat and Sridharan 2015a). The GC theory combines two well-known equations known as Poisson equation and Boltzmann equation that express the variation of electrostatic potential with distance between the clay platelets and the relationship between ion distribution and electric potential, respectively (Reddi and Inyang 2001). Combining these equations with the Langmuir's equation facilitates the determination of osmotic pressure between the clay platelets. The swelling pressure is the difference between the osmotic pressure at the central plane between the clay platelets and the osmotic pressure in the equilibrium solution (Bolt 1956). The swelling behavior of clayey soil depends on physicochemical interaction between the mineral surfaces and the surrounding pore-fluid. Useful theoretical equations for relating the osmotic pressure and the void ratio for different clay–water–electrolyte interactions in compacted clayey soils are given by (Verwey and Overbeek, 1948; van Olphen 1977; Sridharan and Jayadeva, 1982; Bharat et al., 2013; Bharat and Sridharan, 2015a; Bolt 1956):

$$\rho_d = \frac{G_s \rho_w}{1 + G_s \rho_w S d} \tag{3.3}$$

$$kd = -\int_z^u \left(2\cosh(y) - 2\cosh(u)\right)^{-1/2} dy \tag{3.4}$$

$$\left(\frac{dy}{d\xi}\right)_{x=0} = -\frac{C}{S}\sqrt{\frac{2\pi}{\varepsilon n K T}} \tag{3.5}$$

$$\left(\frac{dy}{d\xi}\right)_{x=0} = -\left(2\cosh(z) - 2\cosh(u)\right)^{1/2} \tag{3.6}$$

$$P = 2nRT\left(\cosh u - 1\right) \tag{3.7}$$

where, ρ_d is the dry density of clay (Mg/m^3), G_s is the specific gravity of clay, S is the specific surface area of soil (m^2/g), C is the cation exchange capacity (meq/100 g), d is the mid-plane distance for the interacting clay plates, P is the swelling pressure (kPa), G is the specific gravity of soil particles, T is the absolute temperature, ρ_w is the density of water (Mg/m^3), R is the universal gas constant, u the scaled mid-plane potential of the interacting clay plates ($u = ve'\phi_d / KT$), y is the scaled potential at any distance, x, from the clay surface, z is the scaled potential at the clay surface ($ve'\phi_0 / KT$), ξ is the scaled distance (κx), $1/\kappa$ is the Debye length (Bharat and Sridharan 2015b) in which $\kappa = \sqrt{\frac{8\pi e'^2 v^2 n}{\varepsilon KT}}$, e' is the elementary electric charge, v is the cation valence, n is ion concentration in the bulk fluid, ε is the dielectric constant, and KT is the thermal energy per ion. Swelling pressure determination using Langmuir's Eq. (3.7) requires an inverse analysis and solution of an elliptical integral of Eq. (3.4). Many approaches (Verwey and Overbeek 1948; Van Olphen 1977; Sridharan and Jayadeva 1982; Bharat et al. 2013) are available to circumvent this problem. Bharat et al. (2013) approach for the estimation of osmotic potential and void ratio relationship is found to be simple and accurate (Haase and Schanz 2016; Puppala et al. 2017). In this approach, an empirical relationship between mid-plane potentials of the interacting clay-water-electrolyte system and electrostatic potential of non-interacting diffuse system is utilized for the estimation of mid-plane potential. The mid-plane potential is then estimated using

$$\phi_d = -6.24\times10^{-4}\phi_{x=d}^2 + 1.205\phi_{x=d} + 8.582 \tag{3.8}$$

Where, $\phi_{x=d}$ the electric potential of a non-interacting plate at a distance, x, equals to the half-space distance d and is given by

$$\phi_{x=d} = \frac{2RT}{vF}\ln\left(\frac{\exp(\xi) + \tanh\left(\frac{z}{4}\right)}{\exp(\xi) - \tanh\left(\frac{z}{4}\right)}\right) \tag{3.9}$$

where F is the Faraday constant. The theoretical swelling pressure–dry density curves for different bentonites were obtained in this study using this approach.

3.8 Study of pore size distribution of compacted sample

After obtaining the swelling pressure data from swelling pressure test, the results were further analysed using mercury intrusion porosimeter (MIP) results done on the same compacted sample. The MIP data gives an insight of the pore size distribution of soil. The MIP data was obtained for each and every stages of swelling and for different compaction densities of bentonite B1 and B2.

3.8.1 *Mercury Intrusion Porosimeter*

The bentonite specimens were carefully extruded from the rings using the sample extruder, with minimal disturbance. The specimens were then freeze-dried (Choudhury and Bharat 2017) using the Lyophilizer (LabconcoFreeZone®) at −60° C for freezing the pore water and changing the water phase to gas phase by sublimation process that offers a minimal disturbance to the fabric of the compacted specimen. A representative freeze–dried specimen of size 5 mm containing a large surface area of the sample volume used for the MIP testing. The PSDs of the freeze-dried specimens were determined using Pascal 140–440 porosimeter (Thermo Scientific®), which is capable of measuring the pore sizes from 100 μm to 3 nm, by increasing the pressure from vacuum to 414 MPa. The size of the pores that mercury penetrates at different pressure steps calculated from the Washburn equation which is given by

$$P = \frac{4T_s \cos\theta}{d} \tag{3.2}$$

where d is the pore diameter, T_s is the surface tension, θ is the contact angle, and P is the applied pressure. The volume change of mercury under each pressure increment provides the pore size distribution of the specimen (Dhandapani and Santhanam 2017). The differential pore volume with respect to the pore diameter indicates critical pore sizes of the system.

3.9 Study of soil fabric

This part deals with the study of soil fabric of powder/compacted kaolin and bentonites used in the study. The instrument used in this study was FESEM sigma 300. The working principle of the instrument was discussed in the next section.

3.9.1 Field emission scanning electron microscope

The fabric of the compacted sample studied under FESEM sigma 300 instrument. FESEM produces clearer, less electrostatically distorted images with high spatial resolution less to 1 nm. FESEM gives improved spatial resolution and minimized sample charging damage to the sample as the field–emission cathode in the electron gun of the instrument provides narrower probing beams at low as well as high electron energy.

3.10 Study of shrinkage behavior of slurried soil

The shrinkage behavior of slurried soil samples was studied from volumetric shrinkage curve (VSC), which is a relationship between the specimen volume and the corresponding water content. Accurate measurement of VSC data is important for accurate determination of the unsaturated soil characteristics (Wijaya et al., 2015). The details of the measurement technique used in the study to measure volumetric shrinkage curve are discussed below.

3.10.1 Measurement of volumetric shrinkage curve

The shrinkage property of the studied sample was measured using direct volume measurement technique. This method was initially proposed for low plastic soil (Péron et al. 2009; Saleh-Mbemba et al. 2016). The test set-up consists of a rectangular box (shrinkage mould), made up of a perspex glass plate (Fig. 3.4). The dimension of the shrinkage mould is 200 mm x 30 mm x 10 mm. The soil samples were prepared with water content equal to 1.2 times of liquid limit water content. The soils were thoroughly mixed with water and transferred into a sealed plastic bag and kept in a desiccator for seven days for moisture equilibration. The prepared soil samples were filled in the shrinkage box in three layers with a gentle tapping on the side during the placement to remove any entrapped air bubbles. The excess soil sample was removed by carefully trimming the top surface with the help of a spatula. The

initial water content was measured for each specimen by carefully weighing the mould with the soil sample on the scale. The initial volume of the sample was equal to the mould volume. After initial measurement, the shrinkage box was kept laboratory condition for air drying. With the elapsed time, the volume of the specimen will slowly reduce, as the water will evaporate due to drying. The volume of the specimen was calculated by measuring the specimen dimensions at frequent time intervals. The weight of the specimen was also obtained at the same time to establish volumetric shrinkage behavior of different clayey soils.

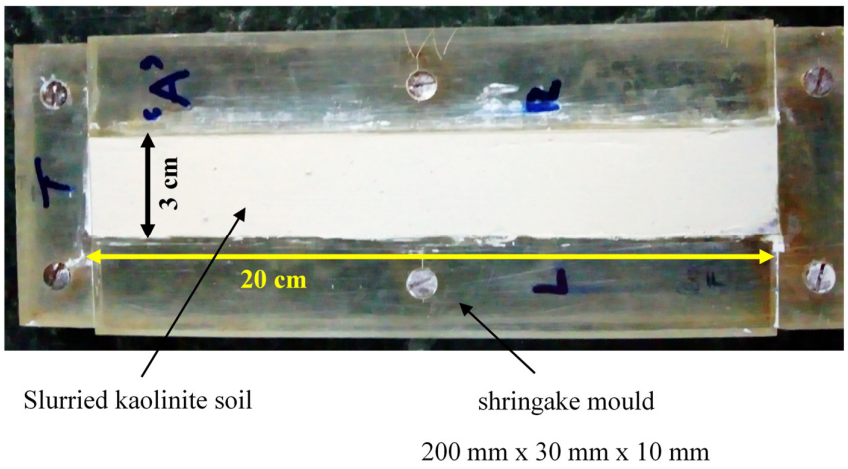

Fig. 3.4 Shrinkage box with the specimen at the initial state

3.11 Measurement of suction for slurried soil

This part will cover all the measurement techniques that were used to measure the SWCC of slurried clayey soil. The understanding of the effect of SWCC on soil behavior is an important aspect from an engineering point of view. The knowledge of SWCC is the first and foremost thing for any unsaturated soil.

The SWCC data of the slurried sample were established using three different techniques independently namely, osmotic technique, method of vapor equilibrium, and vapor pressure measurement technique. The soils specimen were prepared similar to the direct volume measurement technique as discussed in the previous paragraph. The soils were thoroughly mixed with water equal to the 1.2 time liquid limit and transferred in sealed plastic bags. The plastic bags were then put in a closed container and kept 7 days for moisture equilibration prior to the test.

3.11.1 *Osmotic technique*

In the osmotic technique, the specimens were wrapped in a semi-permeable membrane, having molecular weight cut-off (MWCO) value of 14,000, and placed in polyethylene glycol (PEG) solution having an average molecular weight of 6000 and 20,000. The membrane restricts the large sized PEG molecules to enter into the sample by allowing only water to flow through it. There will be an osmotic flow of soil pore water into the PEG solution takes place until the equilibrium. Once both clay specimen and the PEG solution are equal come to equilibrium, i.e., the chemical potentials will be same on both sides, the flow ceases. The concentration of the PEG solution was monitored by measuring the refractive index using a handheld refractometer in 24 hours interval of time to estimate the equilibration time. Based on the soil specimen the equilibration time varied from 10 to 14 days. The gravimetric water content of the clay specimen was estimated using oven drying method (ASTM D2216–10, 2010). The matric suction corresponding to measured concentrations of the PEG 20000 was estimated using the standard calibration curve (Delage et al. 1998). This technique was used to obtain SWCC data for a suction range of 20–1600 kPa.

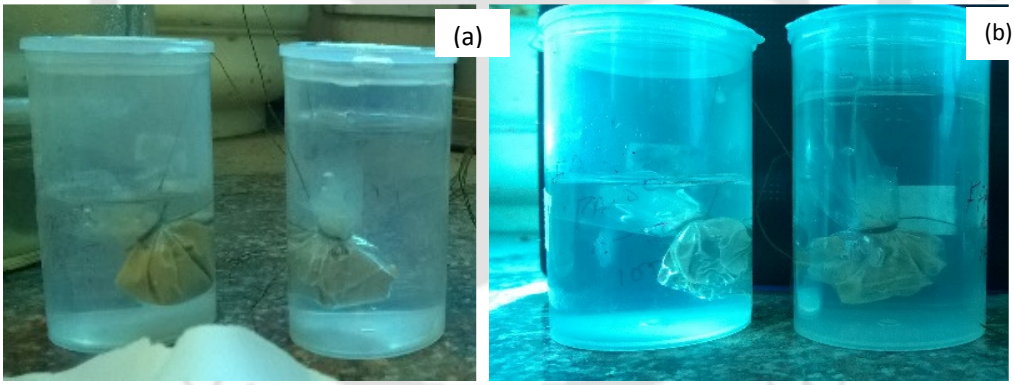

Fig. 3.5. Osmotic test where the slurried clayey soil wrapped in the semipermeable membrane and kept in PEG solution for (a) 1 day (b) 14 day (equilibrium)

3.11.2 *Method of vapor equilibrium*

Saturated salt solutions are generally used in the vapor equilibrium technique. Soil samples were put in a desiccator totally closed and the samples being supported by a rigid grid, which contained a given saturated saline solution at the bottom. Fig. 3.6 shows a schematic view of the experimental setup. The soil samples were brought to equilibrium under different humidity environments. The relative humidity of the

closed containers was regularly monitored using calibrated RH measuring hygrometers. The saturated solutions of KNO_3, KCl, NaCl, K_2CO_3, and LiCl, were used in the glass containers to apply suctions of 7.5, 21.9, 38.2, 114.1, and 296.7 MPa respectively (ASTM E104-02, 2012).

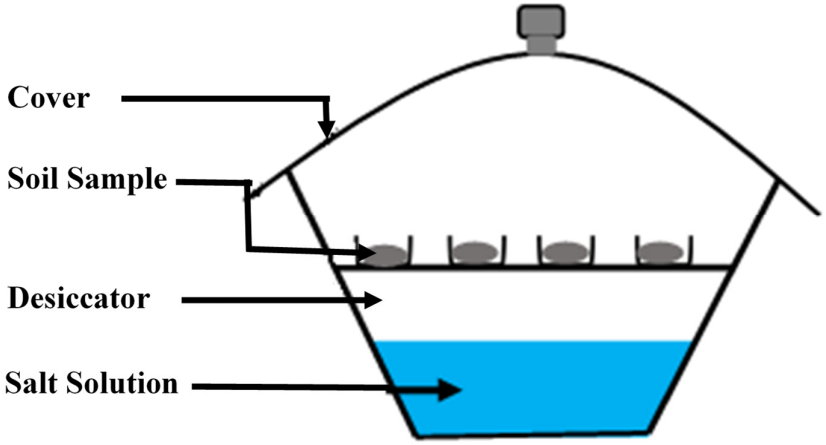

Fig. 3.6. Illustration showing for vapor equilibrium method for suction controlled SWCC test

3.11.3 *Vapour pressure measurement technique*

In this technique, the saturated soil specimens were placed in a plastic container, the volume of approximately 15 cm^3. The thickness of the soil specimens was approximately 5 mm. The saturated specimens were kept for air-drying under the laboratory conditions. After different drying periods, the samples were placed inside the closed chamber and allowed to thermodynamically equilibrate with the chamber environment. The vapor pressure above the soil specimen in the chamber and the saturated vapor pressure at the same temperature are computed using the dew-point and specimen temperatures, respectively. The software internal to the WP4-T device automatically performed the calculation of total suction from the measured vapor pressure. The WP4-T provides excellent results in the high suction range device to measure suction reduces the time and costs associated with suction measurements in the high suction range.

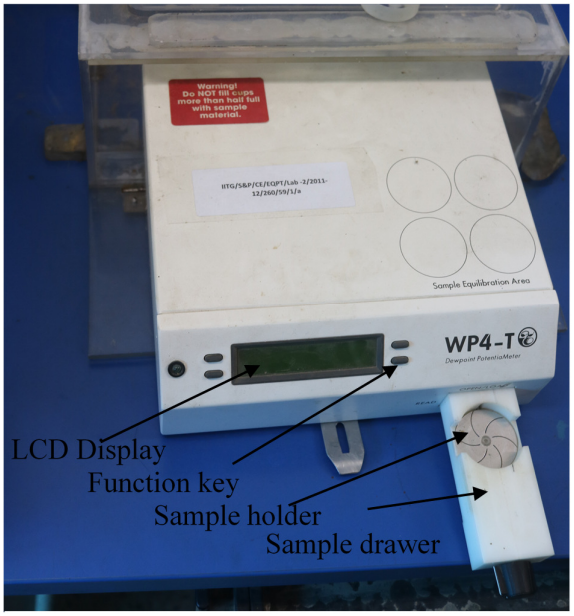

Fig. 3.7. Dew point potentiometer for vapor pressure measurement technique

3.12 Suction Control Test

This part focused on the measurement of the SWCC for compacted soil for different dry densities and loading conditions. A series of suction control swelling pressure and collapse test were carried out on compacted kaolin and bentonite samples to measure the SWCCs undergoing wetting conditions. The uniqueness of the soil water retention behavior was examined and provided the basis or deducing the representative SSCC from the SWCC. Collapse test of kaolin and swelling pressure test of the bentonites were conducted for different suction ranges conduction suction controlled test. The collapse potential of kaolin was measured for suction 37-1108 kPa and swelling pressure was measured for suction 1-4500 kPa. The osmotic technique was used for controlling the matric suction.

3.12.1 *Suction Control Collapse potential test Test*

A series of collapse test of kaolin were conducted for a dry density of 1.25 Mg/m^3 under controlled suction condition by using osmotic technique. The sample preparation forthe controlled suction test was similar to the collapse test. The similar test set-up of collapse test was used to do the suction-controlled collapse test. The collapse potential for each suction was calculated from the dial gauge attached to the top cover plate of the oedometer cell. The collapse potential was measured three

inundation pressure such as 100 kPa, 400 kPa, and 800 kPa. The semipermeable membrane molecular weight cut–off (MWCO) value of 14,000 was placed between the sample and the bottom porous stone. After placing the sample the vertical pressure was applied in increment to reach the predetermined pressure. Once the sample comes to equilibrium under the vertical pressure, the polyethylene glycol (PEG) solution having an average molecular weight of 20,000 was supplied from the bottom of the oedometer cell as shown in Fig. 3.8. The membrane restricts the large-sized PEG molecules to enter into the sample. Therefore, the osmotic flow will take place from PEG solution into soil sample until the equilibrium. Due to the osmotic flow, the collapse will take place which can be observed from the dial gauge reading. The changes in suction were monitored by measuring the refraction index after a definite time interval of 24 hours. At equilibrium, there will no changes in the concentration of PEG solution as well in the dial gauge reading. The equilibration time generally varied from 10 to 14 days for different specimens. Once the sample reaches equilibrium, the sample was extruded carefully from the consolidation mould for water content determination. The gravimetric water content of the clay specimen was estimated using oven drying method (ASTM D2216–10, 2010) and the concentration of the PEG solution was determined using the optical refractometer (Delage et al. 1998). The matric suction corresponding to measured concentrations of the 20000 was estimated using the standard calibration curve (Delage et al. 1998).

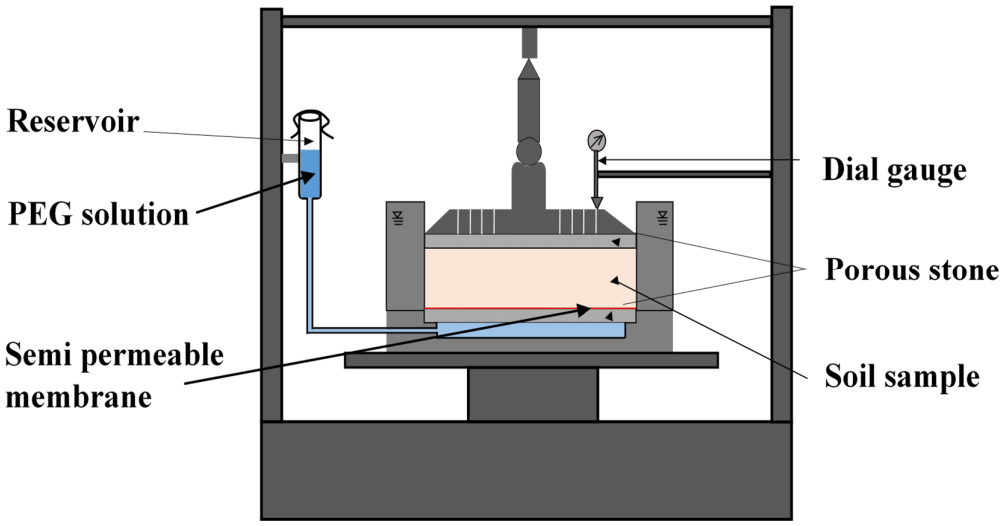

Fig. 3.8. Illustration of single oedometer test set-up for suction controlled collapse test

3.12.2 *Suction Control Swelling pressure test*

The test setup for suction control swelling pressure test was similar to the laboratory swelling pressure test. In the suction control technique, a semi–permeable membrane placed between the bottom porous stone and the compacted specimen as shown in Fig. 3.9. The molecular weight cut–off (MWCO) value of 1500 and 14,000. The polyethylene glycol (PEG) solution having an average molecular weight of 6000 and 20,000 were supplied from the bottom of the oedometer cell (Fig. 3.9). The membrane acts as a filter for the large sized PEG molecules to enter into the sample. Therefore, the osmotic flow of soil pore water into the PEG solution continues until the equilibrium. Due to the osmotic flow, the soil sample will exert swelling pressure. The flow of water ceases when equilibrium chemical potentials of both clay specimen and the PEG solution are equal. The swelling pressure corresponding to the equilibrium will be considered as the final swelling pressure. The changes in the concentration of the PEG solution was monitored to estimate the equilibration time. The equilibration time varied from 10 to 14 days for different specimens. Once the sample reaches equilibrium, the sample was extruded carefully from the consolidation mould for water content determination. The gravimetric water content of the clay specimen was estimated using oven drying method (ASTM D2216–10, 2010) and the concentration of the PEG solution was determined using the optical refractometer (Delage et al. 1998). The matric suction corresponding to measured concentrations of the PEG 6000 and 20000 was estimated using the standard calibration curve (Delage et al. 1998). Using this technique, the SWCC data was obtained for a suction range of 20–9000 kPa.

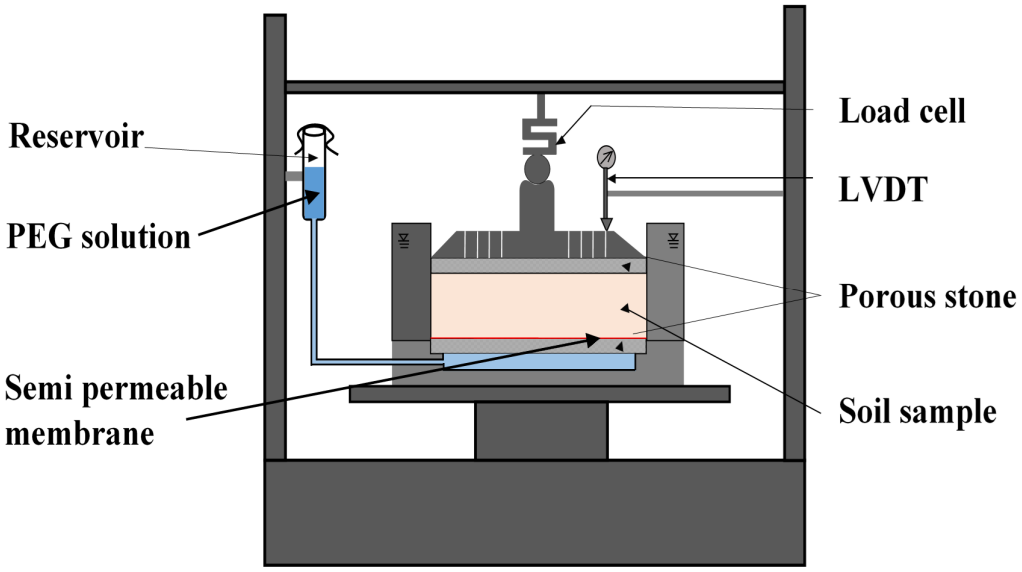

Fig. 3.9. Illustration showing swelling pressure measurement test set-up under controlled suction and isochoric condition

CONCLUDING REMARKS

In this chapter, the procedures adopted for determining the basic physical properties of soils, such as the particle size distribution, the liquid limit, the plastic limit, the compaction characteristics, the field density, the natural moisture content, and the specific gravity were described. The specimen preparation conditions and experimental methods for various tests were explained in detail. The procedures adopted for measuring the collapse potential of Kaolin soil under mechanical loading were described. Similarly, the procedures adopted for measuring the swelling pressure of bentonite for different compaction condition were presented in detail. The measurement of shrinkage limit and suction for slurried soils were presented. The method of conduction single oedometer test and swelling pressure test under controlled suction were discussed in detail. The suction controlled test was conducted up to a maximum of 14 days due to the limitation associated with the semipermeable membrane.

CHAPTER 4

WETTING-INDUCED COLLAPSE BEHAVIOR OF KAOLIN: INFLUENCE OF FABRIC AND INUNDATION PRESSURE

4.1 GENERAL

A series of sedimentation tests over a pH range of 3–8 was conducted to study the variation in equilibrium sediment volume data with pH of the bulk solution. The pH of the clay solutions was adjusted using 0.1 mol/L concentration of NaOH and 0.1 mol/L HCl solutions. The pH of the clay suspensions in sediment volume tests was monitored using a pH meter. The IEP_{edge} was determined from the equilibrium sediment volume data to analyze the influence of pH-dependent charges on the kaolin behavior (Lyklema 1995; Israelachvili 2011). As mentioned earlier, the IEP is the pH value of a pore fluid at which the electrophoretic mobility of the clay particle is zero.

Three different pH solutions (3.1, 6.1, and 8), two different electrolyte concentrations (0.1 and 0.01 mol/L NaCl), and different dielectric solutions were used for studying the effect of fabric on the sedimentation behavior. Different ethanol/water mixtures and kerosene were used to vary the dielectric properties of the pore medium. The dielectric constants of the pore fluids were measured using a 5TM water content and temperature probe (Decagon Devices, Inc.). The probe uses an oscillator to measure the dielectric permittivity of the medium. The measured dielectric constant data of different dielectric pore fluids are reported in Table 4.1.

Table 4.1. Measured dielectric constant data for different pore fluids

Pore-fluid	Dielectric constant, ε
Distilled water	77.8
Mixture1 (25% ethanol + 75% water)	60.28
Mixture2 (50% ethanol + 50% water)	45.32
Mixture3 (75% ethanol + 25% water)	33.04

Ethanol	20.1
Kerosene	2.78

4.2 SEDIMENTATION RATE AND EQUILIBRIUM VOLUME

The measured equilibrium sediment volume (ESV) data over a wide pH range are shown in Fig. 4.1. The ESV data decreased with increase in pH from 3.1 to 5.6 and the decrease in volume with pH became insignificant with further increase in pH. The fabric of the kaolin changed abruptly from flocculated to dispersed beyond pH = 5.3, indicating the development of a negative charge on the edge. The IEP_{edge} was thus estimated to be 5.3. A more accurate estimation of IEP_{edge} may require the measurement of ESV data between 5.3 and 5.6. As IEP_{edge} is used to understand qualitative behavior of kaolin at pH < IEP_{edge} and pH > IEP_{edge}, the obtained accuracy was acceptable. The estimated IEP_{edge} was consistent with earlier work on untreated kaolin (Braggs et al. 1994) and the colloidal nature of the kaolin mineral (Gupta 2011).

The influence of pH, NaCl concentration, and dielectric constant on the time rate of sedimentation was studied. The pH of the solution became altered from the targeted value during the sedimentation phase due to reaction between the particle surface and the pore fluid. The pH values, therefore, were adjusted to the targeted values in the sedimentation tests. The effect of pH on the sedimentation rate is shown in Fig. 4.2 for different pH solutions while electrolyte concentration was adjusted to 0.001 mol/L. After some initial time, a sharp interface formed, for pH = 3.1, at the top of the sediment between clear solution and the kaolin. This interface followed a linear settling mode with a constant settlement rate for 1 day and reached equilibrium after which the settlement ceased completely. The linear settling mode with a distinct and unique interface in kaolinwas observed when the particle association was flocculated. The observed mode of particle association was EF as the pH of the solution was below IEP_{edge}. Two distinct interfaces (AB and CD in Fig. 4.3) were noted in the case where pH > IEP_{edge}. After some initial time, a sharp interface, AB, developed between the clear solution and clay dispersion at the top of the cylinder. This interface settled at a constant velocity. The dispersion at the base of the cylinder, however, settled into a high and this interface, CD, propagated upwards with a steady velocity. The two interfaces moved towards each other with steady velocity as illustrated in Fig. 4.3. The interfaces merged into a distinct

and unique interface after achieving the equilibrium in the case of pH = 6.1. The volume of sediment did not change

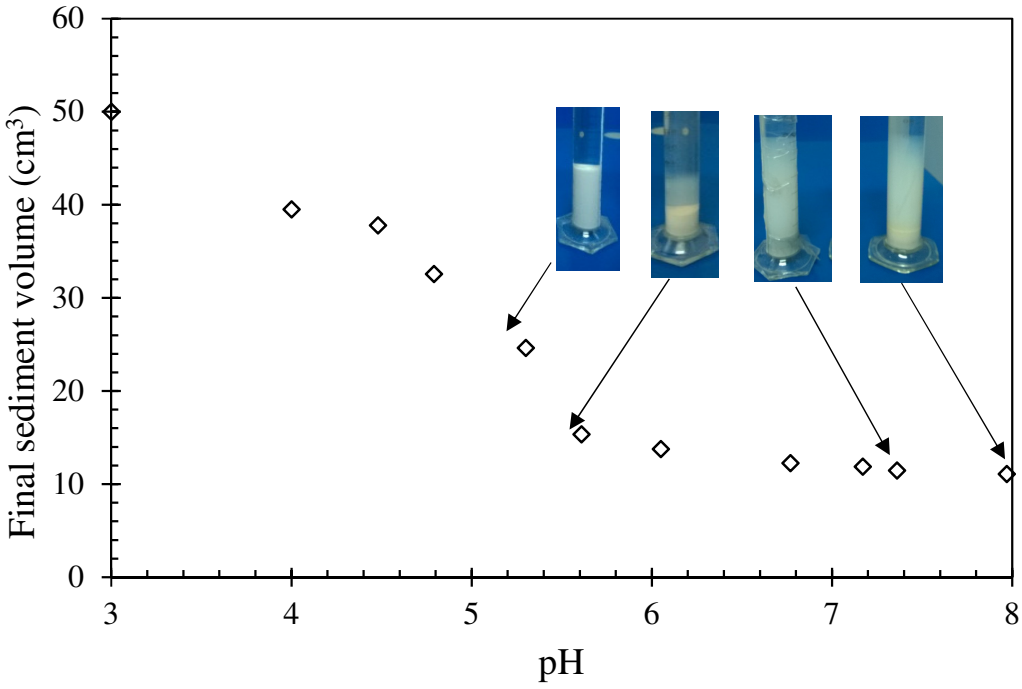

Fig. 4.1. Estimation of IEP_{edge} from equilibrium sediment volume data

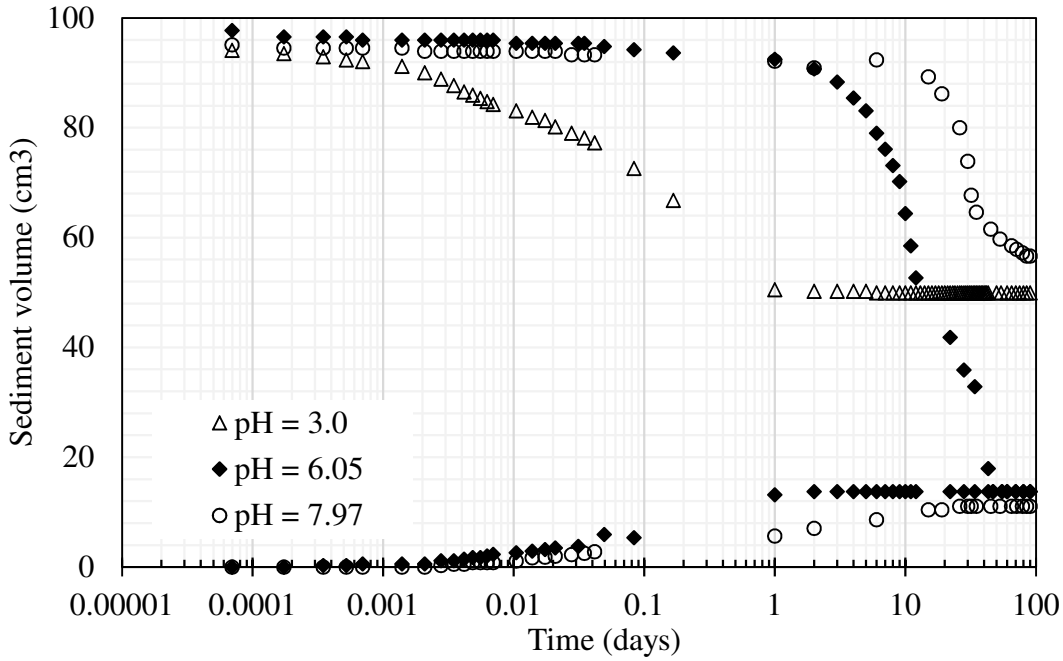

Fig. 4.2. Settlement behavior of kaolin soil in the presence of different pH solutions (n = 0.001 mol/L NaCl)

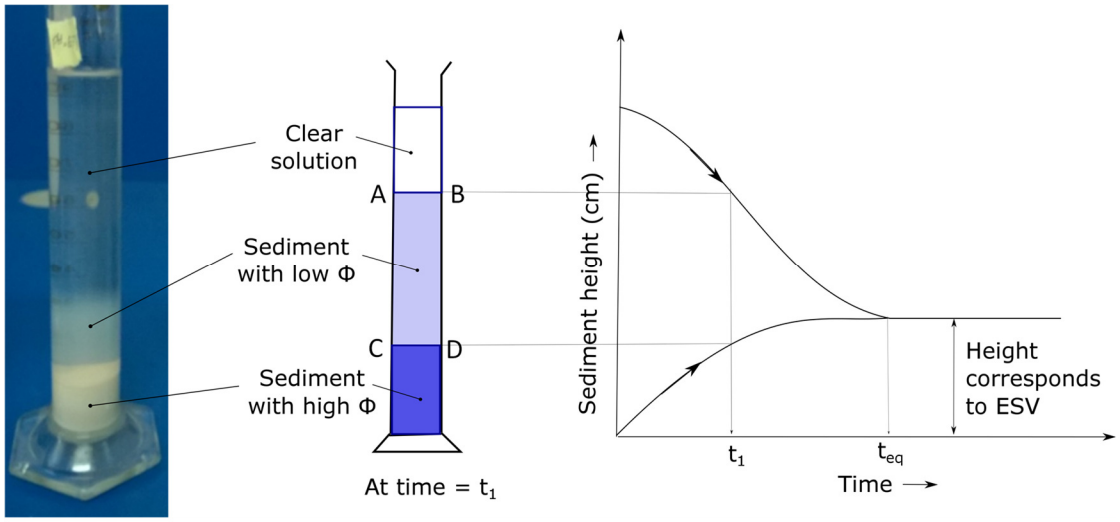

Fig. 4.3. Illustration of sedimentation behavior of kaolin in dispersed particle association

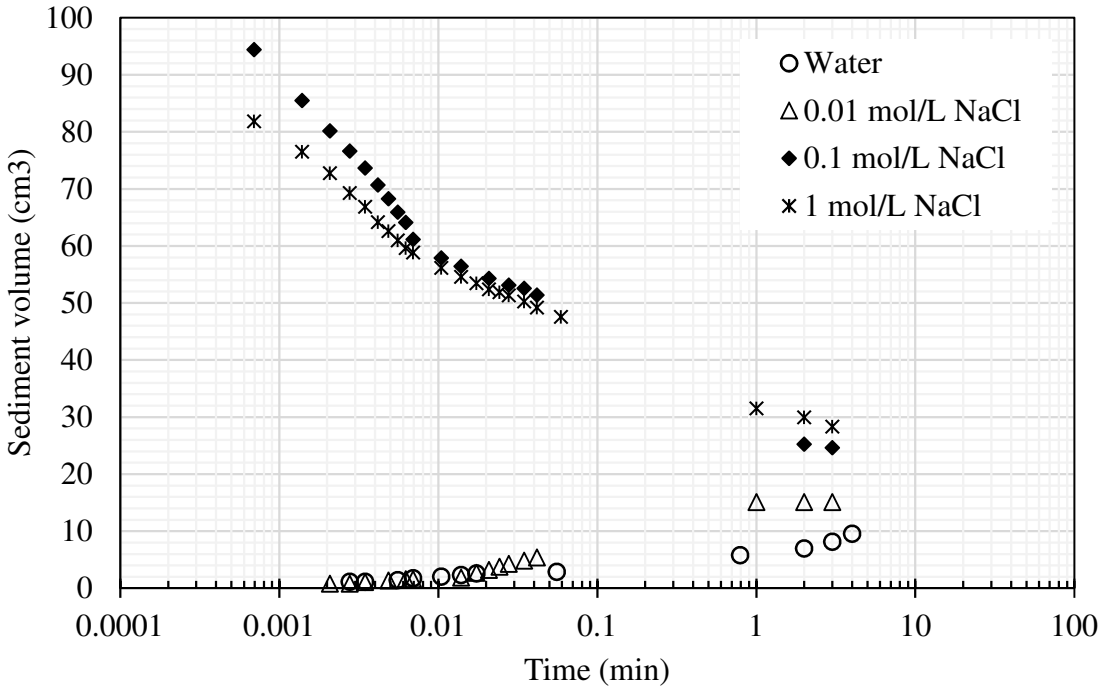

Fig. 4.4. Settlement behavior of kaolin at different salt concentrations

after this equilibrium time. The time rate of change of these two interfaces for pH = 6.1 in terms of sediment volume is shown in Fig. 4.2. However, the top interface did not merge with the bottom interface with further increase in pH of the pore fluid even when time, t > 90 days, as shown in Fig. 4.2. As the volume of the sediment contributed by the dispersed suspension (between AB and CD) is insignificant after reaching the steady state, the volume corresponding to the lower interface, CD, alone was considered for estimating the equilibrium sediment volume after the lower interface reached steady state. Therefore, sediment volume based on the upper interface, AB, was not shown for the other dispersed cases where these interfaces did not merge. The settlement behavior at pH > IEP_{edge} was in accordance with the observation made by Wang and Siu (2006a) for a dispersed system due to the presence of negative charges on both edge and face surfaces of the particle. The time rate of sediment volume showed an increase in volume with time when the particle association was dispersed, but decreased with time when the particle association was flocculated. The rate of change in sediment volume with time in the presence of different salt concentrations is shown in Fig. 4.4. The pH of the solutions in these tests varied between 6 and 7. The sediment volume increased with time in the case of water and 0.01 mol/L NaCl solution by exhibiting a dispersed mode of particle association. In contrast, the particle association was flocculated in the presence of higher salt concentrations

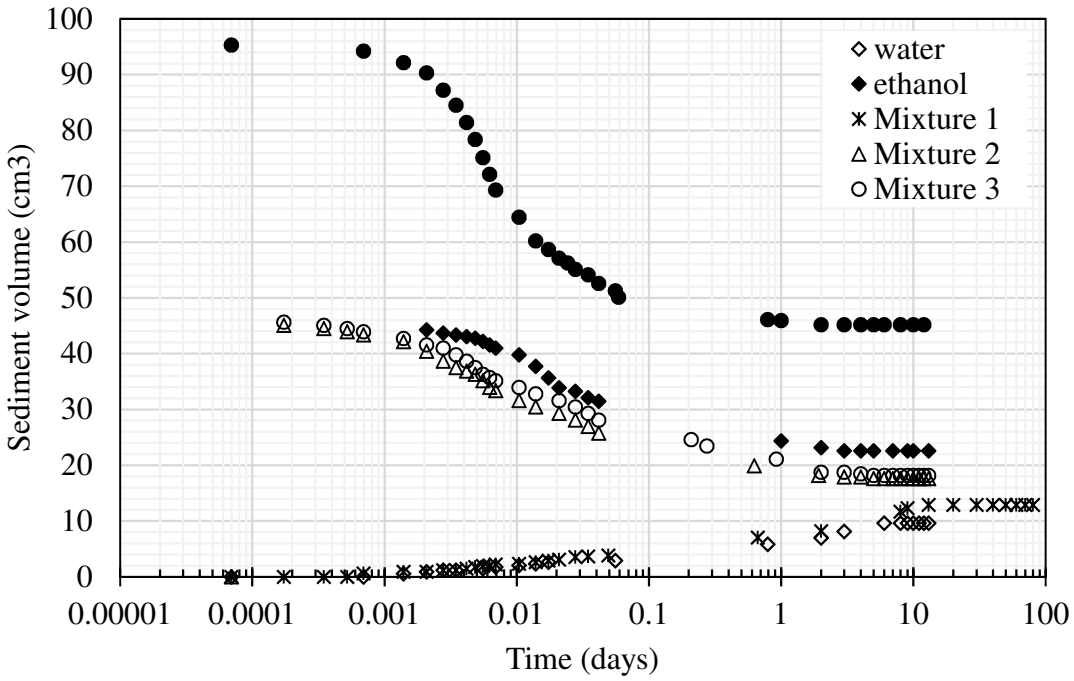

Fig. 4.5. Settlement behavior of kaolin in the presence of different dielectric solvents

(n = 0.1 and 1 mol/L), which was evident from the decrease in sediment volume with time. The particle association at different electrolyte concentrations is in agreement with the earlier observations (Palomino and Santamarina 2005) where it is concluded that the kaolin behavior is pH-dependent at low ionic concentrations, but is pH independent at higher electrolyte concentrations. The influence of the dielectric constant, on the settlement rate is shown in Fig. 4.5. The sediment volume decreased with time in the presence of kerosene and ethanol, but a small and insignificant percentage of clay was in a dispersed state even after equilibrium, in the case of ethanol. The mode of particle association in the presence of kerosene was flocculated, but was considered to be mixed mode (combination of FF and EF) in the case of ethanol. The particle association was also mixed in the presence of mixture 3 and mixture2. However, the particle association changed to dispersed in the presence of mixture1 (25% ethanol : 75% water). The particle association, therefore, changed from dispersed to mixed and mixed to flocculated with the decrease in as observed in the settlement behavior. The ESV data of kaolin in different pore fluids are presented in Table 3. The ESV was lowest in the presence of distilled water where the clay was in a dispersed arrangement as the pH of the

suspension was 6.46 (>IEP_{edge}). The ESV value was highest in the presence of kerosene (= 2.78) and pH = 3.1 (where background concentration, n = 0.001 mol/L NaCl) as the mode of particle association was EF, which was evident from the settlement behavior. The increase in pH, at low salt concentration (n = 0.001 mol/L), decreased the sediment volume five fold due to the change in particle association from EF to dispersed. The sediment volume behavior was pH-dependent at this salt concentration. The sediment volume in the presence of 0.01 mol/L NaCl was slightly higher than the observed data in the presence of water as the observed mode of particle association in water was dispersed. The higher sediment volume due to disperesed particle association at a salt concentration of 0.01 mol/L NaCl is consistent with the settlement rate shown in Fig. 10 and earlier observations (Rand and Melton 1977; Nicol and Hunter 1970; Michaels and Bolger 1962). The particle association at low ionic concentration and moderate pH (i.e., 0.01 mol/L NaCl and pH = 7.21 in the present study) was, therefore, dispersed. The sediment volume at 0.1 mol/L NaCl concentration was significantly higher than the observed value at 0.01 mol/L, indicating the mode of particle association changed to EF even though the pH was nearly the same. Further increase in the concentration did not significantly influence the volume as the particle association remained the same. However, a slight decrease in the sediment volume with concentration was observed, which can be attributed to the increase in face-to-face aggregation due to double-layer thinning and subsequent dominance of van der Waals attractive forces (Schofield and Samson 1954; Rand and Melton 1977). The decrease in the dielectric constant from 77.8 (for water) to 20 (for ethanol) increased the sediment volume several fold due to changes in the particle association from dispersed to mixed mode. The decrease in the dielectric constant from 20 to 2.78, with the replacement of ethanol to kerosene as the pore fluid, increased the sediment volume two fold due to the particle association changing from “mixed” to EF mode. Overall, the equilibrium sediment volume increased with salt concentration up to 0.1 mol/L. The sediment volume decreased with increase in dielectric constant from 2.78 to 77.8 due to alteration in particle association with different dielectric pore fluids. Similarly, sediment volume decreased with increase in pH of the solution from 3.1 (<IEP_{edge}) to 8 (>IEP_{edge}) due to different particle associations.

Table 4.2. Summary of the equilibrium sediment volume data and mode of particle association

Pore-fluid	Equilibrium pH	ε	Equilibrium sediment volume (cm^3/g)	Particle association
0.001 mol/L NaCl	3.05	–	5.0	EF
	6.05	–	1.37	Dispersed
	7.97	–	1.11	Dispersed
0.01 mol/L NaCl	7.21	–	1.46	Dispersed
Water	6.5	77.8	1.05	Dispersed
0.1 mol/L NaCl	7.06	-	2.71	EF
1 mol/L NaCl	6.59	-	2.66	EF
Mixture1	–	60.28	1.29	Dispersed
Mixture2	–	45.32	1.76	Mixed
Mixture3	–	33.04	1.81	Mixed
Ethanol	–	20.1	2.26	Mixed
Kerosene	–	2.78	4.26	EF

4.3 COLLAPSE RATE AND COLLAPSE POTENTIAL

Different pH solutions, dielectric solutions, and salt solutions used in the sedimentation tests were also used in the collapse tests to study the effect of fabric under mechanical stresses. Fabric changes in the clay specimen due to interaction with different pore fluids in the collapse tests were analyzed using a multi-scale approach consisting of scanning electron microscopy (SEM) image analysis on lyophilized specimens and corroborating with IEP_{edge} obtained from sedimentation tests. The specimens for FESEM images were prepared using the following procedure. The compacted clay specimens, before and after the inundation, were obtained by unloading and extracting the specimen from the ring with minimal disturbance. The representative specimens for SEM analysis were obtained using a freeze-drying technique in a Lyophilizer (FreezeDry System, LabconcoFreeZone) at –60 °C

(i.e., using the sublimation process) to preserve the fabric of the specimens. The equilibrium pH of the compacted specimens in the collapse tests was measured by placing a reactive portion of the pH strip (Fisher Scientific) on the specimen to allow the pore fluid to leach onto the paper and comparing the color of the strip with the standard database. The sensitivity of the pH strip was ±0.5.

The particle association in the powder sample was an open, card-house structure (Fig. 4.6) and the formation is due to the presence of different charges on the basal surface and edges (Gupta 2011). Different particle associations were observed with pore fluid interaction due to the difference in IEP of the face and edges.

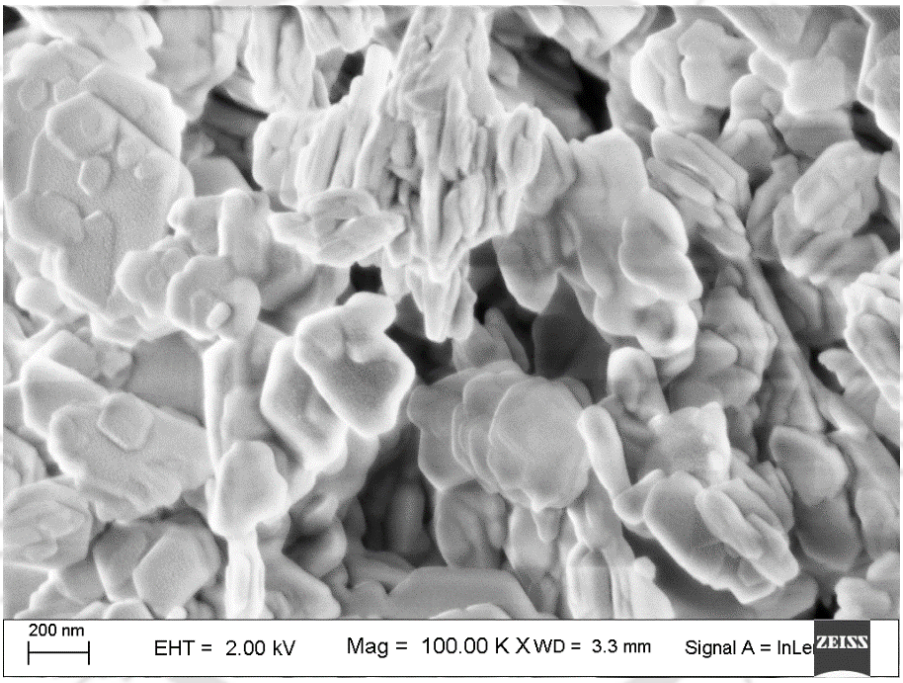

Fig. 4.6. SEM image of kaolin soil in powder form

As the equilibrium specimen volume and settlement rate were altered significantly with the particle association, the volume change behavior of kaolin under the mechanical loads was investigated. Single oedometer tests were performed by inundating the compacted air-dry kaolin specimen with different pore fluids under different normal stresses. The changes in void ratio due to water inundation under different normal stresses are shown in Fig. 4.7a. Compression of the specimen in the air-dried state under the application of loads is shown

with lines; the equilibrium void ratio before and after the inundation is indicated by the symbols. Tests with duplicate specimens were conducted for the

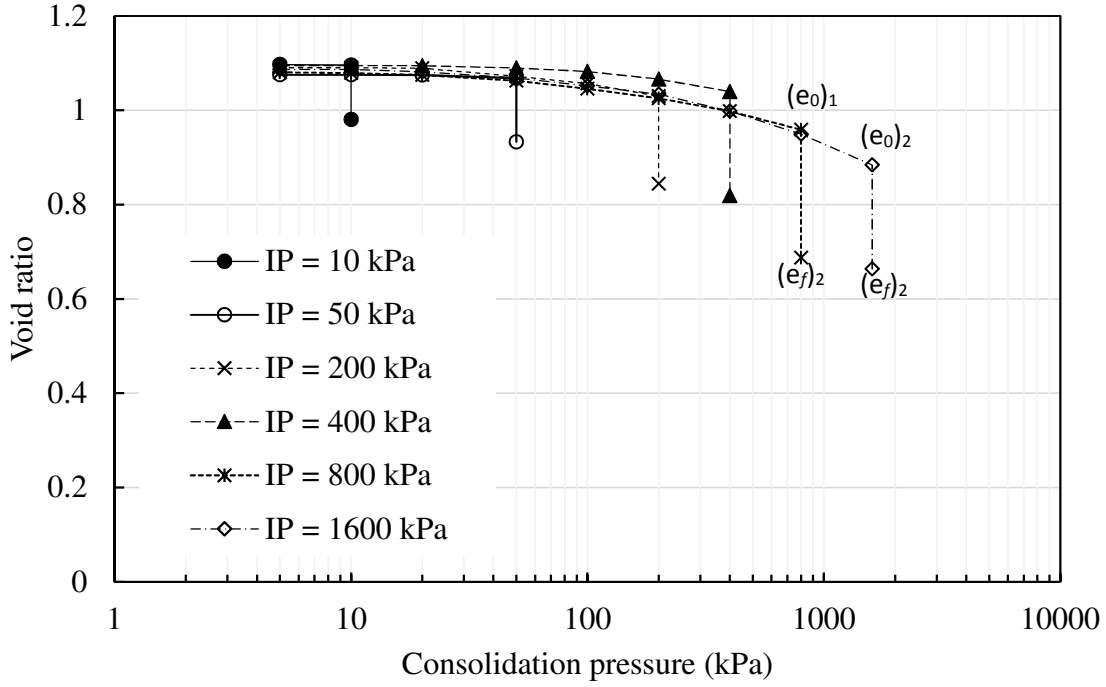

Fig. 4.7a. Compression behavior of kaolinsoil under different inundation pressures using distilled water as the inundation fluid

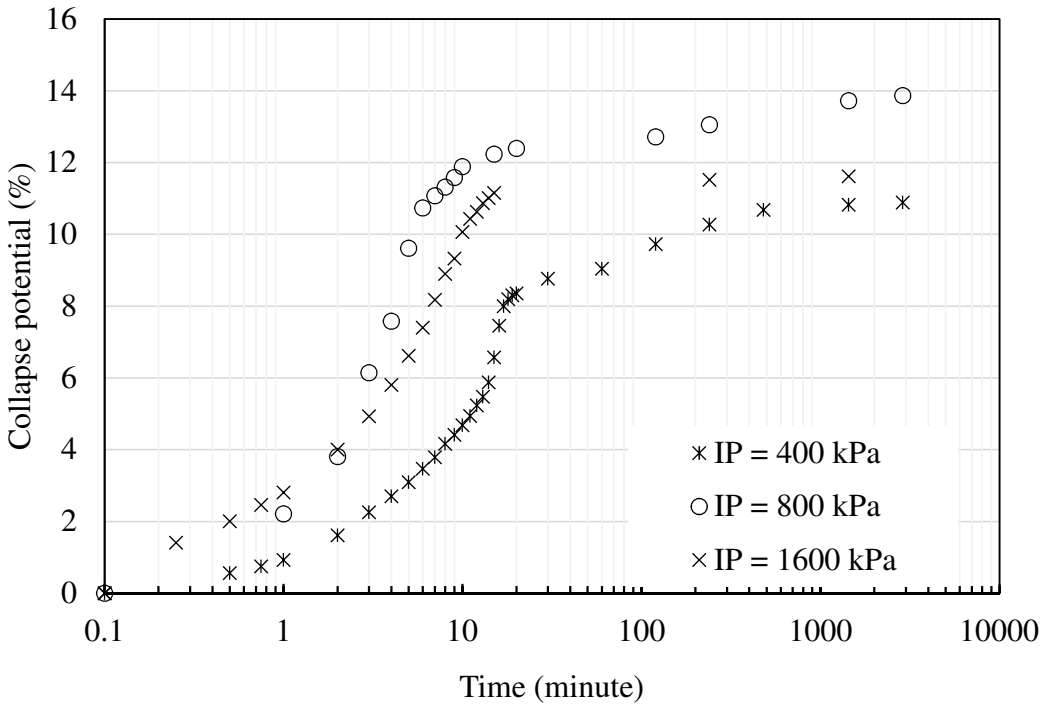

Fig.4.7b. Rate of collapse for different inundation pressures using distilled water as an inundation fluid

determination of equilibrium void ratio under different inundation pressures. The compression curve, in the air-dried state, corresponding to 400 kPa inundation stress deviated slightly from the other compression lines due to slight variation in the initial compaction density. However, this deviation was insignificant in the estimation of volume change due to inundation. The void ratio decreased consistently due to water inundation under different normal stresses indicating the collapse behavior of the soil. The collapse rate due to inundation is shown in Fig. 4.7b as collapse potential versus time under three inundation pressures. The collapse data followed a typical s-shaped curve. The time required for achieving the equilibrium void ratio (or collapse potential) varied from 30 min to 34 h for different inundation pressures. However, the significant amount of collapse settlement took place within 30 min from the beginning of the test. The equilibrium void ratio decreased consistently with the inundation pressures, exhibiting a collapse behavior similar to the loess. The collapse mechanism was studied by measuring the pH of the pore solution and using microscale analysis (i.e., SEM analysis). The inundated specimens were extruded carefully, from the oedometer, after attaining the

equilibrium void ratio and then the pH was measured by placing the pH strips on the saturated specimens. The pH of the specimens varied between 6 and 7 for different inundation pressures. A slight variation in the measured pH under different inundation pressures may be due to the difference in the void ratio (or water content) was different. The SEM images of the compacted, lyophilized specimens before and after water inundation under 400 kPa normal pressure are shown in Figs. 4.8a and 4.8b, respectively. The fabric of the compacted specimen before inundation was similar to the powder specimen (Fig. 4.6) with an open and well-defined card-house structure (Fig. 4.8a). The fabric of the inundated specimen was dispersed due to the presence of water as shown in Fig. 4.8b and as illustrated in the inset of the same figure. The measured pH data of the specimens and sediment data under different pore-fluid environments were well corroborated with the microscale analysis. The face and edge surface charges were negative in this pH range and a dispersed particle association was expected. The volume of the specimen decreased due to chain the particle association from EF (air-dry specimen) to dispersed (after inundation). The volumetric collapse behavior of kaolins was, therefore, due to the fabric changes. The collapse potential of the soil under different inundation pressures is shown in Fig. 4.9. The collapse potential increased with the inundation pressure up to 800 kPa, but decreased beyond that pressure, exhibiting a peak collapse potential at a specific inundation pressure. The peak behavior was also analyzed using the microscale analysis. SEM images of the powder and compacted specimens in the air-dry state (Figs.4.6 and 4.8a) show that the fabric of the kaolin was not affected by the mechanical stresses, which is also evident from the compression behavior of the air-dry specimen (lines in Fig. 4.6). The mechanical stresses only decreased the macrovoids in the specimen by maintaining the EF association between the particles. The particle association changed to dispersed only after the water inundation. The increase in inundation pressure only resulted in bringing the dispersed particles closer to each other in the dispersed fabric and, therefore, increased the collapse with the pressure, as shown in Figs. 4.10a and 4.10b under different inundation pressures. This is evident from the observed particle association under 400 kPa inundation pressure, which was shifted face-to-face as the applied pressure was not sufficient to bring the particles to FF orientation. The particle interaction after water inundation was, therefore, governed by the electrostatic repulsion between the particles. The equilibrium, saturated void ratio, therefore, decreased with the increase in inundation pressure up to 800

kPa. The decrease in equilibrium void ratio with inundation pressure reduced beyond this pressure due to increase in the electrostatic repulsion between the particles. The air-dry specimen volume under normal loads, however, decreased continuously by decreasing the volume of the macropores. The collapse potential, which is represented by the ratio of Δe to $1 + e$ (eq. (1)), decreased beyond 800 kPa due to a significant decrease in Δe with load, while changes in $1/(1 + e_0)$ were insignificant. The decrease in Δe was due to the decrease in e_0 with load, but the final void ratio (e_f) after inundation was insignificant. For example, the void ratios of the specimen before inundation under 800 and 1600 kPa loading were 0.95 and 0.8 (Fig. 4.7a), respectively. The e_f values after the inundation were 0.687 and 0.664 at these loads, respectively. The difference in the ef values under 800 and 1600 kPa loading was insignificant, but the void ratios before the inundations were significantly different. The collapse potential values at these loads were, therefore, 13.4% and 11.7%, respectively. As a result, the maximum collapse potential corresponding to an inundation pressure signifies the lowest void ratio achieved under mechanical stresses by a saturated specimen. The inundation pressure corresponding to the maximum collapse potential was also not related to the maximum applied static compaction pressure, which was 3.6 MPa in this study. The maximum collapse potential was 14%, which is significantly higher than some loess soils (Liu et al. 2016).

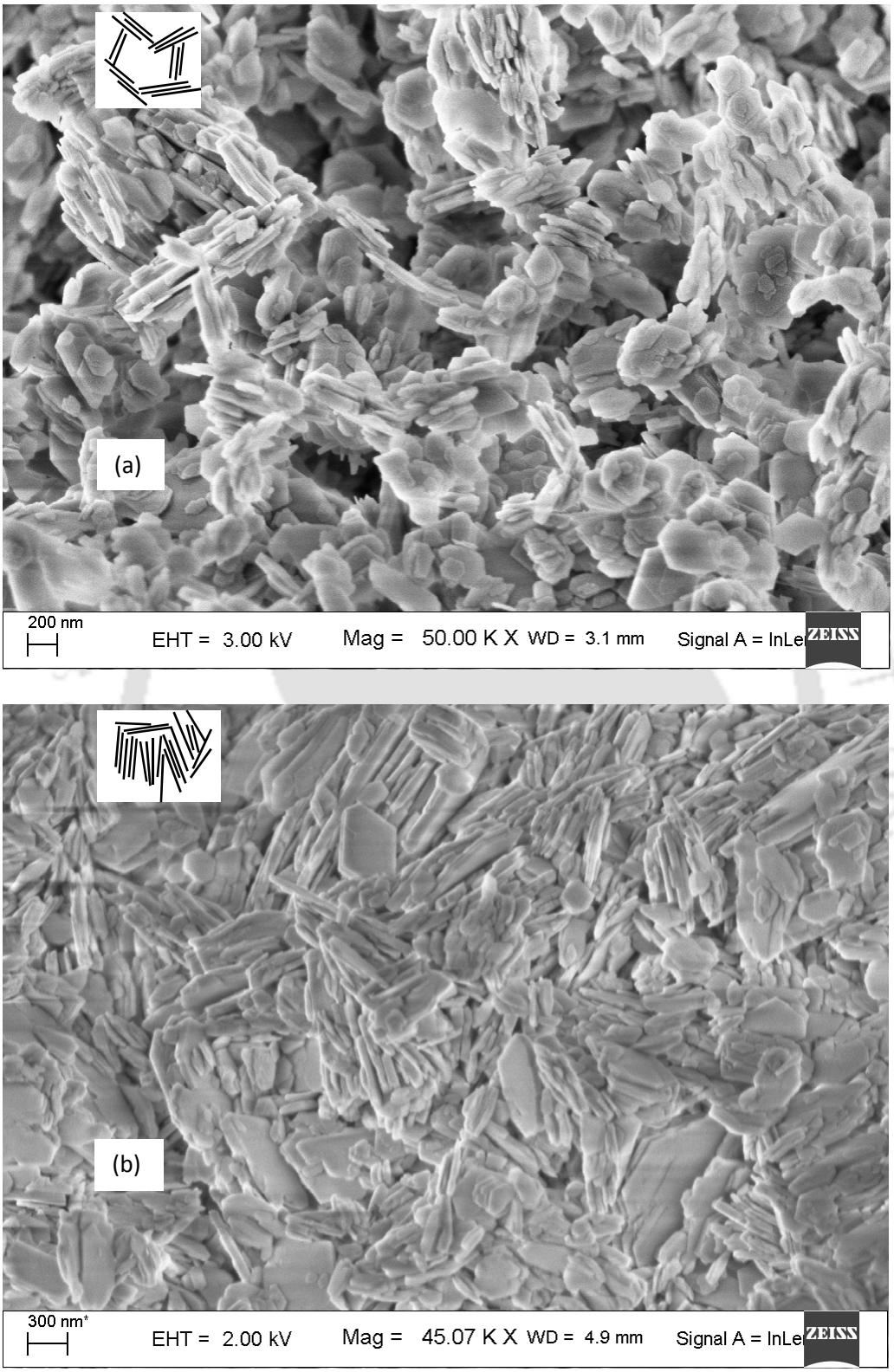

Fig. 4.8. SEM image of compacted specimen under 400 kPa normal pressure (a) before inundation and (b) after inundation

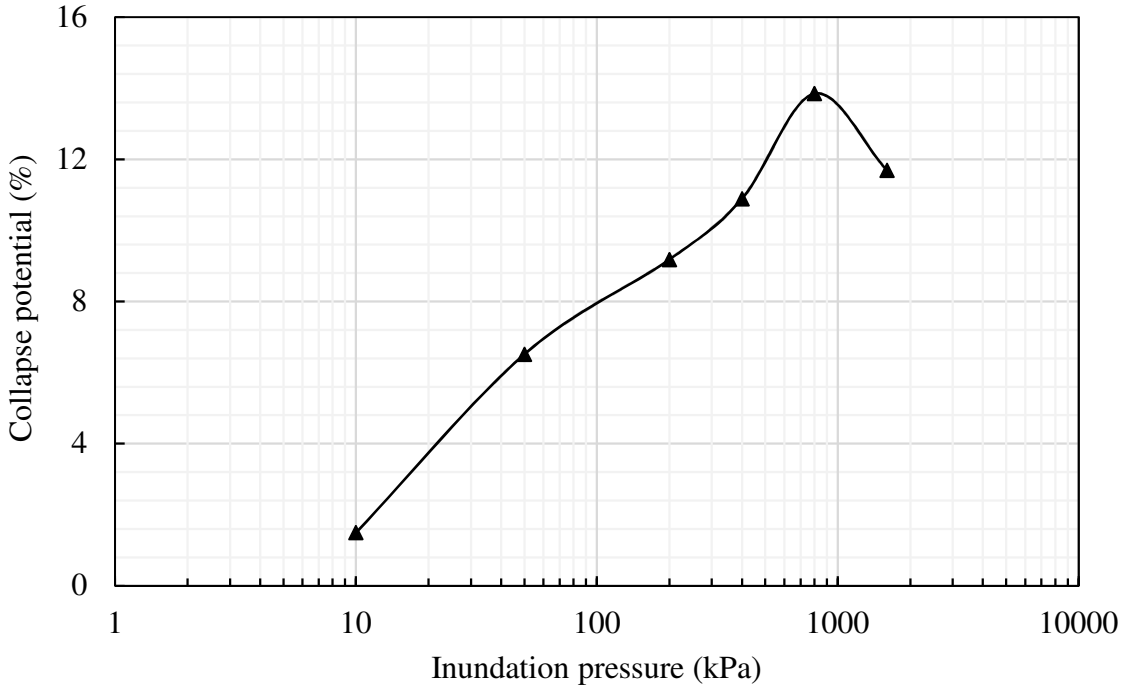

Fig. 4.9. Collapse potential variation with inundation pressure

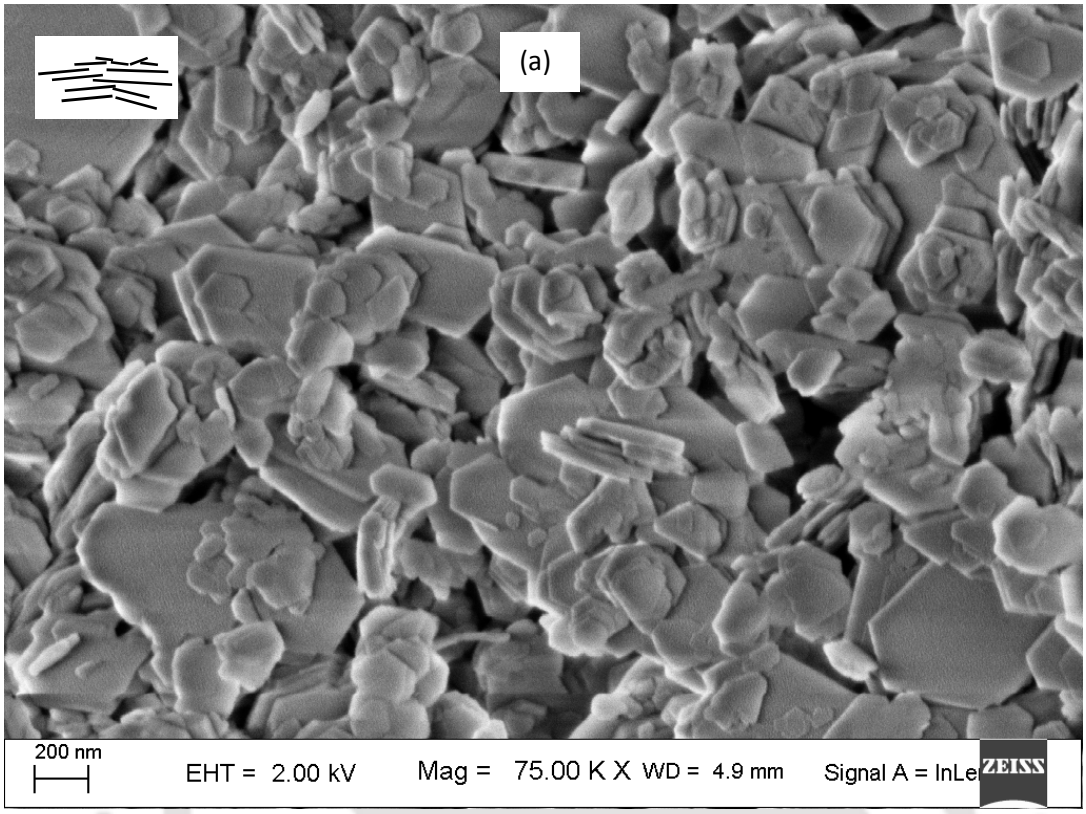

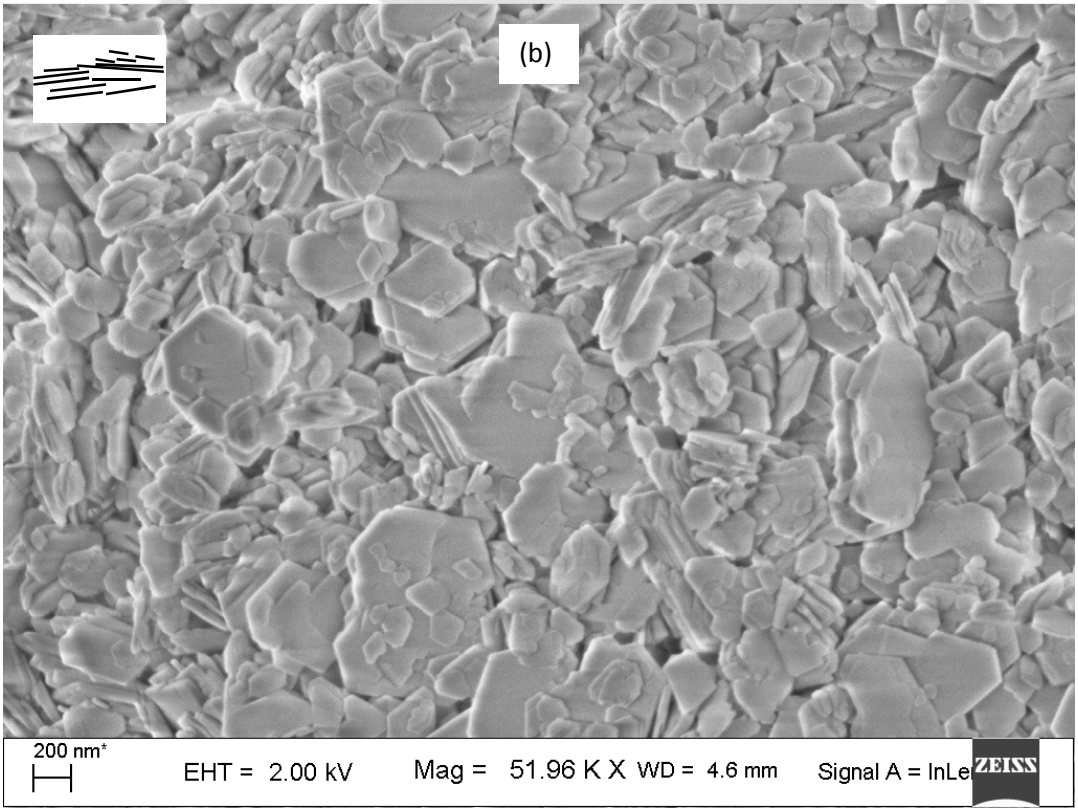

Fig. 4.10. SEM image of compacted specimen at an indundation pressure of (a) 800 kPa and (b) 1600 kPa

As the collapse behavior of kaolin was physicochemical in nature, the effect of different inundation fluids on the collapse potential was also studied. The influence of electrolyte presence on the collapse behavior of kaolin was studied at 0.01 and 0.1 mol/L NaCl concentrations as shown in Figs. 4.11a and 4.11b for different inundation pressures. The collapse behavior of kaolin in the presence of different ionic concentrations was qualitatively similar to the water inundated case, but the magnitude of peak collapse potential and corresponding inundation pressure decreased. The measured pH values varied in the range of 5.5–7.0 (>IEP_{edge}) in spite of wide variation in the targeted pH solutions. The particle association remained, therefore, dispersed due to collapse as inundated with different pH solutions. The equilibrium void ratio became nearly constant after 400 kPa inundation pressure in the presence of both the concentrations (Figs. 4.11a and 4.11b). The magnitude of the collapse potential decreased slightly with the increase in concentration (Table 4.3), which was in accordance with the sediment volume tests data. The influence of pH on the collapse behavior was studied only under 800 kPa inundation pressure, shown in Figs. 4.12 and 4.13 for two different NaCl concentrations. Three different targeted pH solutions were used for a given electrolyte concentration. The measured pH, however, varied between 5.5 and 7, indicating the particle association was dispersed. The collapse rate was similar for all three pH solutions at n = 0.01 mol/L as the measured pH was nearly the same. The collapse potential and collapse rate were not affected by the targeted pH for n = 0.1 mol/L as the soil behavior was pH-independent at higher concentrations. The observations were qualitatively similar with different inundation pressures and, therefore, are not presented. The pH of the pore fluids in the collapse tests could not be controlled unlike the sediment volume tests. The mode of association was dispersed, independent of the targeted pH solution. The influence of the EF particle association on the collapse potential was, therefore, studied by varying the dielectric constant of the pore fluid.

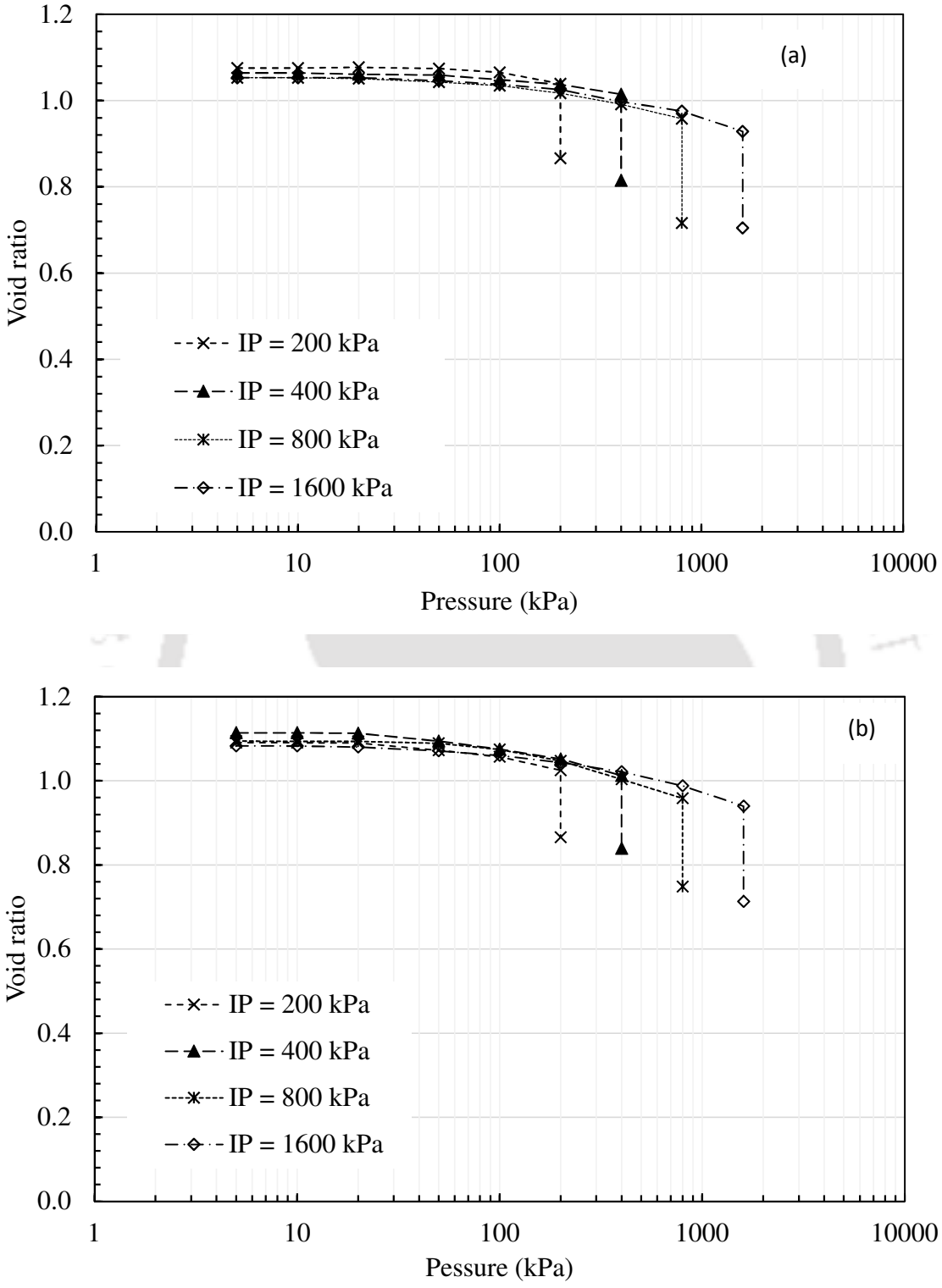

Fig. 4.11. Compression behavior of kaolinunder different inundation pressures using (a) 0.01 mol/L NaCl as inundation fluid and (b) 0.1 mol/L NaCl as inundation fluid

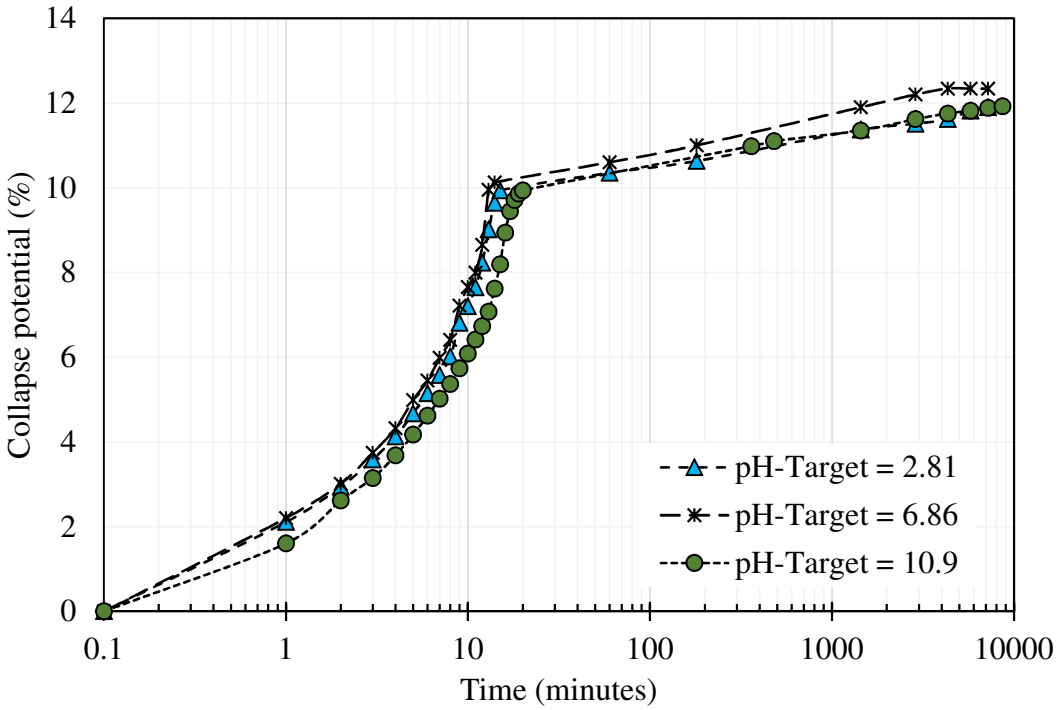

Fig. 4.12. Rate of collapse potential under 800 kPa inundation pressure in the presence of different pH solutions and 0.01 mol/L NaCl electrolyte concentration

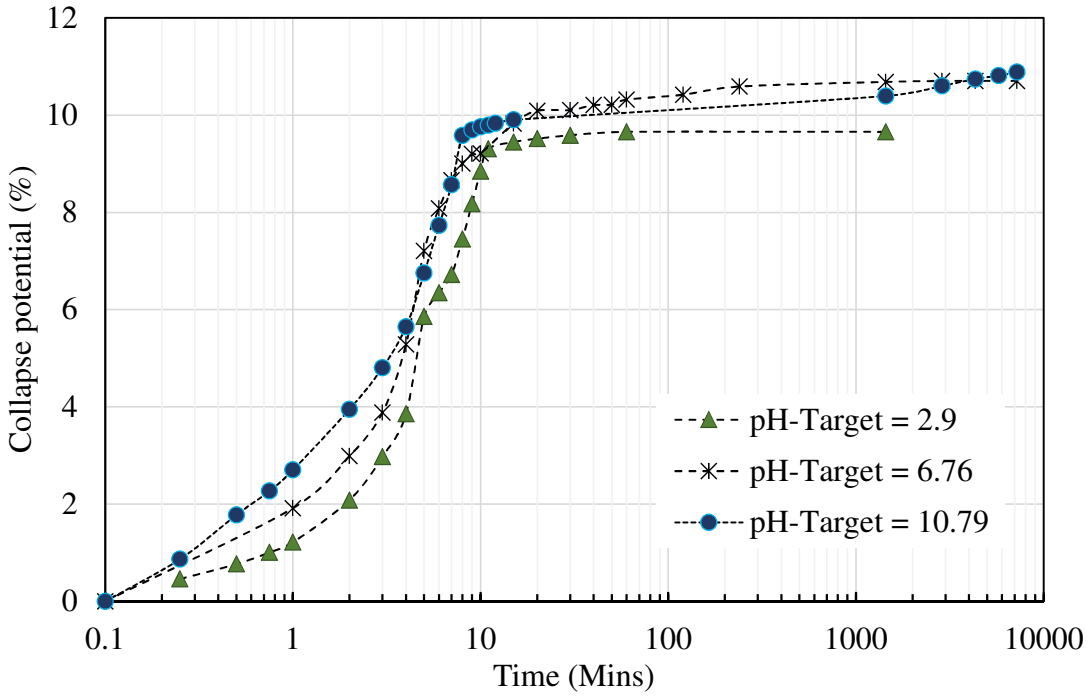

Fig. 4.13. Rate of collapse potential under 800 kPa inundation pressure in the presence of different pH solutions and 0.1 mol/L NaCl electrolyte concentration

The influence of the dielectric constant on the collapse rate and collapse potential of kaolin was studied by inundation with a wide range of dielectric fluids. The collapse rate in the presence of different dielectric fluids under 800 kPa inundation pressure is shown in Fig. 4.14. The collapse potential decreased with the decrease in dielectric constant. Kaolin attained maximum collapse in the presence of water, with = 77.8, and minimum in the presence of kerosene, = 2.78. An insignificant collapse was noticed in the presence of kerosene just after 1 day. The open structure was evident from the FESEM image of the specimen inundated with kerosene under 1600 kPa as shown in Fig. 4.15. As the particle association was EF (or card-house) before the inundation (Fig. 3.1) and after the inundation with kerosene (Fig. 4.15), the collapse was insignificant. The compression behavior of kaolin in the presence of ethanol under three different inundation pressures is shown in Fig. 4.16. The observed collapse was insignificant up to 400 kPa inundation pressure. The dielectric fluid could not change the particle association under lower pressures, but the mechanical load assisted the partial collapse of the structure at higher pressures (≥800 kPa) in the presence of ethanol. The FESEM image of the post-inundation compacted specimen under 800 kPa inundation pressure in Fig. 4.17 shows that the van der Waals forces were still dominant (due to low dielectric constant) and the card house structure existed with larger macrovoids. The collapse potential data under different inundation pressures in the presence of different pore fluids are given in Fig. 4.18. The observed maximum collapse potential was highest in the presence of water and lowest in the presence of kerosene. The maximum collapse potentials were not influenced by the electrolyte concentration, but shifted towards the right of the graph with the decrease in dielectric constant. The maximum collapse potentials were, however, not observed for different dielectric fluids due to a limitation with the oedometer load application.

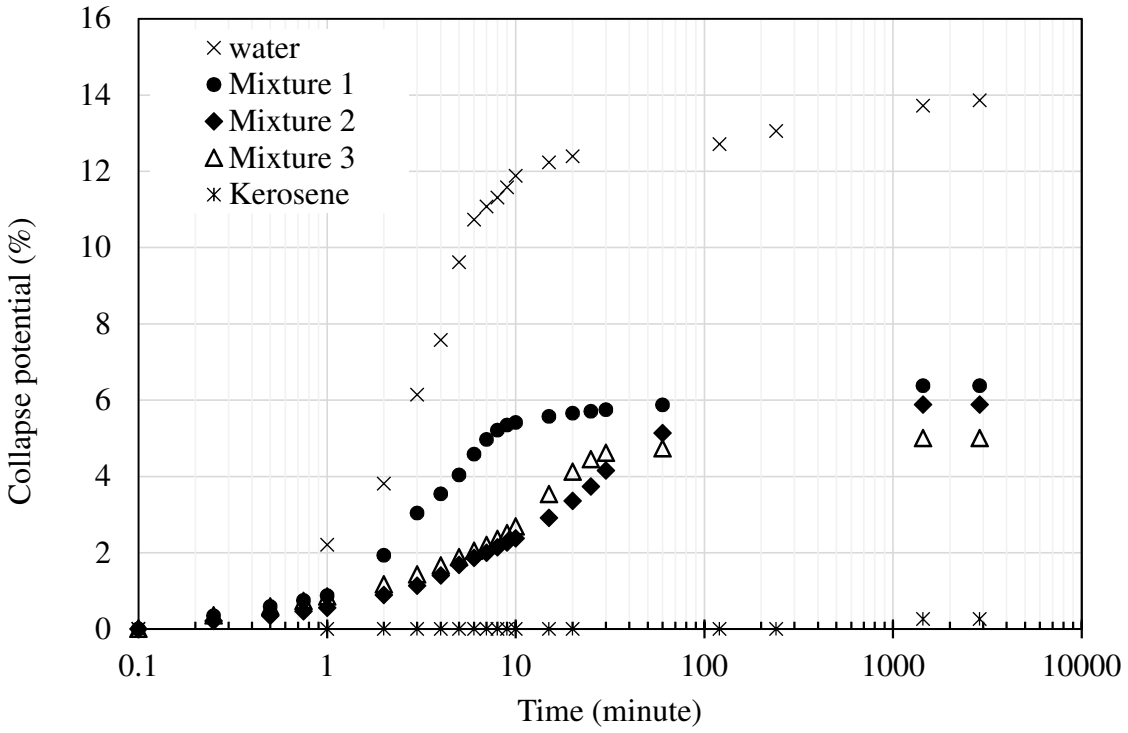

Fig. 4.14. Effect of dielectric pore fluids on the collapse rate under 800 kPa inundation pressure

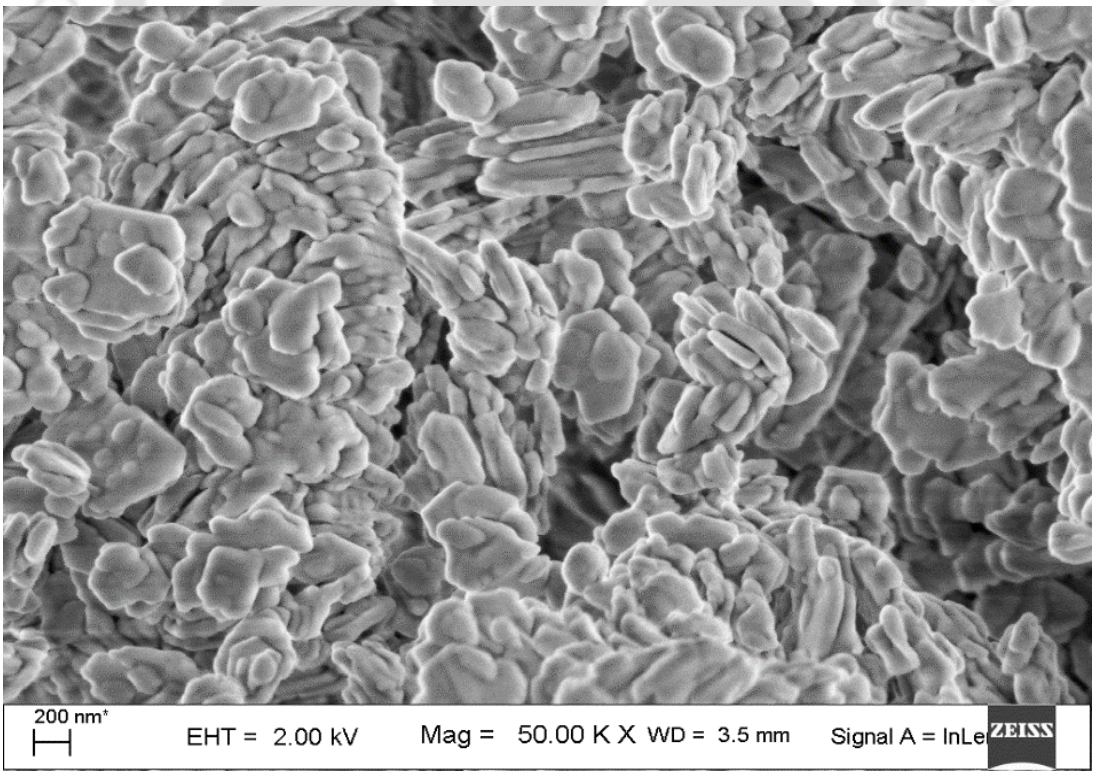

Fig. 4.15. SEM image of compacted specimen at1600 kPa inundation pressure in the presence of kerosene

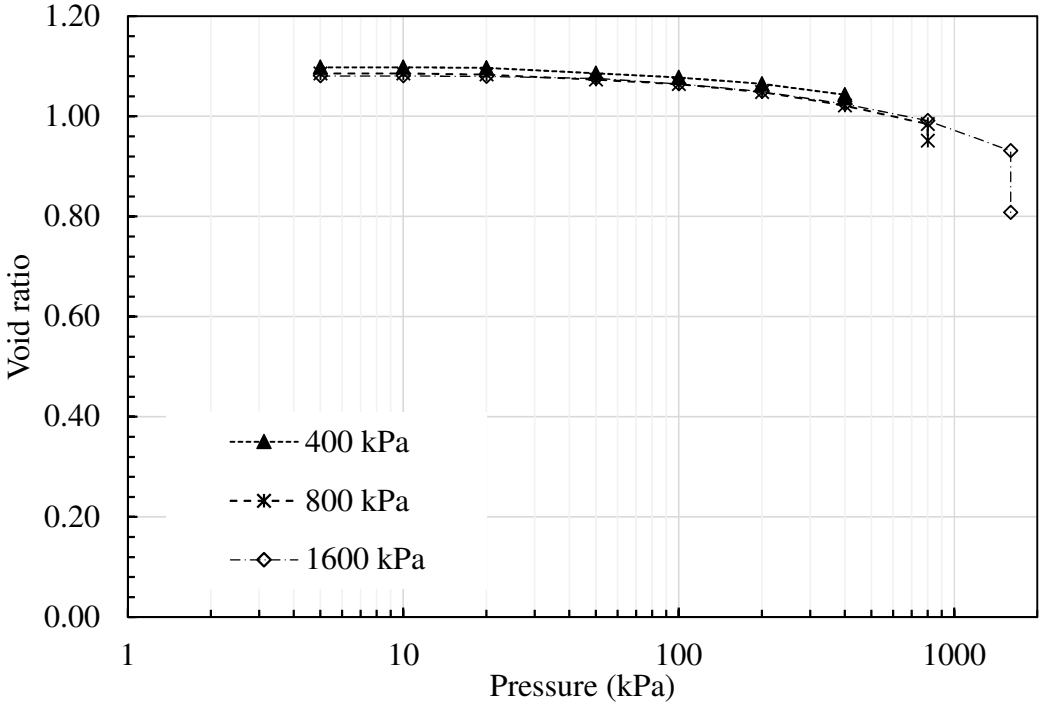

Fig. 4.16. Compression behavior of kaolin soil under different inundation pressures using ethanol as inundation fluid

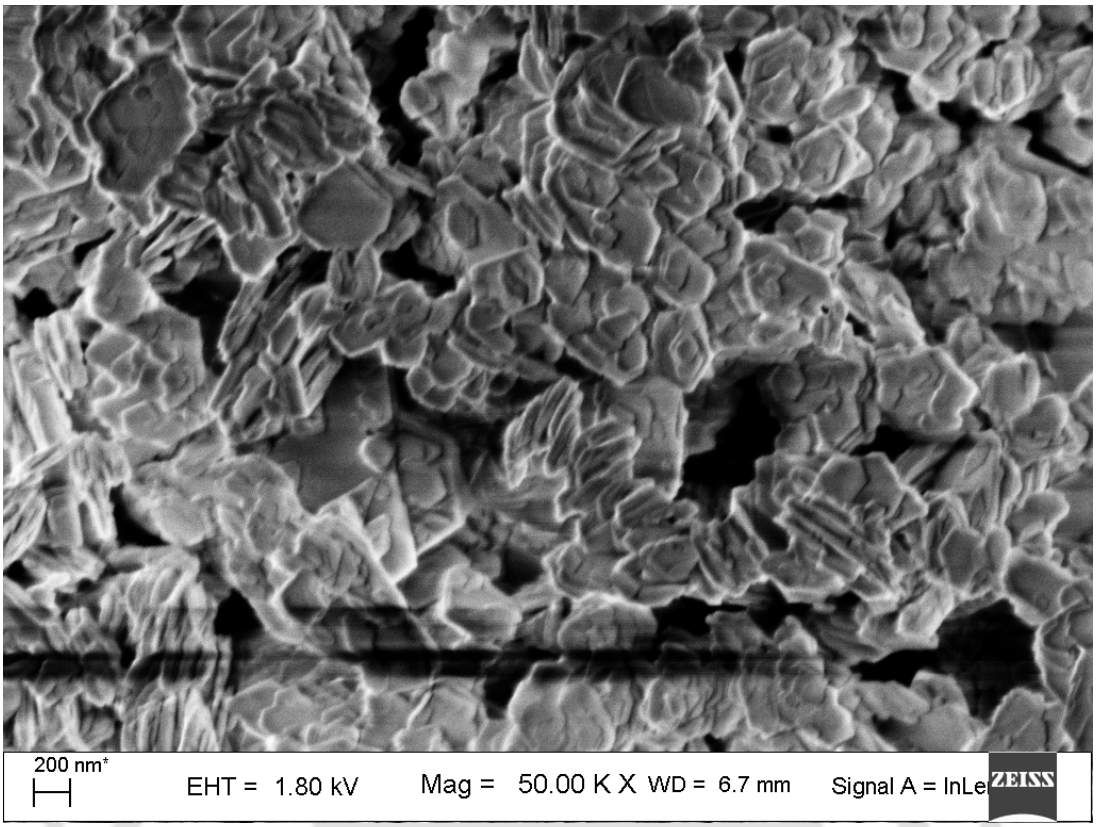

Fig. 4.17. SEM image of compacted specimen at 800 kPa inundation pressure in the presence of ethanol

Table 4.3: Measured collapse potential (CP) in the presence of different inundation fluids and inundation pressures

Inundating fluid	CP at different Inundation stress				
	50	200	400	800	1600
Water	6.515	9.18	10.89	13.85	11.695
0.01 mol/L NaCl	-	8.47	9.905	11.92	11.612
0.1 mol/L NaCl	-	7.52	8.614	10.70	11.596
Ethanol	-	-	0.260	1.67	6.370
Kerosene	0.00	0.00	0.00	0.27	0.5674

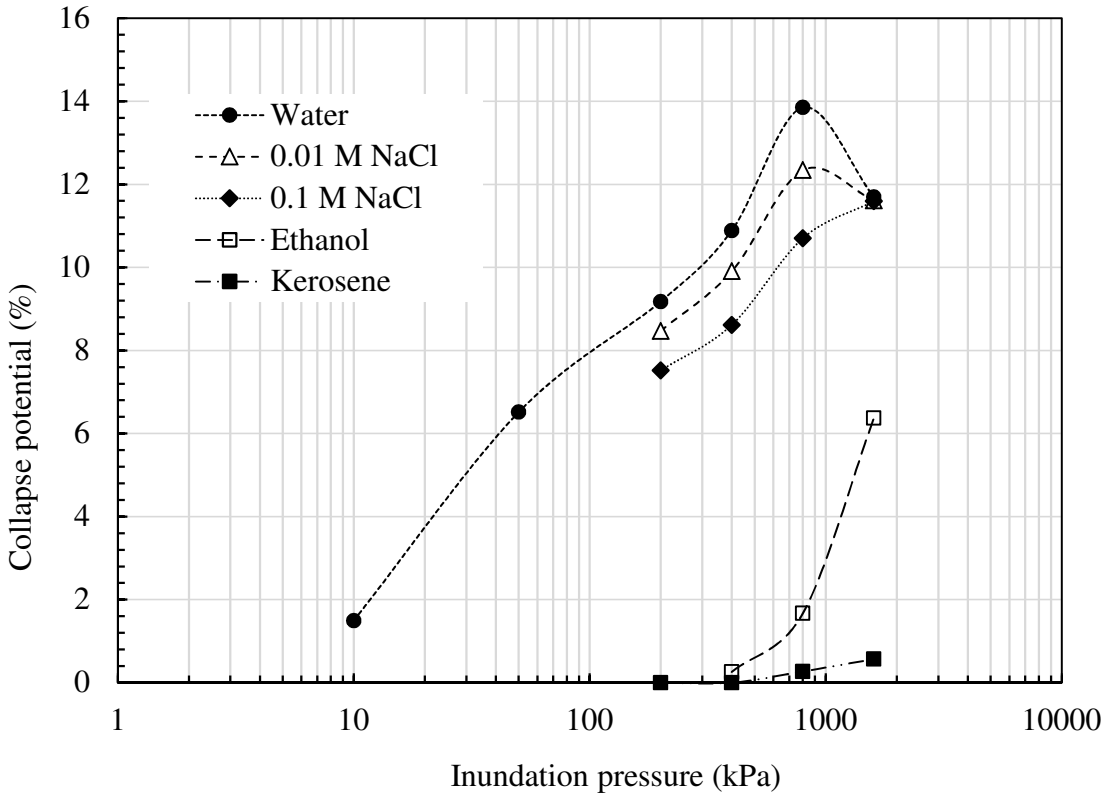

Fig. 4.18 Variation of collapse potential with inundation pressure and pore fluid chemistry

CONCLUDING REMARKS

A detailed study was conducted on the collapse behavior of kaolin under mechanical load for the first time and was found that the behavior is physicochemical in nature. Compacted kaolin specimens were able to withstand large mechanical loads in the air-dry state, but a significant collapse was noticed on wetting, similar to the loess soil. The collapse behavior of kaolin, however, was observed to be due to physicochemical interaction between the particle and pore fluids. The collapse potential of the compacted kaolin specimens due to fabric changes under the application of mechanical loading was analyzed. The rate of volumetric collapse and collapse potential in the presence of different pore fluids was investigated.

The variation in equilibrium sediment volume data with pH of the bulk solution was studied by conducting the sedimentation tests over a pH range of 3–8 was. The IEP_{edge} was determined from the equilibrium sediment volume data. The measured IEP_{edge} was 5.3 for the studied kaolin. The influence of pH-dependent charges on the kaolin behavior was analyzed

base on IEP_{edge}. The effect of fabric on the sedimentation behavior was studied by using three different pH solutions (3.1, 6.1, and 8), two different electrolyte concentrations (0.1 and 0.01 mol/L NaCl), and different dielectric solutions. The effect of fabric under mechanical stresses was studied from collapse tests by different pH solutions, dielectric solutions, and salt solutions which were used in the sedimentation tests. Fabric changes in the clay specimen due to interaction with different pore fluids in the collapse tests were analyzed using a multi-scale approach consisting of FESEM image analysis on lyophilized specimens. The results were corroborating with IEP_{edge} obtained from sedimentation tests.

CHAPTER 5

SWELLING PRESSURE CHARACTERISTICS OF BENTONITES IN ISOCHORIC CONDITIONS BY MICROSTRUCTURAL ANALYSIS

5.1 GENERAL

A series of swelling pressure test was conducted at five different initial compaction densities viz., 1.2, 1.45, 1.65, 1.8, and 2.0 Mg/m^3 for bentonite B1 and B2 using constant volume swelling pressure test. The temporal variation of swelling pressure for different bentonites and initial compaction densities were reported for understanding the swelling characteristics. The influence of compaction density and bentonite plasticity on the development of swelling pressure was analyzed by understanding the changes to the pore size distribution (PSD) and the clay fabric during the swelling pressure development.

5.2 RESULTS

The observed swelling pressure evolution with time for the bentonites B1 and B2 were presented in Fig. 5.1–5.2. Temporal changes in the swelling pressure for B1 with different compaction densities, varying in the range of 1.2 – 2.0 Mg/m^3, were shown in Fig. 5.1a – 5.1b. The swelling pressure continuously increased up to 4 *h* and 6 *h* for specimens compacted at 1.2 and 1.45 Mg/m^3 (Fig. 5.1a), respectively. The swelling pressure decreased with time for a sufficiently long time after attaining the first peak of swelling pressure, indicating a structural collapse. The decrease in the swelling pressure varied between 10 and 14% for the specimens compacted at ρ_d = 1.2 and 1.45 Mg/m^3, respectively. The swelling pressure further increased temporally after the structural collapse until attaining the equilibrium pressure at full saturation. The decrease in the swelling pressure was sharp and the difference between first pressure peak and equilibrium swelling pressure was insignificant in case of ρ_d = 1.45 Mg/m^3. However, the decrease in the swelling pressure was gradual and a significant increase in the swelling pressure was noticed after the collapse at ρ_d = 1.2 Mg/m^3. The swelling pressure evolution with time at higher compaction densities (viz. 1.65, 1.8, and 2 Mg/m^3) was shown in Fig. 5.1b. The swelling pressure increased continuously and reached a meta-equilibrium state with a plateau. The swelling pressure increased further with further water uptake after 0.5 – 6 d of meta-equilibrium state to reach the final equilibrium state. The temporal behavior of swelling pressure for these densities followed a monotonously increasing function. The results were qualitatively similar at the three compaction densities, albeit the equilibrium swelling pressure significantly varied with the initial compaction density. In summary, the

increase rate of swelling pressure for B1 at different compaction densities was nearly same during the initial water uptake but deviated significantly after 10 minutes. The specimens compacted at lower compaction densities (ρ_d = 1.2 and 1.45 Mg/m^3) exhibited a structural collapse with decrease in the swelling pressure after the initial phase of uptake process, but the other specimens exhibited a plateau for long durations before reaching the final hydro–mechanical equilibrium.

The swelling characteristics of B2 bentonite at different compaction densities were shown in Fig. 5.2a – 5.2b. The temporal evolution of the swelling pressure for all different compaction densities was qualitatively similar to the swelling characteristics of B1 bentonite at higher compaction densities (i.e., ρ_d = 1.65, 1.8, and 2 Mg/m^3). However, the magnitude of swelling pressure significantly higher for B2 compared to B1, even at the same compaction density, due to the presence of higher clay content and montmorillonite content.

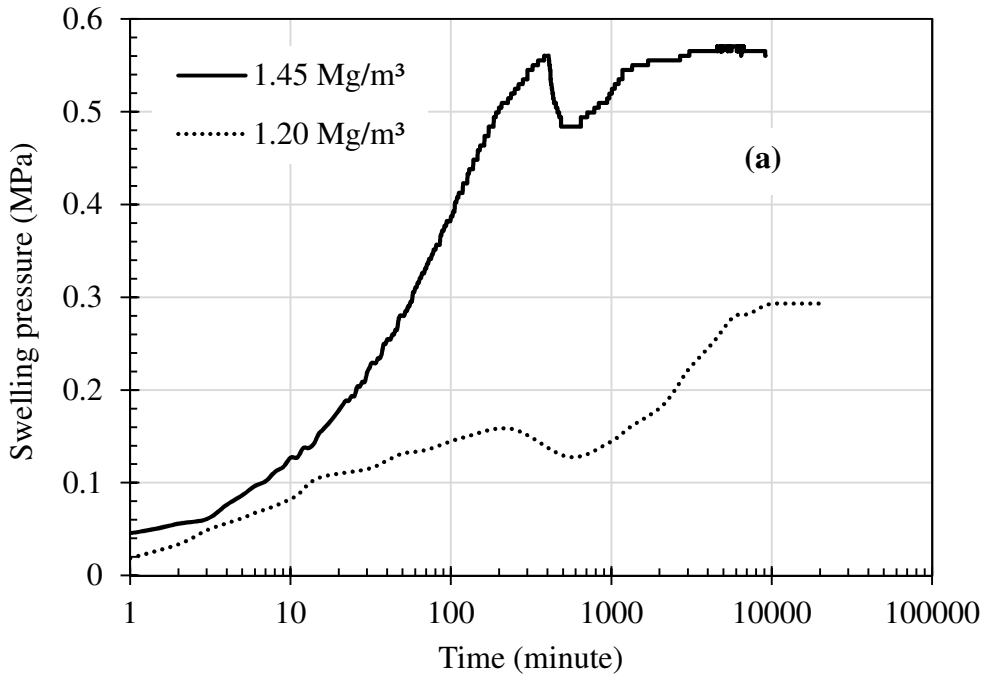

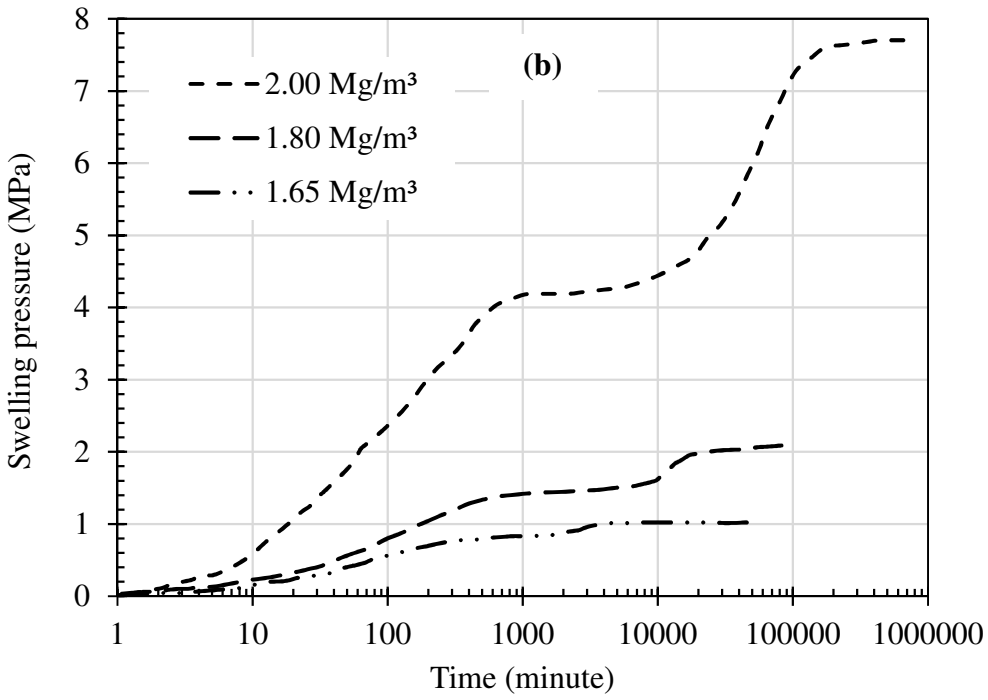

Fig. 5.1. Temporal variation of swelling pressure for B1 at initial dry densities of (a) 1.2 Mg/m^3 and 1.45 Mg/m^3 (b) 1.65 Mg/m^3, 1.8 Mg/m^3, 2 Mg/m^3

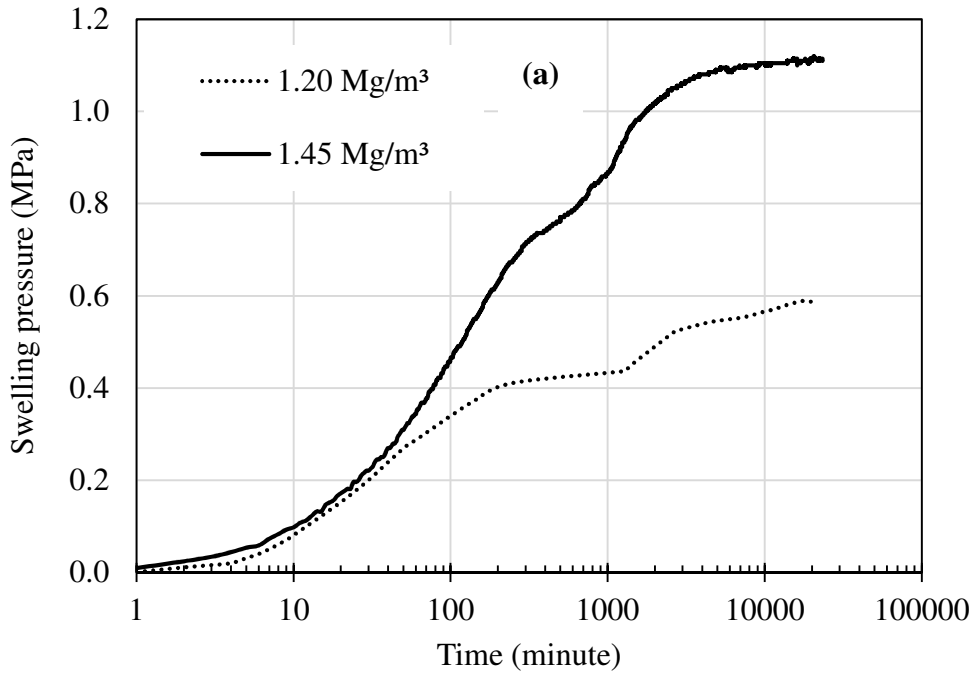

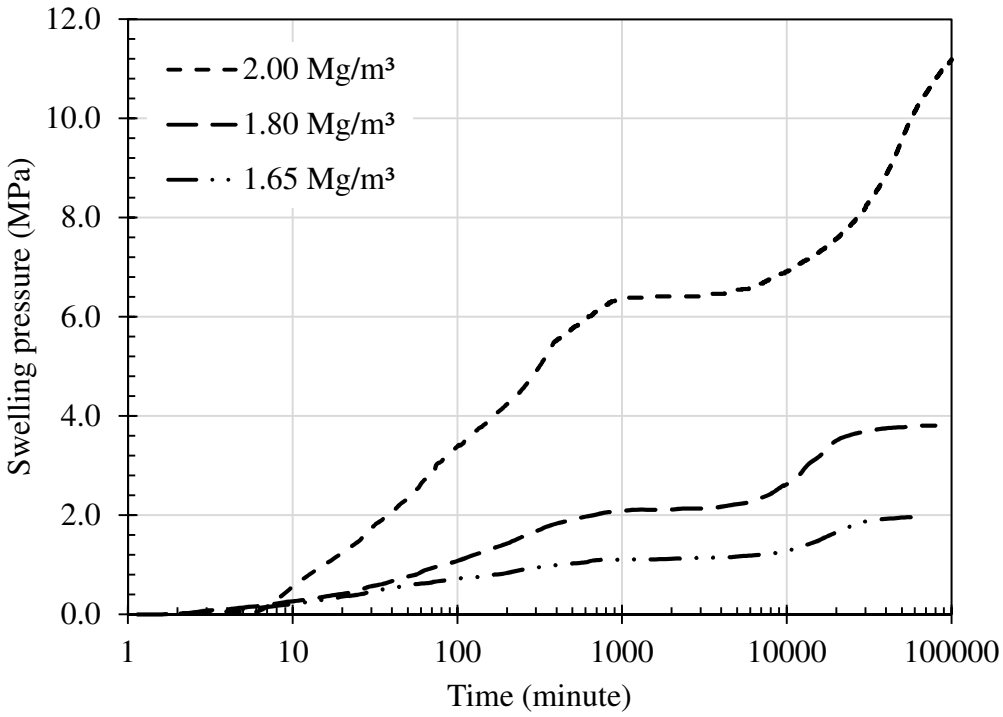

Fig. 5.2. Temporal variation of swelling pressure for B2 at initial dry densities (a) 1.2 Mg/m^3 and 1.45 Mg/m^3 (b) 1.65 Mg/m^3, 1.8 Mg/m^3, and 2 Mg/m^3

Thus, the swelling behavior of bentonites exhibited either a bimodal behavior or monotonously increasing behavior depending on the bentonite quality and initial compaction density as illustrated in Fig. 5.3a – 5.3b. The influence of bentonite quality and compaction density on the pore sizes evolution during the water uptake was studied in the following section to bring out the responsible micro-mechanisms for different swelling characteristics.

5.3 PORE SIZE AND FABRIC EVOLUTION

The PSDs and fabric of the bentonite specimens under the influence of different hydro-mechanical loads were obtained by Mercury Intrusion Porosimetry (MIP) and Field Emission Scanning Electron Microscope (FESEM). Different stages of swelling pressure development were noted on the swelling pressure evolution curve (SPEC) as shown in Fig. 5.3a – 5.3b. Increase in the swelling pressure due to initial water uptake was depicted by *OP* or *OP'*, followed by decrease in the swelling pressure or no change in swelling pressure with time using *PQ* or *P'Q'*, and immediately followed by a very slow rate of swelling pressure development until the equilibrium value as shown by *QR* or *Q'R'*. The B1 bentonite at lower

compaction densities (ρ_d = 1.2, 1.45 Mg/m^3) exhibited the bimodal curvature, *OPQR*. The monotonously increasing curve *O'P'Q'R'* was observed by B1 bentonite at higher compaction densities and by B2 bentonite at all the studied densities. The pore size and fabric evolution for B1 and B2 bentonites due to water uptake at *O, P, Q,* and *R*; *P', Q',* and *R'*, respectively, were analyzed only at compaction density of ρ_d = 1.45 Mg/m^3. Both bimodal and monotonously increasing behaviors were exhibited by the bentonites at this density. The soil specimens at different stages were carefully extruded and lyophilized from the duplicate tests for the MIP and FESEM testing. The influence of compaction density on the PSDs and fabric were studied using the "as – compacted" specimens

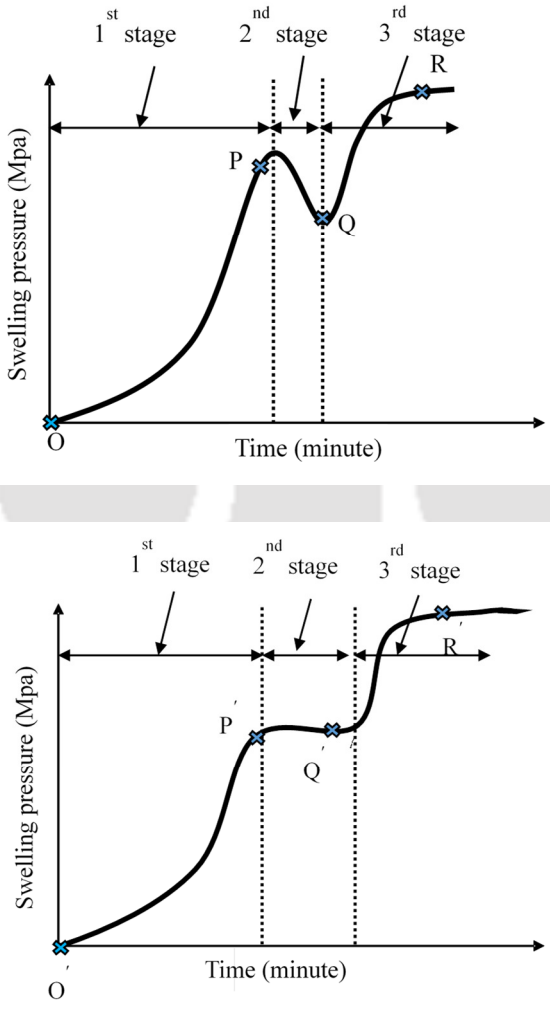

Fig. 5.3 Typical swelling pressure evolution curve exhibiting (a) bimodal and (b) monotonously increasing behavior

5.4 SPEC evolution for different bentonites

The differential specific intrusion volume variation with pore diameter for B1 at *O*, *P*, *Q*, and *R* on the SPEC was presented in Fig. 5.4. The normalized pore volumes based on the contributions from different pore size classes at these stress states were also presented using the bar diagram in Fig. 5.5. The intrusion volume at the "as-compacted" condition, point '*O*', showed a relatively uniform distribution of the pore sizes with no significant sharp peak. The FESEM figure (Fig. 5.6) also showed the aggregate formation with several pores of different pore size classes. The water enters into the micro pores and small crevices during the initial water uptake due to higher hydration energy. The hydration of interlayers of the aggregate forming particles decreased the distance between the aggregates that was inferred from the decrease in the pore volume contribution from the pore size class of 10 – 100 μm and simultaneous increase in the pore size class of 10 – 1 μm. Similarly, the pore volume contribution of pore size class of 0.1 – 1 μm decreased and the contribution to the total volume by the smaller pore class of 0.01 – 0.1 μm increased simultaneously during the initial water uptake from *O* to *P* as shown in Fig. 5.5. The increase in the volume contribution of the smaller pore size class resulted in the development of non-uniform pore size distribution with a sharp and high intensity peak in the differential intrusion volume plot for *P*. A peak in the differential intrusion volume plot at a particular pore diameter indicates the presence of more number of similar size pores. Further uptake of water reduced the pore volume contribution from 10 – 100 μm pore size class to an insignificant value where the decrease in the swelling pressure was observed. The collapse of this pore size class contributed to the swelling pressure reduction in the *PQ* segment of the SPEC. The FESEM figure (Fig. 5.7) of the specimen at point "*R*" showed a parallel arrangement of the clay plates revealing the fabric change. A sudden drop in the normalized pore volume in the bar diagram also indicated the fabric change which resulted in the formation of tiny pores that were inaccessible to the mercury. The increase in the swelling pressure with a very slow rate in the *QR* segment (compared to *OP*) of the SPEC was observed to be due to the DDL formation which increased the amount of pore size classes of 0.1 – 1 μm and 1 –10 μm significantly.

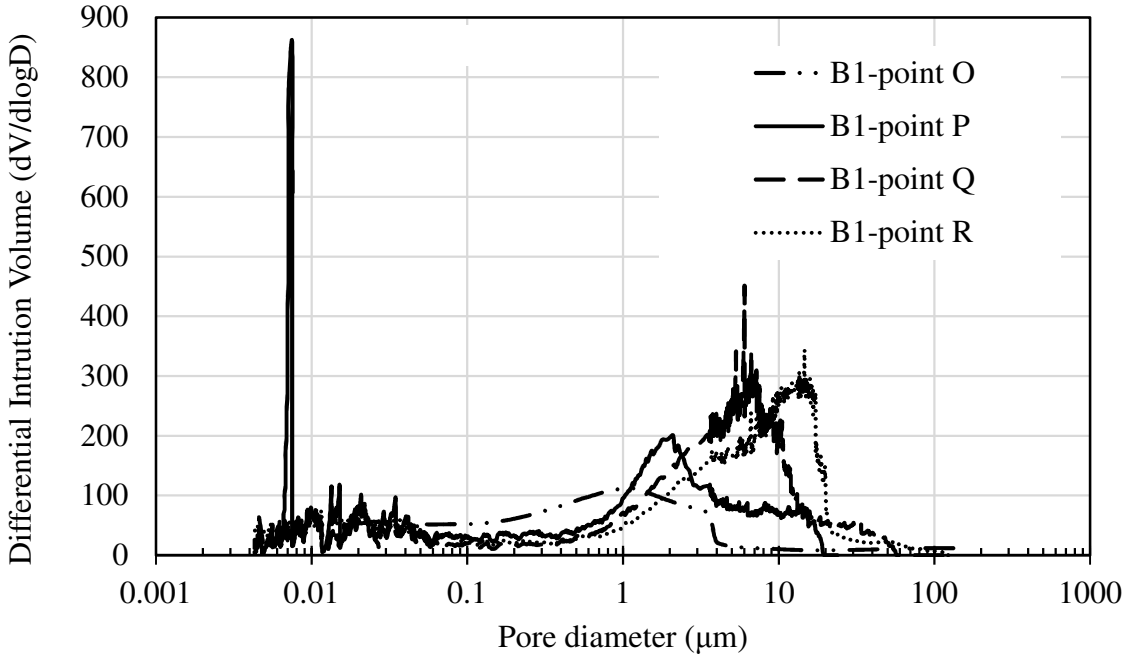

Fig. 5.4. Typical data differential intrusion volume from intrusion porosimetry for bentonite B1

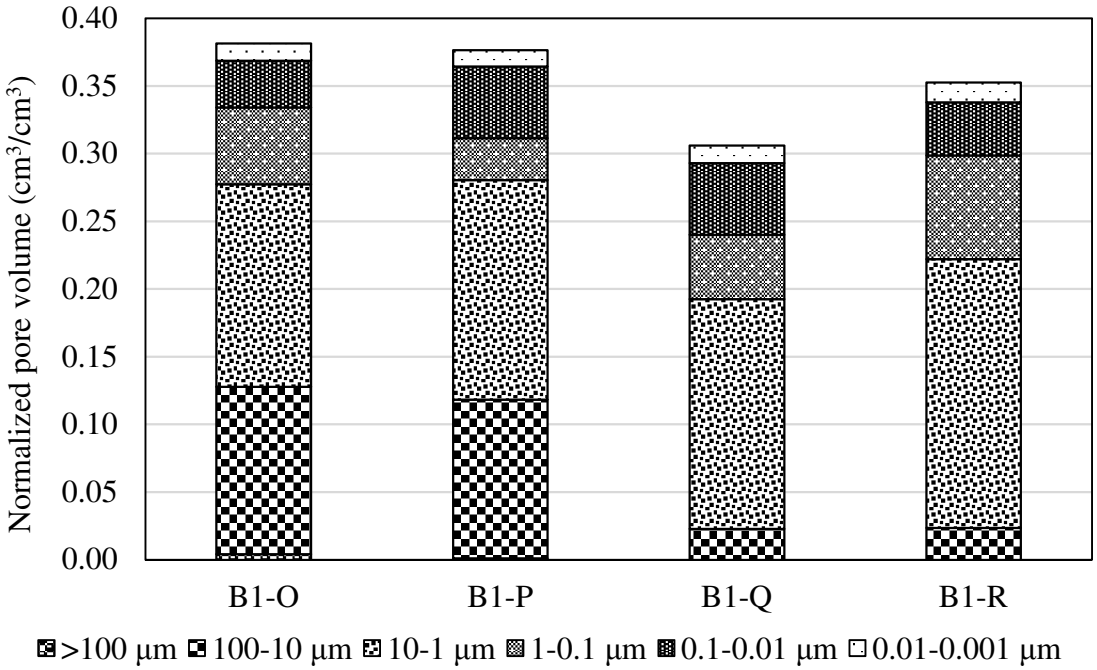

Fig. 5.5. Typical pore size distribution bar diagram of B1, ρ_d = 1.45 Mg/m^3

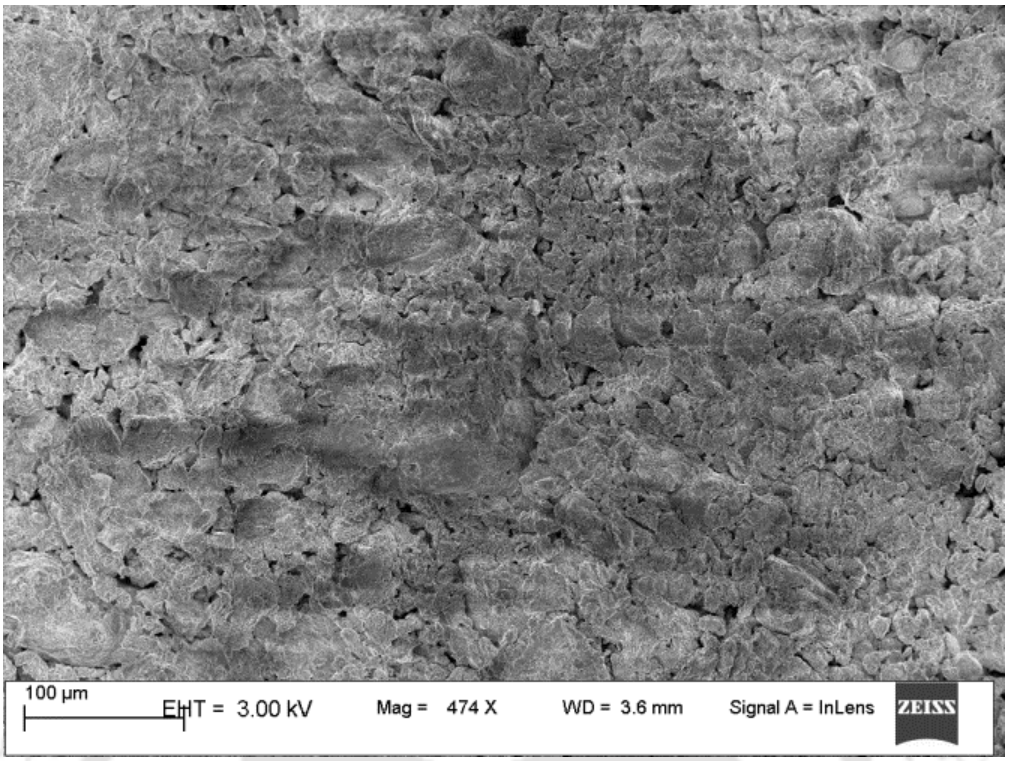

Fig. 5.6. FESEM figure for "as – compacted" specimen of B1 bentonite at ρ_d = 1.45 Mg/m^3

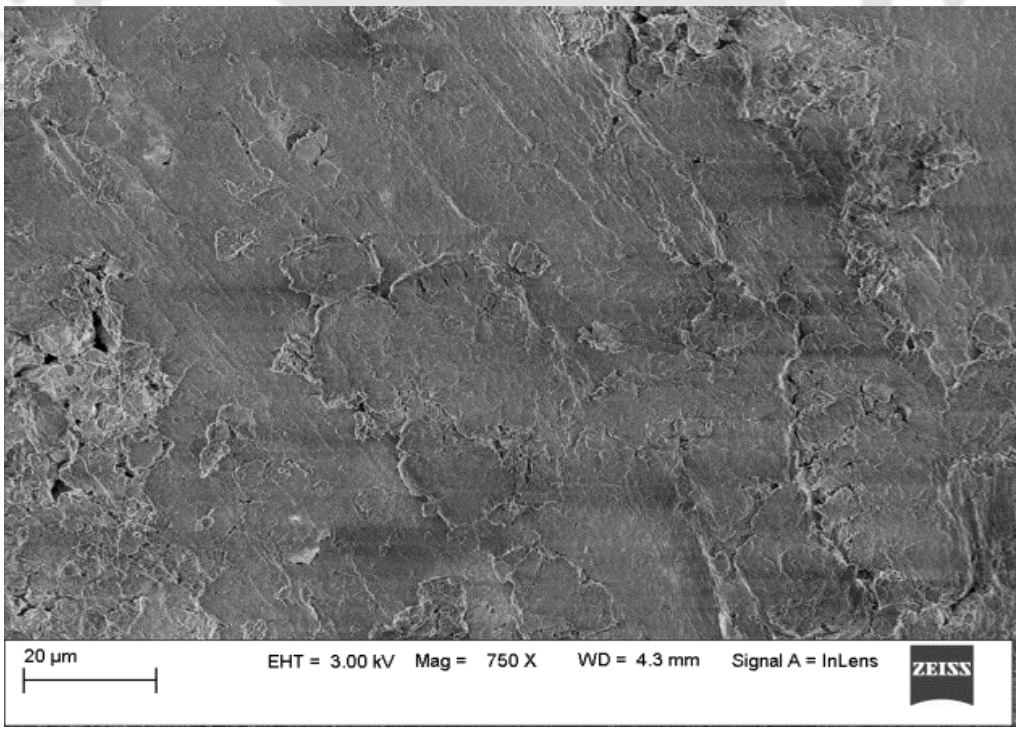

Fig. 5.7. FESEM figure of B1 bentonite at ρ_d = 1.45 Mg/m^3 at point "*R*" on SPEC

The differential specific intrusion volume variation for B2 at *O´*, *P´*, *Q´*, and *R´* on the SPEC was presented in Fig. 5.8. The normalized pore volumes based on the contributions

from different pore classes at these stress states were also presented using the bar diagram in Fig. 5.9. In contrast to B1 specimen, the pore size class of 10 – 100 μm was insignificantly available in B2 specimen at the same compaction density. The intrusion volume at the "as-compacted" condition, point '*O´*', showed a relatively uniform distribution of the pore sizes except with a presence of low intensity, smooth peak at 1 μm. The FESEM figure (Fig. 5.10) showed the aggregate formation with relatively smaller pore size classes. The hydration of interlayers of the aggregate decreased the pore volume contribution of the pore size class of 1 – 10 μm and simultaneous increase in the pore volume significantly due to other smaller pore size classes. The increase in the volume contribution of these pore size classes exhibited sharp and high intensity peak on the differential intrusion volume plot for *P'*. Further uptake of water increased the pore volume contribution from 10 – 1, 0.1 – 1, and 0.01 – 0.001 μm pore size classes to a significant value, but by compensating the 0.01 – 0.1 μm pore size class indicating the redistribution of water. The FESEM diagram, at *P´* also showed not a significant variation in the fabric compared to *O´* and plates are aligned more parallel to each other at *Q´* (Fig. 5.11). The plateau on the SPEC thus signifies the redistribution of pore size classes due to more alignment of particles in parallel orientation. Swelling pressure didn't decrease unlike for B1 bentonite at this density, during this stage, because the absence of larger pore size class such as 10 – 100 μm, which contributed for the structural collapse during the water uptake. The increase in the swelling pressure with a very slow rate in the *Q´R´* segment of the SPEC was observed to be due to the DDL formation which increased the amount of pore size classes 0.1 – 1 μm for *R*'.

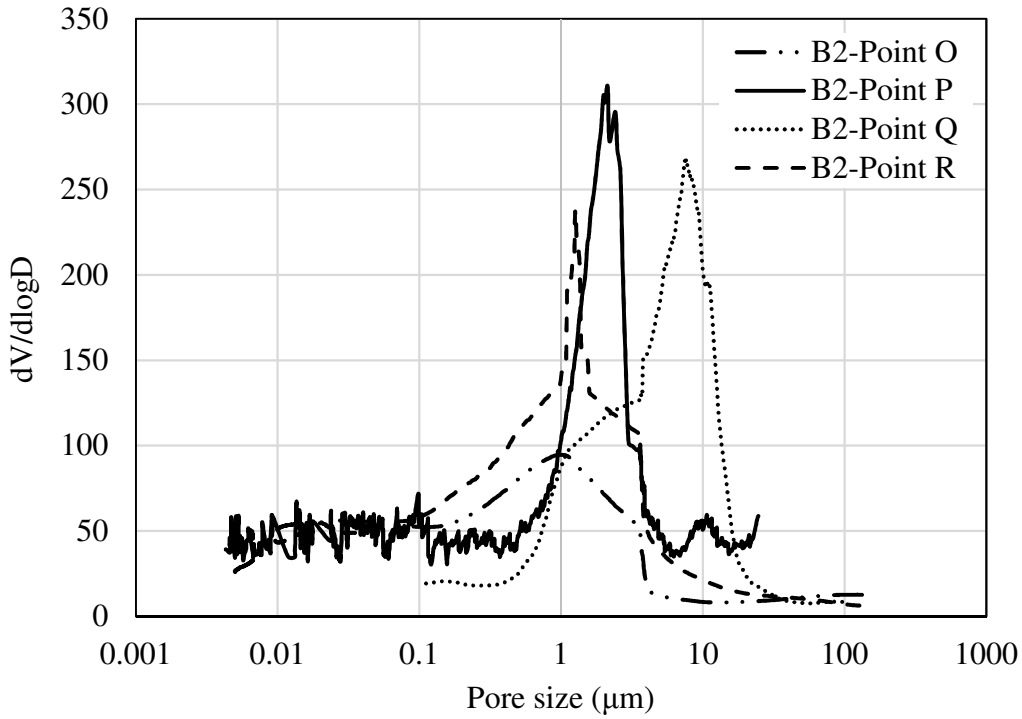

Fig. 5.8. Typical data differential intrusion volume from intrusion porosimetry for bentonite B2

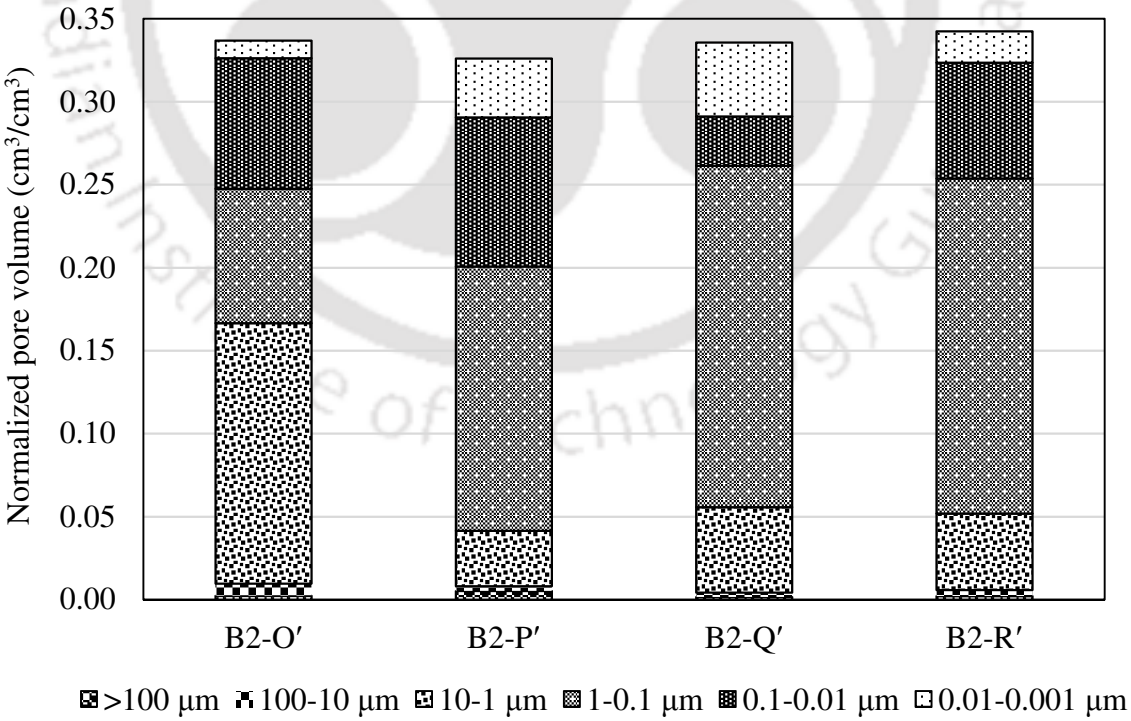

Fig. 5.9. Typical pore size distribution bar diagram of B2, ρ_d = 1.45 Mg/m^3

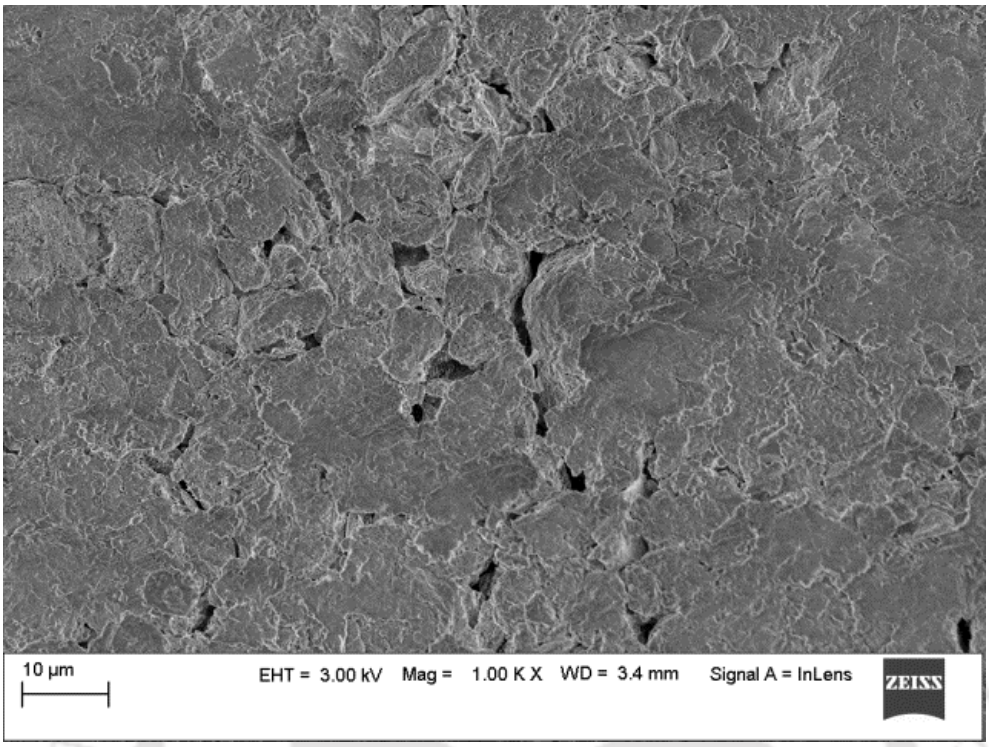

Fig. 5.10. FESEM figure for "as – compacted" specimen of B2 bentonite at ρ_d = 1.45 Mg/m^3

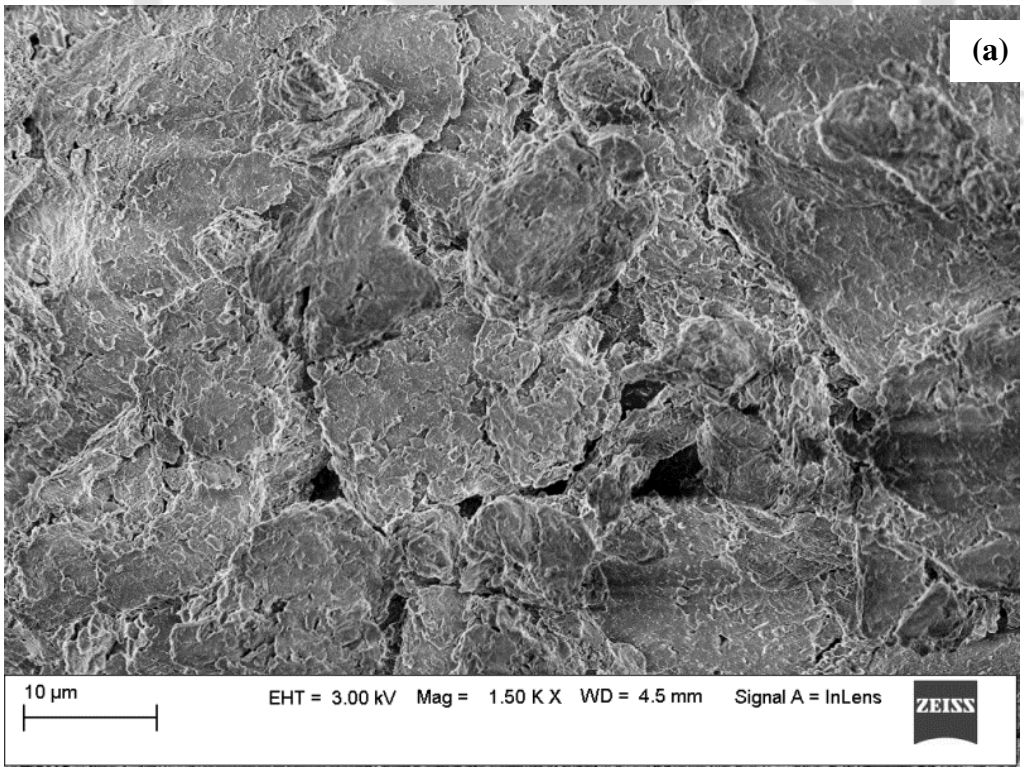

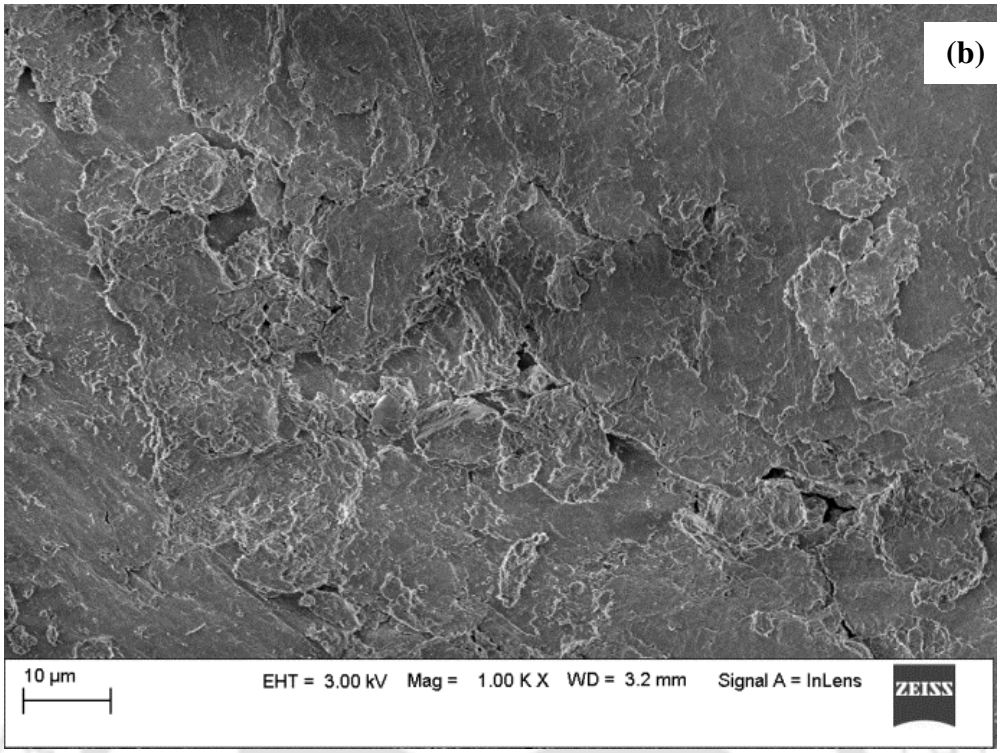

Fig. 5.11. FESEM figure of B2 bentonite at ρ_d = 1.45 Mg/m^3 at (a) *P´* and (b) *Q´*

5.5 Influence of compaction density and bentonite plasticity

The influence of compaction density on the PSDs was analyzed using the MIP data on the "as-compacted" specimens of B1 and B2 for three different densities. The variation in differential mercury intrusion volume with pore diameter was presented for the "as-compacted" specimens of B1 and B2 in Fig. 5.12. The differential mercury intrusion volume data for both the bentonites at a given density were qualitatively similar. The differential volume exhibited a sharp peak for density ρ_d = 1.2 Mg/m^3 for both the bentonites and the distribution of pore sizes were uniform for the other densities. The normalized pore volumes for these cases were presented using the bar diagram in Fig. 5.13. The contribution of different pore-size classes on the total pore volume was clearly brought by the bar diagram. The volume contribution of macro pore-size class 10 – 100 μm was significant for B1 at ρ_d = 1.2 Mg/m^3 and increased to maximum at ρ_d = 1.45 Mg/m^3. The percentage reduction in the swelling pressure was thus maximum at ρ_d = 1.45 Mg/m^3. Further increase in the compaction effort decreased the volume of macro pore size class to insignificant value which prompted the change in SPEC from bimodal to monotonously increasing behavior. In contrast to B1, the

macro pore size class was insignificantly available in B2 at any given compaction density. The SPEC followed monotonously increasing behavior for B2 due to the presence of insignificant amount of macro pore size class as shown in Fig. 5.13. More amount of soil was present in the B2 specimen at any given compaction density due to the presence of higher percentage of clay fraction compared to B1. The inter-particle distance in B2 was thus smaller compared to B1 bentonite at the same compaction density. The volume of given smaller pore-size classes (≤ 10 μm) was higher in B2 compared to B1 for any given density. The increase in bentonite plasticity, therefore, reduced the presence of macro pore size classes and altered the structural collapse behavior. The FESEM diagrams of B1 at different compaction densities (Fig. 5.6) showed no noticeable variation, but for B2 (Fig. 5.10) showed unnoticeable pores and very smooth surfaces.

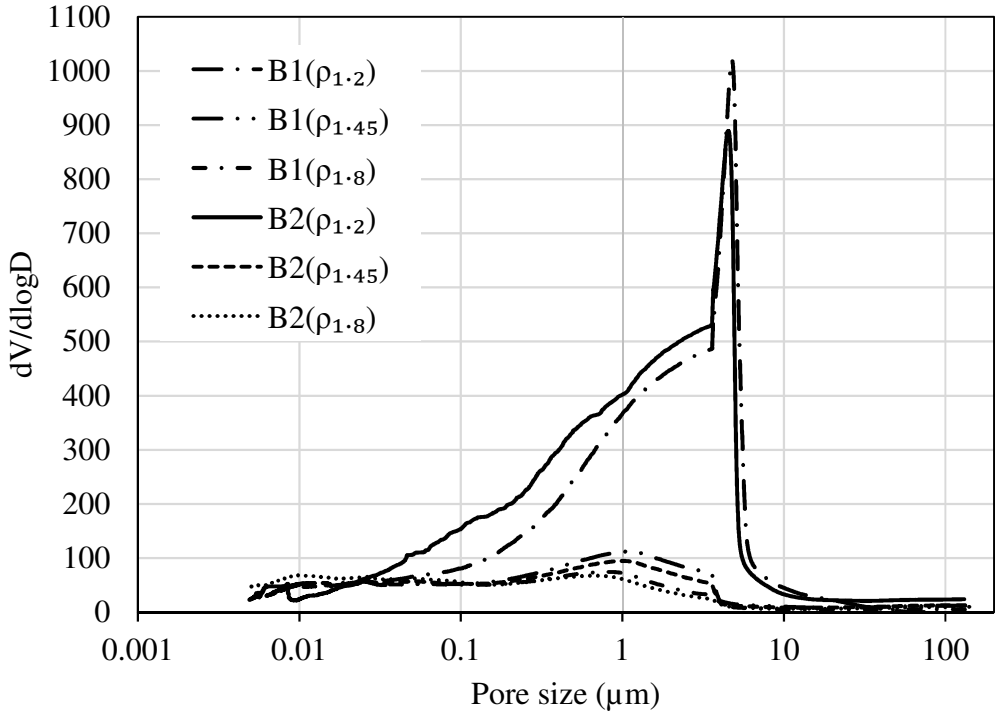

Fig. 5.12. Typical data from mercury intrusion porosimetry of bentonite B1and B2 for as compacted state differential intrusion volume

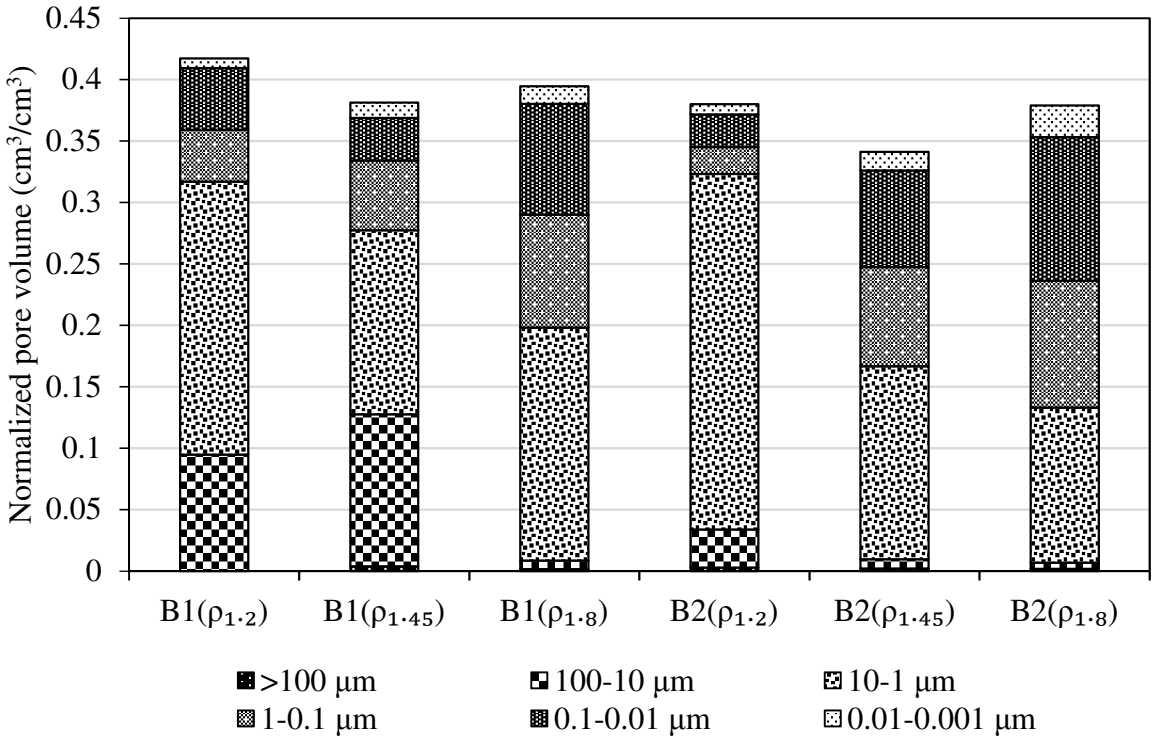

Fig. 5.13. Typical pore size distribution bar diagram of B1 and B2 for as compacted state

CONCLUDING REMARKS

The swelling pressure data were obtained at five different initial compaction densities for bentonite B1 and B2 using constant volume swelling pressure test. The swelling pressure characteristic curve was studied for the bentonites. The temporal variation of swelling pressure for different bentonites and initial compaction densities obtained for the swelling characteristics. The swelling behavior of bentonites exhibited either a bimodal behavior or monotonously increasing behavior depending on the bentonite quality and initial compaction density. The influence of compaction density and bentonite plasticity on the development of swelling pressure was analyzed by understanding the changes to the pore size distribution (PSD) using MIP data and the clay fabric using FESEM image during the swelling pressure development. The drop in SPEC after the initial water uptake is due to the collapse of 10 – 100 μm pore size class present in the soil sample.

CHAPTER 6

SWELLING PRESSURE PREDICTION FOR COMPACTED BENTONITES AND BENTONITE – SAND MIXTURES

6.1 General

In this chapter, a new model was proposed for predicting the swelling pressure variation over a wide range of dry densities. The proposed model was an extension of Bharat and Sridharan, 2015 earlier work for predicting the compressibility curves of highly plastic clays, but deviates significantly from the earlier model due to the mechanisms associated with the swelling pressure variation with dry density. The proposed model considered the influence of quality of clayey soil and associated mechanisms in the swelling pressure variation with density for the prediction.

6.2 Measured data of swelling pressure – dry density

The measured swelling pressure–dry density data of the Indian bentonites from the present study and the literature data for different plastic clays presented in Table 3.4 were shown in Fig. 6.1a. The variation of swelling pressures over a wide range of dry densities i.e., 1.0 – 2.1 Mg/m^3 was presented in this figure. The void ratio varied from 1.86 to 0.36 for different clayey soils and with dry density. The variation in the void ratio with compaction density signifies the variation in the inter-platelet distance. Thus the void ratio is smaller at densely compacted state compared to the lower dry density. The diffuse double layer (DDL) repulsion at full saturation is relatively higher at high compaction state and thus the measured swelling pressures are higher significantly with increase in the compaction density. Swelling pressure data of different compacted bentonites and bentonite-sand mixtures showed that the swelling pressures varied significantly with the clay quality/plasticity. The swelling pressure of the higher quality bentonite, B2, is consistently higher than B1 at a given compaction density. The presence of higher surface properties such as specific surface area and cation exchange capacity in the higher plastic clays contain more DDL water which increases the repulsion between the hydrated clay plates. As the variation in the swelling pressure was significantly large (~700 – 32,000 kPa), especially at high compaction densities, the variation

was also presented in semi-log scale in Fig. 6.1b. The bentonites MX80, Montigel, GMZ-1, and Kunibond bentonites showed highest swelling pressures, at any given compaction density, due to the presence of higher percentage of montmorillonite content, which is apparent from their high surface properties. The swelling pressure is about 32 MPa at ρ_d = 2 Mg/m^3 for MX80 and is about 3 MPa at ρ_d = 1.43 Mg/m^3 for Kunibond bentonite. The swelling pressure data of Kunibond (Komine and Ogata, 2004) was not available at densities higher than 1.43 Mg/m^3, but the swelling pressure data of MX80 and Kunibond are comparable at this particular density (Fig. 6.1b). The swelling pressures of the sand-bentonite (SB) mixtures at a given density reduced significantly due to the addition of different percentages of sand as indicated by SB1 – SB5. The swelling pressure data of the SB mixtures are available only in the higher density range (ρ_d > 1.4 Mg/m^3). Thus the swelling pressure varied with plasticity in a thick band for the studied clays as shown in the figure.

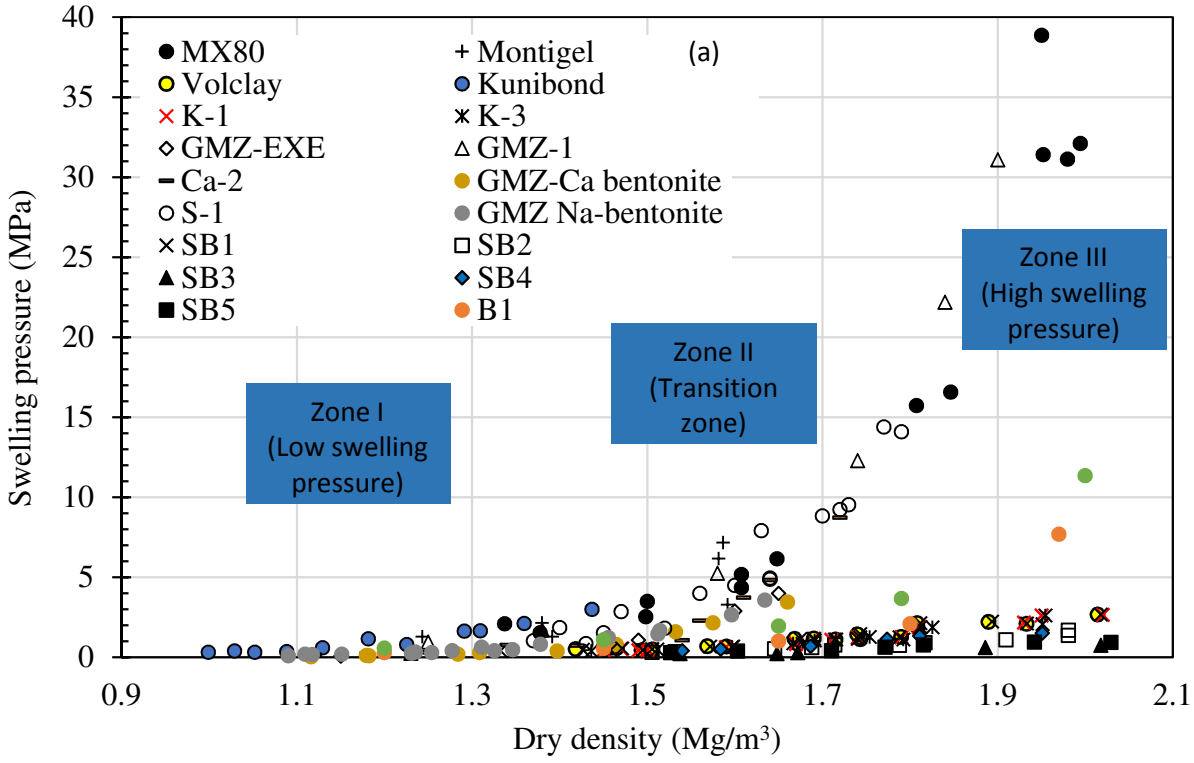

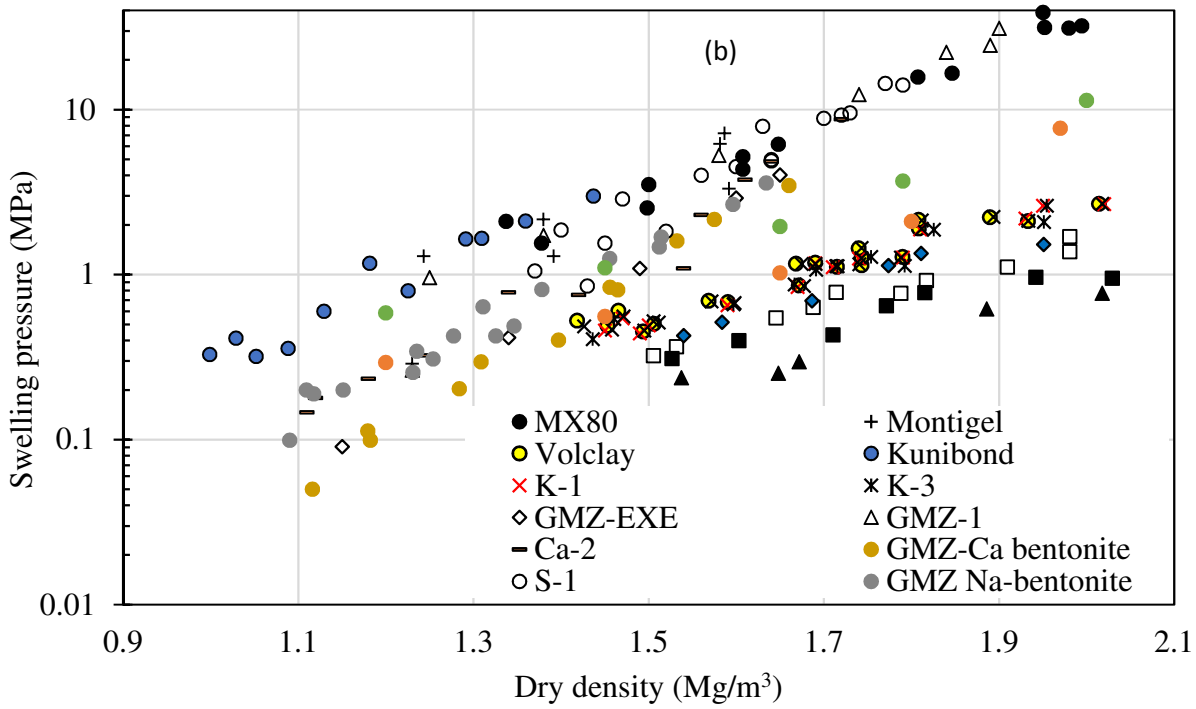

Figure 6.1. Swelling pressure vs. dry density data of B1, B2, and the studied soils from the literature (a) in normal scale and (b) in semi-log scale

6.3 Prediction by GC theory

The swelling pressure – dry density relationship is often estimated theoretically using the GC theory. In this study, simplified method given by Bharat et al. (2013) was used for predicting the theoretical relationship. The mid-plane distance between the two interacting plates was obtained by knowing the dry density of the soil using Eq. (2.1). The non-interacting plate potential at a distance equal to the mid-plane distance was computed using Eq. (2.7) and this value was used to estimate the mid-plane potential, ϕ_d, using Eq. (2.6). The swelling pressure was then estimated using Eq. (2.5) by considering mid-plane potential in non-dimensional form and knowing the pore-fluid characteristics. The estimated theoretical curves of swelling-pressure – dry density for B1, B2, MX80, and Montigel were shown in Fig. 6.2a – 6.2b along with the experimental data. Theoretical curves for all the clays over-predicted the swelling pressures slightly in the lower density range and significantly undermined the pressures in the higher density range. This observation was consistent with the earlier studies (Bharat et al., 2013).

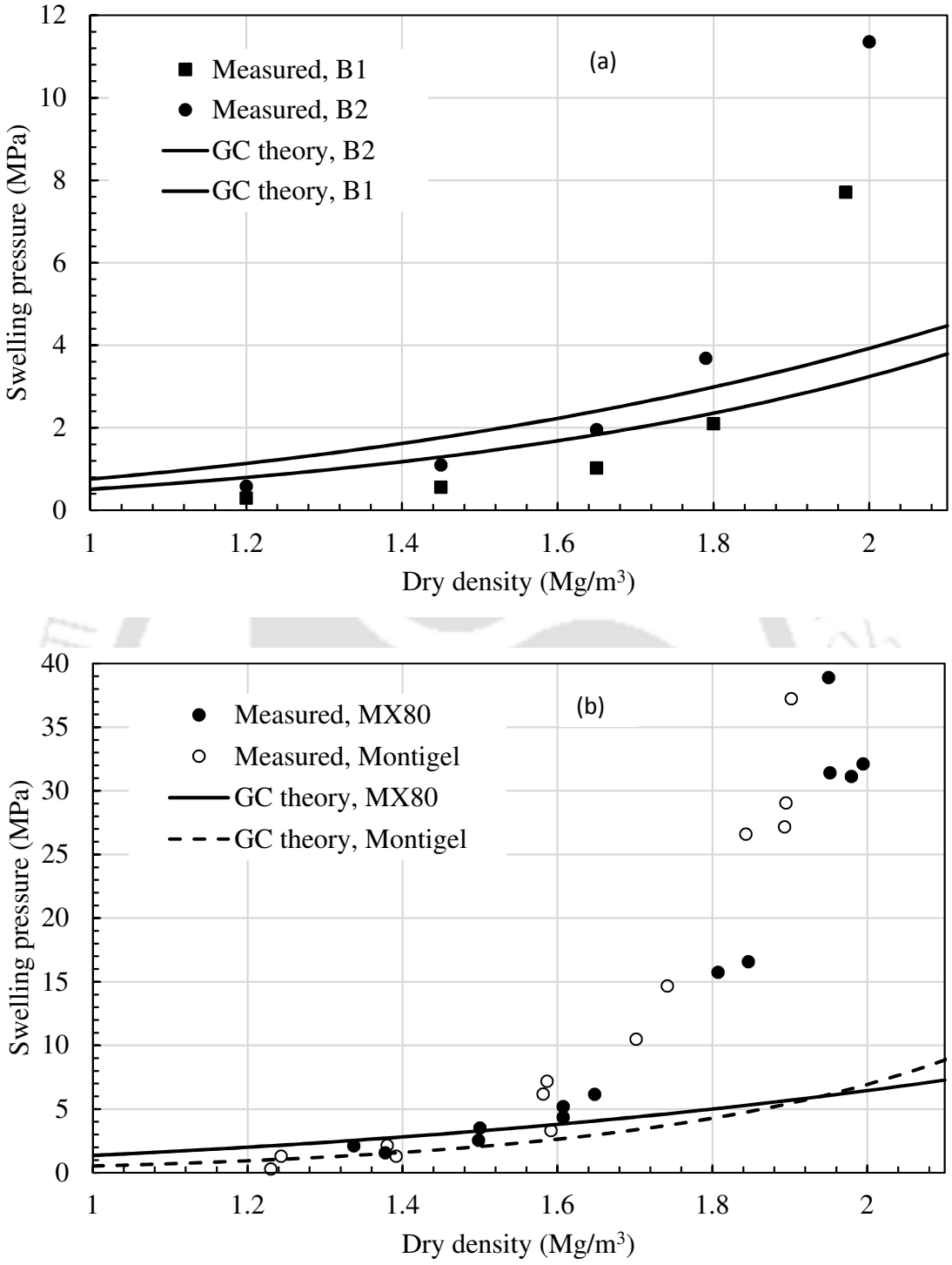

Figure 6.2. Measured and estimated swelling pressure-dry density curve of (a) bentonite B1 and B2 (b) MX80 and Montigel bentonite

Recent studies showed that the density of clay surface water is not unity in bentonites and found to influence the compacted bentonite behavior (Villar and Lloret 2008; Jacinto et

al. 2016; Zhang and Lu 2018). The upper bound of adsorbed water density near the clay surface is reported between 1.4 Mg/m^3 (Martin 1960) and 1.872 Mg/m^3 (Zhang and Lu 2018) in different studies. The number of hydration layers around the clay platelets after the crystalline swelling is influenced by the compaction density which in turn influences the inter-particle distances. Thus the increase in the compaction density limits the complete formation of DDLs and increases the overall density of the clay water. Villar and Lloret (2008) provided a useful relationship between the compaction density and average water density which accounts for the increase in water density from 1 Mg/m^3 to 1.36 Mg/m^3 due to decrease in the pore volume. The variation in the water density with compaction density was incorporated in the GC theory for theoretical estimation of swelling pressure – dry density curves for MX80 and montigel bentonites as shown in Fig. 6.3a-6.3b. The influence of water density on the predicted swelling pressure was appreciable (i.e., 40 – 50% of higher pressures) as the water density is directly proportional to the swelling pressure at a given compaction density. However, the theory still significantly underpredicted the observed swelling data. The influence effect of siloxane cavity formation at the higher inter-particle interactions (i.e., higher dry densities) and the distribution of charge (Sposito 2008) might increase the swelling pressure of the bentonite appreciably. However, the DDL theories do not consider the siloxane cavities on montmorillonite surfaces and thus limit the inter-particle interactions at higher compaction densities. The theoretical swelling – pressure vs. dry density relationships by the GC theory is often underestimated for many clayey soils due to limitations associated with the diffuse double layer theory. Normalization approach based on the linearization model is recently introduced for predicting the compressibility data of highly plastic clays (Bharat and Sridharan 2015a). The method requires a single measured data point (i.e., consolidation pressure and corresponding void ratio) to predict the entire compressibility curve. The predictive equation is given as

$$\frac{e_{P^*}}{e} = \left(\frac{P^*}{P}\right)^n \tag{6.1}$$

where e_{P^*} and P^* are the normalization data; n is an empirical parameter; P is the consolidation pressure; and e is the void ratio corresponding to P. The Eq. 6.1 with $n = 0.5$ is found to be applicable for compressibility data of highly plastic clays. This model is found to

be advantageous as it requires no knowledge of the clay surface or pore-fluid characteristics, or the computation of midway potentials to relate with the distance between clay platelets (Bharat and Sridharan 2015a). The applicability of this model for predicting the swelling pressure – dry density data was studied here.

6.4 Linearization of the swelling pressure data

Normalization and linearization of the compressibility data provide useful equations for accurately predicting the compressibility data for highly plastic clays (Bharat and Sridharan 2015a). Although the swelling pressure is measured by controlling the dry density in constant volume swell pressure tests unlike the compressibility tests, where the void ratio is estimated under applied pressure, the void ratio was normalized for a given swelling pressure in this study to understand the applicability of linearization model for swelling data. The void ratio data were normalized using the void ratio corresponding to two different swelling pressures viz. 0.8 MPa and 1.6 MPa and were presented in Fig. 6.4a-6.4b, respectively. The void ratio data converged to a band beyond the normalization void ratio $e_{0.8}$, but the void ratio data varied in a thick band for the other swelling pressures. This indicates the dependency of chosen normalization void ratio on the swelling curves, unlike for the compressibility curves. Further, the linearization of the swelling data using Eq. 8 with $n = 0.5$ was presented in Fig. 6.5a – 6.5b for the studied clayey soils using two normalization void ratios namely, $e_{0.8}$ and $e_{1.6}$, respectively. The predicted swelling pressure – dry density curves based on the measured data at 0.8 MPa and 1.6 MPa swelling pressures were also presented along with the measured data. The predicted lines deviated from the measured data significantly for all the clayey soils, especially in the range $1/\sqrt{P} > 1.5$ using $e_{1.6}$ and $1/\sqrt{P} > 1.7$ using $e_{0.8}$. A careful observation showed that the theoretical lines matched the experimental data for low plastic clays such as SB1 – SB2 with $e_{1.6}$. Thus $n = 0.5$ may not be applicable for all the clayey soils with different plasticity and normalization factor influences the prediction.

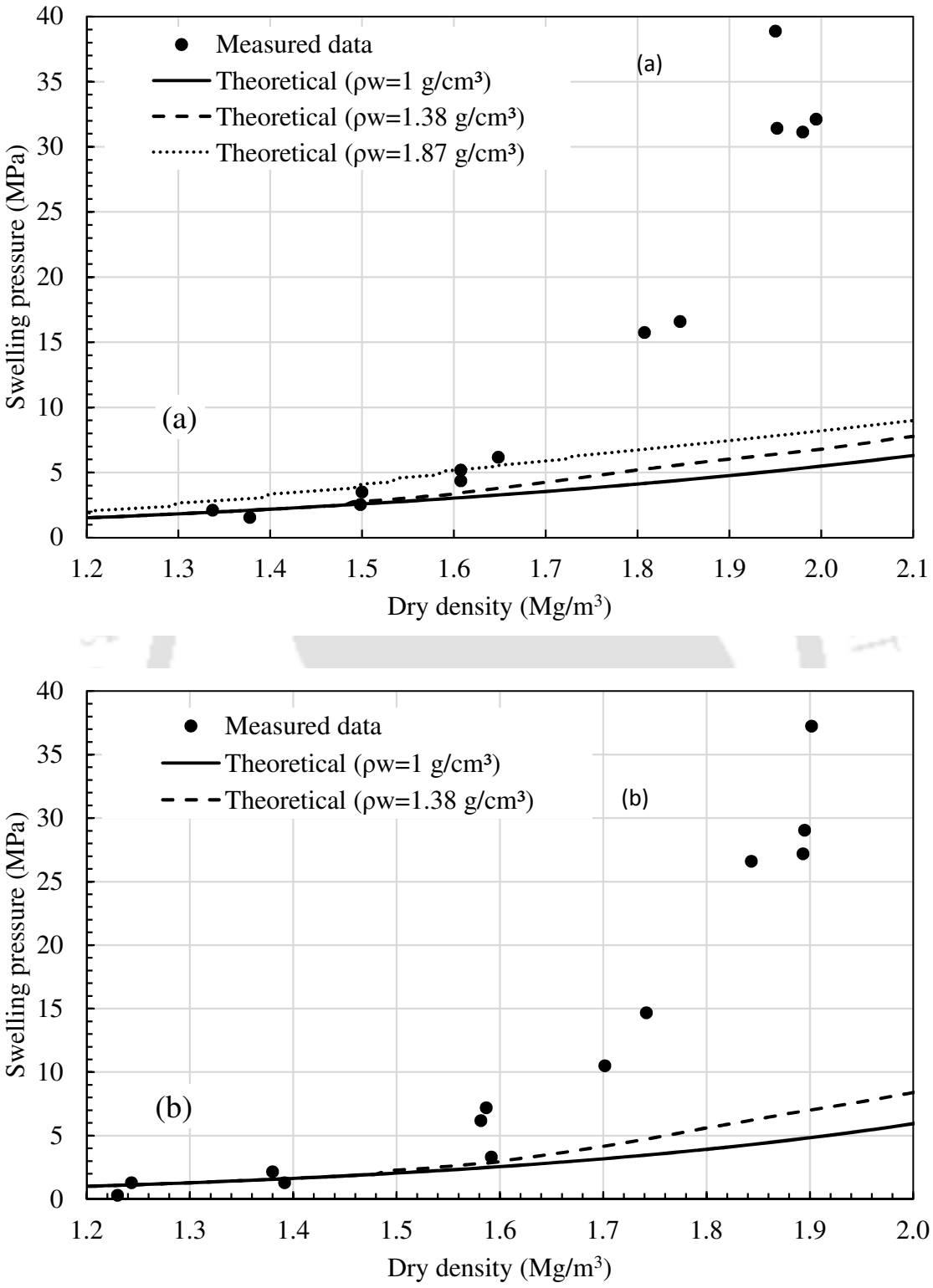

Figure 6.3. Measured and estimated swelling pressure-dry density curve of (a) MX80 bentonite (b) Montigel bentonite based on GC theory by changing the water density

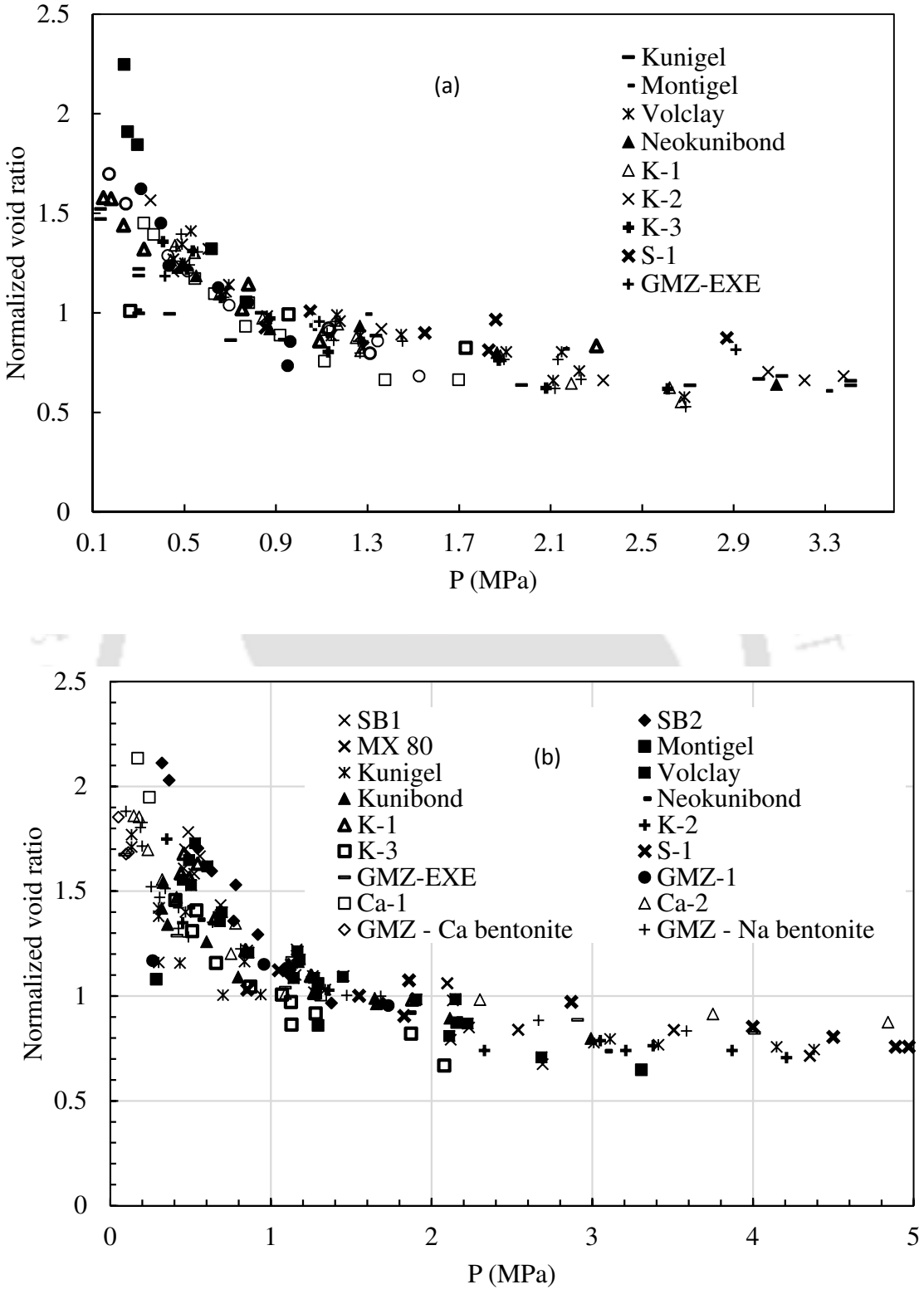

Fig. 6.4. Normalized compression curves using (a) $e_{0.8}$ and (b) $e_{1.6}$ as the normalizing factor

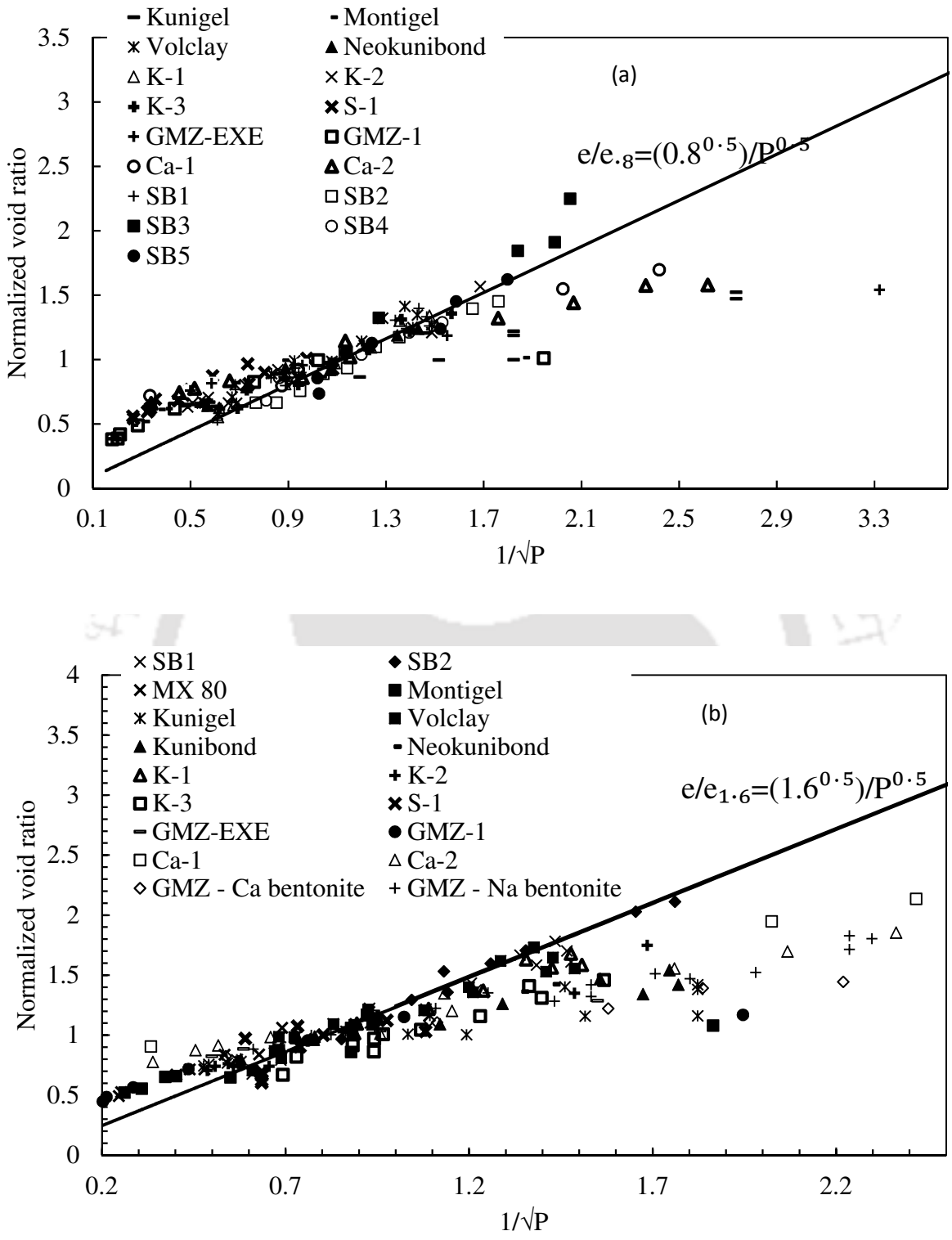

Fig. 6.5. Linearized swelling pressure data using void ratio at swelling pressures of (a) 0.8 MPa and (b) 1.6 MPa

6.5 PROPOSED APPROACH

As the swelling pressure is measured while maintaining a constant dry density in the constant volume swelling pressure tests, Eq. 6.1 was re-written in the following form in terms of dry density to develop the proposed predictive model for developing the theoretical swelling pressure – dry density curves:

$$P = P_{\rho_d^*}\left(\frac{G_s\rho_w - \rho_d^*}{G_s\rho_w - \rho_d}\right)^n \tag{6.2}$$

where P is the swelling pressure, $P_{\rho_d^*}$ is the swelling pressure at normalization dry density, ρ_d^*. The choice of the measured normalization data (ρ_d^*, $P_{\rho_d^*}$) and empirical factor, n, for the swelling curve prediction was explored here based on the knowledge of underlying swelling mechanisms. The prediction of compressibility curves for highly plastic clays in the earlier work (Bharat and Sridharan 2016a) is based on the yield point or the compressibility data point beyond the preconsolidation pressure (i.e., curvature change from concave to convex). The chosen data point anywhere beyond the preconsolidation pressure does not influence the compressibility prediction. However, such sharp distinction in the swelling pressure – dry density relationship is not observed for swelling pressure data which poses difficultly in choosing the normalization factor for the prediction of the swelling pressure – dry density curve. Three distinct zones in the swelling pressure variation with dry density were made as shown in Fig. 2a to circumvent this problem and to understand the influence of normalization data.

6.5.1 *Zoning*

The variation of swelling pressure with dry density was significantly low in zone–I, moderately high in zone–II, and significantly high in zone–III. The maximum dry density for zone–I was less than 1.45 Mg/m^3 for all the studied soils. The increase in swelling pressure with density was not significant for different soils in zone – I due to the presence of significant percentage of macro-voids in this density range. The macro voids nearly accommodates the increased volume of the aggregates due to hydration and diffuse double layer formation. This hypothesis is in accordance with the recent findings by Matusewicz and Olin (2019) that showed the perchlorate accessible (macro) pore volume is comparable to the macroscopic

porosity at low compaction densities for MX80. On the other hand, the interlamellar porosity (micro pore volume) increases with the density and approaches nearly macroscopic porosity at the lower bound value of zone – II for MX80 (Matusewicz and Olin 2019). The considered dry density range for zone–II varied between 1.45 – 1.7 Mg/m^3. Thus due to the availability of dominant micro-pore volume in the zone – II and zone – III, the pore volume is congested in accommodating the DDL formation which resulted in significant swelling pressure development. The dominance of hydration forces due to the availability of limited pore space for swelling in the density range considered for zone – III resulted in significantly high swelling pressures. The swelling pressures in this zone varied between 2 – 39 MPa for different clayey soils. The measured swelling pressures for MX80, Montigel and GMZ-1 were more than 30 MPa while for the swelling pressures of K-1, K-3, and sand-bentonite mixtures were less than 3 MPa. The laboratory measured swelling pressure for B1 and B2 showed a significant difference in zone-III while the difference was little in zone – I and II.

The influence of chosen normalization data on the estimated swelling curves was shown on two bentonites of different quality in Fig. 6.6a – 6.6b along with the measured data. A normalization factor, ρ_d^* , and the respective measured swelling pressure $P_{\rho_d^*}$ was considered from all the three zones (as shown in Fig. 6.6a – 6.6b) and using n = 0.5 in Eq. 9 for understanding the predicted swelling pressure change with the density. Normalization data for SB3 was not considered from zone – I as the measured swelling pressure data were available only in zone – II and zone – III for sand – bentonite mixtures (Komine and Ogata 2003). The variation in the predicted swelling curves was significant with the chosen normalization data for MX80, especially beyond zone – II (Fig. 7a), and the theoretical curves deviated from the measured data. The theoretical curves based on the normalization data from zone – I and II (i.e, ρ_d^* = 1.37 and 1.64 g/cm^3) severely underpredicted the measured swelling pressures in zone – III, but theoretical curve based on ρ_d^* = 1.64 g/cm^3 matched well in zone – I and II of the swelling pressure – dry density relationship. On the other hand, the variation to the theoretical curves is insignificant for SB3 based on different normalization densities. Further, the theoretical curves based on the normalization density from zone – II were more accurate when compared with the experimental counterparts. These results suggested that the empirical parameter is dependent on the soil plasticity. Further, the choice of the normalization dry density influenced the predicted curves if appropriate n was not considered. Thus a suitable

empirical parameter for different plastic clayey soils was explored using parametric analysis and by considering the normalization data from zone – II to capture different swelling mechanisms in the measured data. The swelling pressures of high – moderate plastic clays were ≥1 MPa in this zone and of low plastic clayey soils such as bentonite – sand mixtures were < 1 MPa in this zone.

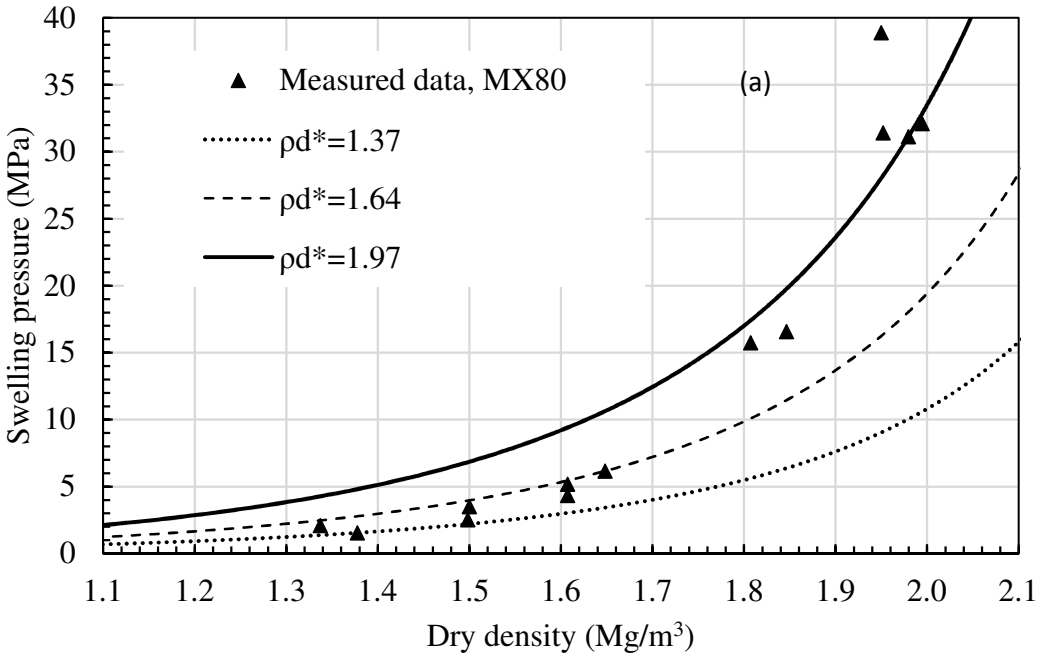

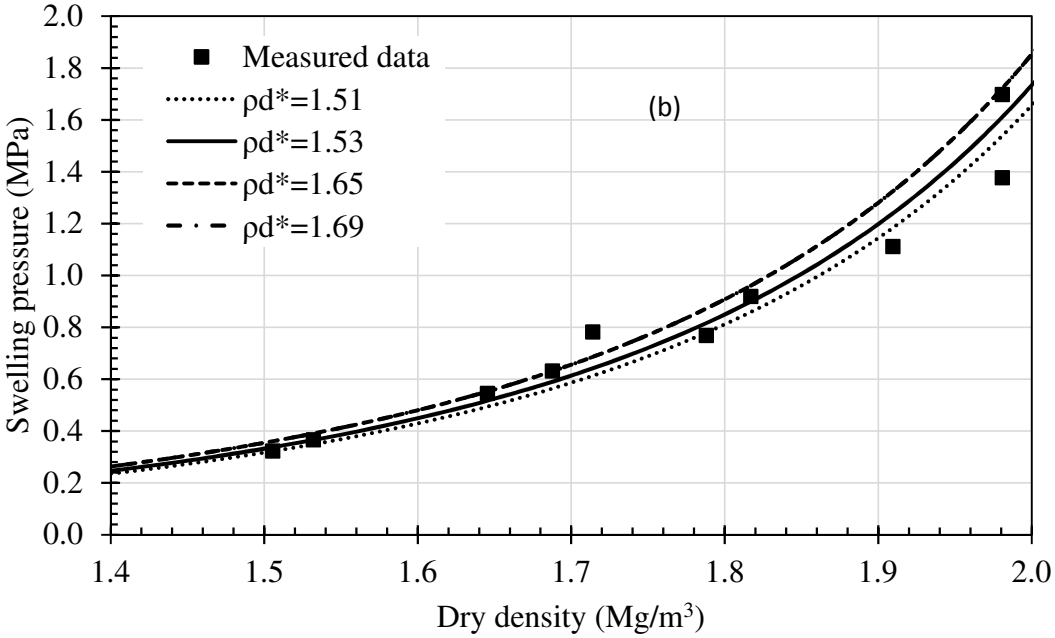

Figure 6.6. Variation of predicted swelling pressure curves using different normalization factors using n = 0.5 for (a) MX80 and (b) SB3

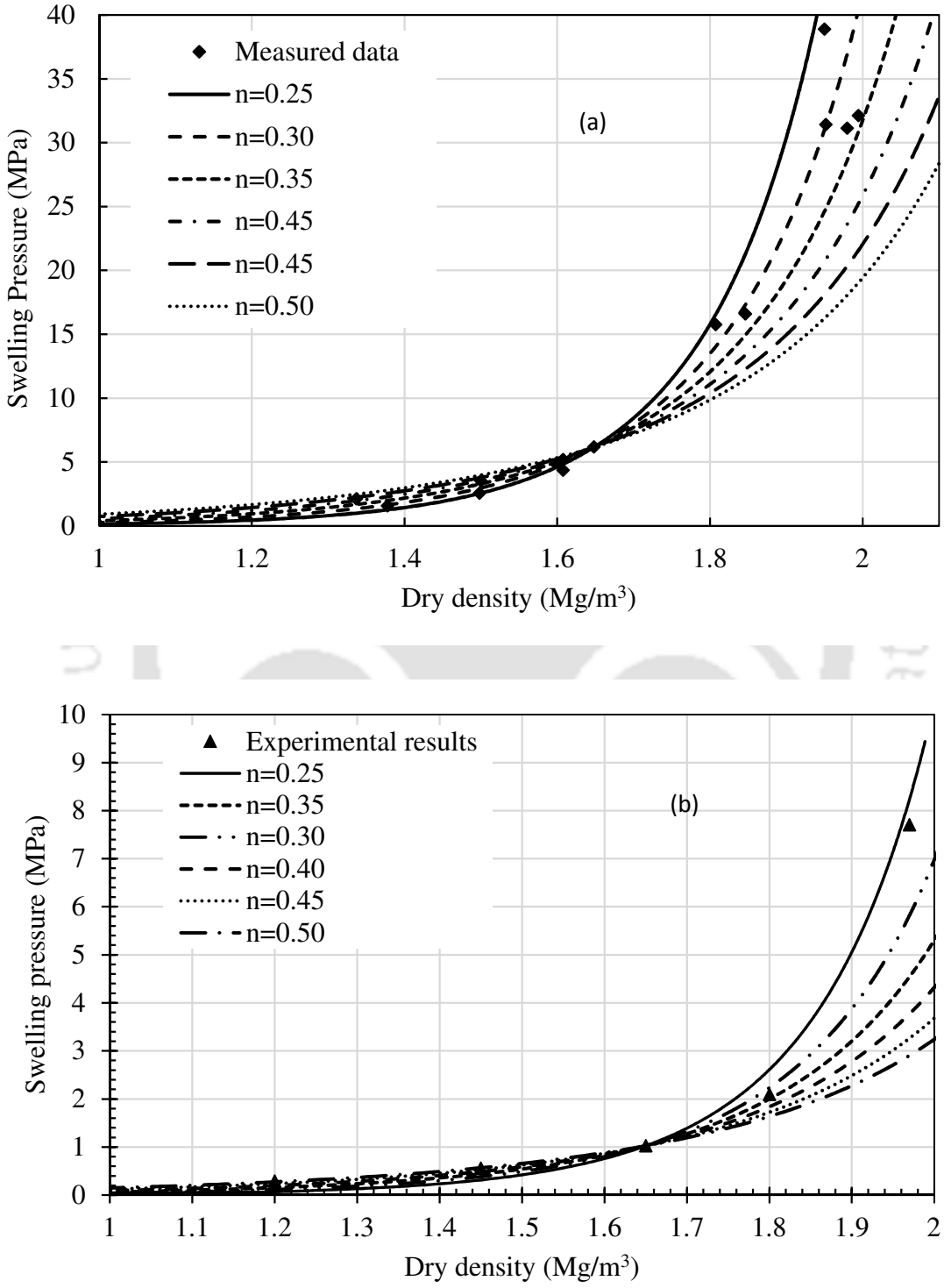

Figure 6.7. Theoretical swelling pressure – dry density curves by the predictive model using different empirical parameter (*n*) along with the experimental data of (a) MX80 (b) B1

6.5.2 *Parametric Analysis*

The experimental swelling pressure data of the bentonites B1, MX80, SB-2, and SB-3 were used in the parametric analysis for determining the appropriate '*n*' in the predictive model. The measured swelling pressure data of the remaining bentonites were used for the experimental validation of the proposed predictive model in the following section.

The theoretical swelling pressure-dry density curves based on Eq. 9 using different *n* values viz. 0.25, 0.3, 0.35, 0.4 and 0.45 were shown in Fig. 6.7a – 6.7b for high – medium quality bentonites such as MX80 and B1 (swelling pressure in zone – II ≥ 1 MPa), respectively, along with the measured data. The normalization data point (ρ_d^* , $P_{\rho_d^*}$) was selected from zone – II as mentioned earlier. The theoretical swelling curve with $n = 0.3$ was in good agreement with the measured data for high – moderate plastic clays considering the significant variability in the measured swelling pressure data. Theoretical curves with $n \neq 0.3$ overestimated the swelling pressures in zone – I and underestimated in zone – III. Thus the appropriate empirical constant for high – moderate plastic clays, whose swelling pressure is more than 1 MPa in zone – II, was found to be $n = 0.3$.

Theoretical swelling pressure curves of low plastic clayey soils such as SB2 and SB3 by varying *n* between *0.25* and *0.5* were presented in Fig. 6.8a – 6.8b. The swelling pressures of these bentonites in zone – II were less than or equal to 1 MPa. The theoretical curve corresponding to $n = 0.5$ showed good agreement with the measured data and theoretical curves based on other *n* values severely overpredicted the swelling pressures in Zone – III. This was also evident in the linearization data shown earlier in Fig. 6.5. Based on the parametric analysis and governing mechanisms for the swelling pressure development at different compaction densities, the following procedure was proposed for the estimation of swelling pressure – dry density curve theoretically based on single measured swelling pressure in zone – II.

i. Determine the swelling pressure of a given clayey soil at any dry density from zone – II (1.45 g/cm^3 ≤ ρ_d ≤ 1.7 g/cm^3). This measured data point (ρ_d^* , $P_{\rho_d^*}$) was used as normalization data in Eq. 6.9.

ii. Adopt *n* value from the following two cases based on the measured swelling pressure value corresponding to the chosen density from zone – II.

Case 1: If swelling pressure $P_{\rho_d^*}$ > 1 MPa, *n = 0.3*

Case 2: If swelling pressure $P_{\rho_d^*}$ ≤ 1 MPa, *n = 0.5*

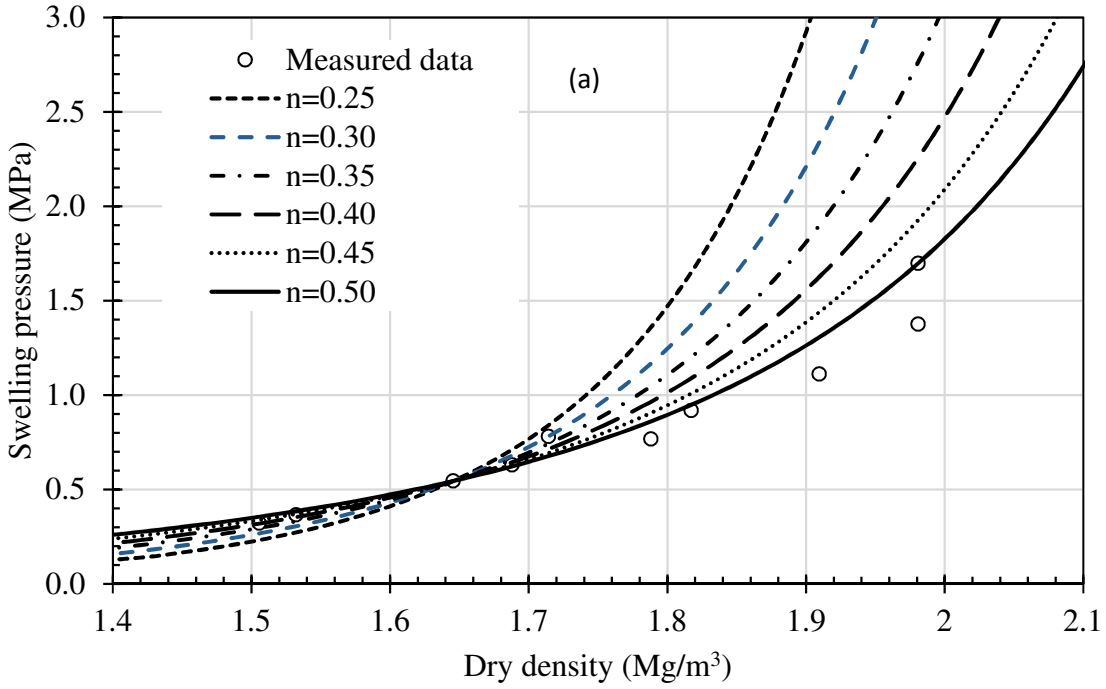

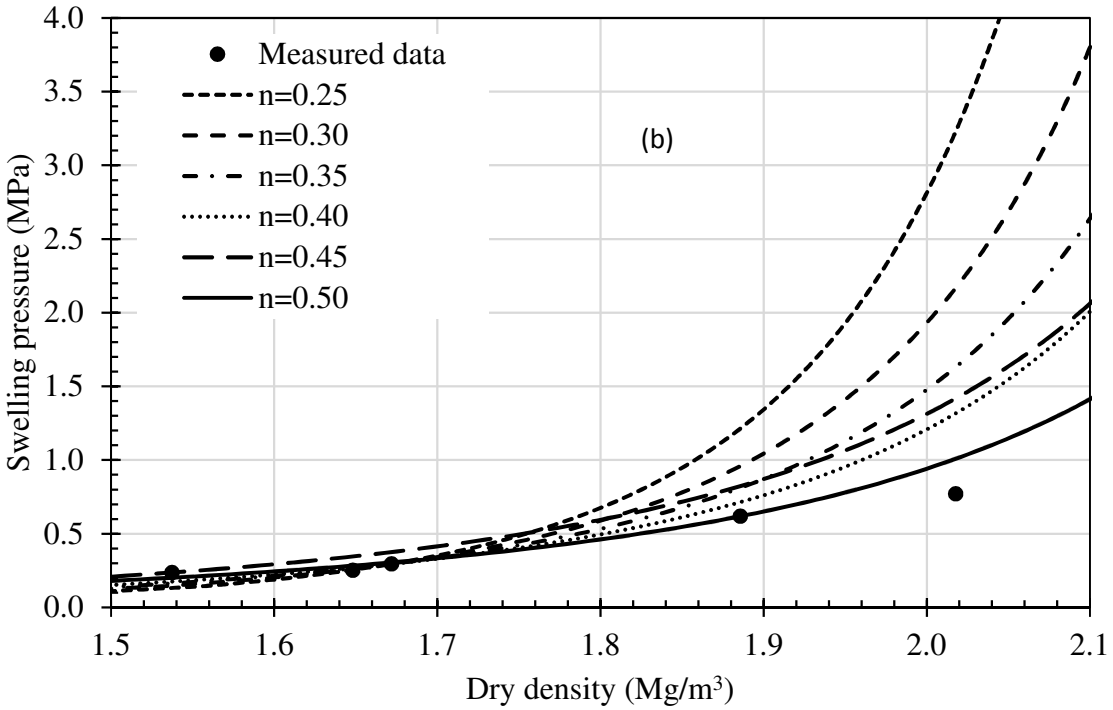

Figure 6.8. Theoretical swelling pressure – dry density curves by the predictive model using different empirical parameter (n) along with the experimental data of (a) SB2 (b) SB3

6.6 EXPERIMENTAL VALIDATION

The proposed procedure was validated on the measured swelling pressure data of fifteen different bentonites and bentonite – sand mixtures that were not used in the parametric analysis. The theoretical curves along with the measured swelling pressure data only for selected bentonites and bentonite – sand mixtures were presented for brevity through Fig. 6.9a–6.9g. The proposed procedure required only a single measured swelling pressure data point corresponding to a dry density from zone – II for the normalization. The normalization data used for the prediction in Eq. (6.2) were shown with open circle (○) in all of the figures. The empirical constant for these bentonites was chosen based on the measured swelling pressure value in zone – II and following the proposed procedure. The bentonites B2, GMZ-EXE, GMZ-1, K-2, Montigel, Calcigel-2, Kunibond, Volclay, GMZ-Na, and GMZ-Ca were considered to be the clays with high – moderate plasticity as per the swelling pressure values in the zone – II. The swelling pressure for all these bentonites in zone-II was higher than 1 MPa and thus n = 0.3 (i.e., case 1) was used in the predictive equation. Theoretical swelling

pressure vs dry density curves along with the measured data was shown for B2, K-2, Volclay, Kunibond, and GMZ-Na in Figs. 6.9a – 6.9e. The R^2 data for all the studied clayey soils were presented in figure legend and Table 6.1. The prediction was found to be extremely good for all the studied high – moderately plastic clays. Further, validation for the low plastic bentonite and bentonite – sand mixtures was done using $n = 0.5$ as the swelling pressure values in zone – II was less than 1 MPa. Theoretical swelling pressure curves for K-3 and SB-1 were presented in Figs. 6.9f – 6.9g and showed a very good agreement with the measured data. The R^2 varied between 0.80 – 0.99 (Table 6.1) for all the studied bentonite and bentonite – sand mixtures. The prediction was extremely good considering the several factors involved in laboratory measurements of swelling pressures.

The predictive model proposed for the clayey soils of different plasticity was, therefore, very useful for predicting the swelling pressure data over a wide range of dry densities using a single data point from the constant volume swelling pressure test carried out at any chosen dry density in zone-II (i.e., 1.45 Mg/m^3 < ρ_d < 1.7 Mg/m^3). The proposed model is very simple considering that the prediction requires only a single swelling pressure value and corresponding dry density.

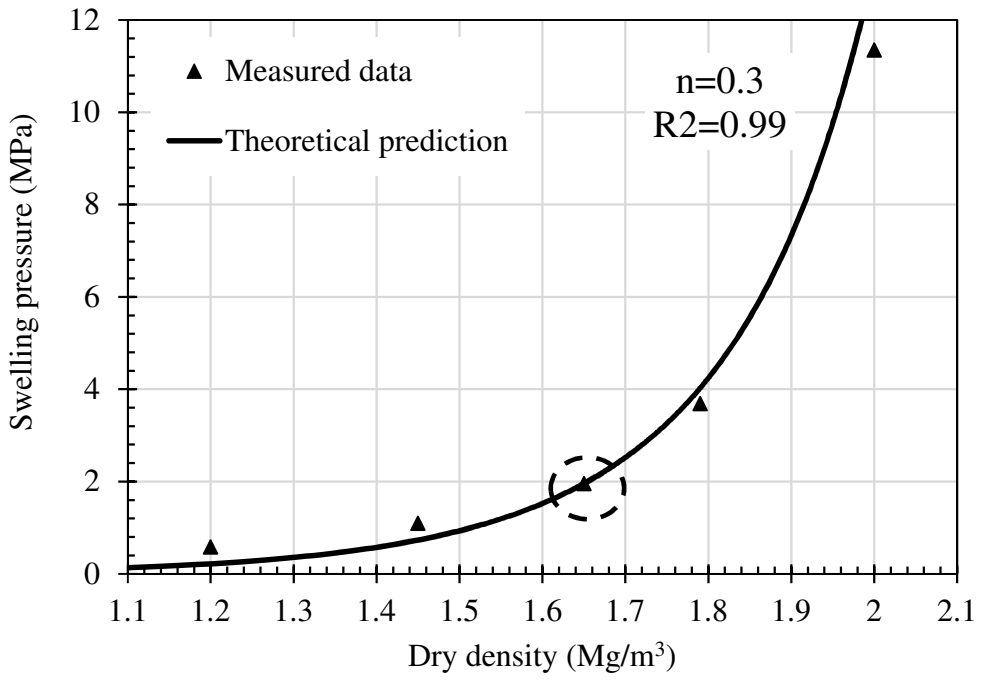

Figure 6.9a. Measured and predicted result of B2

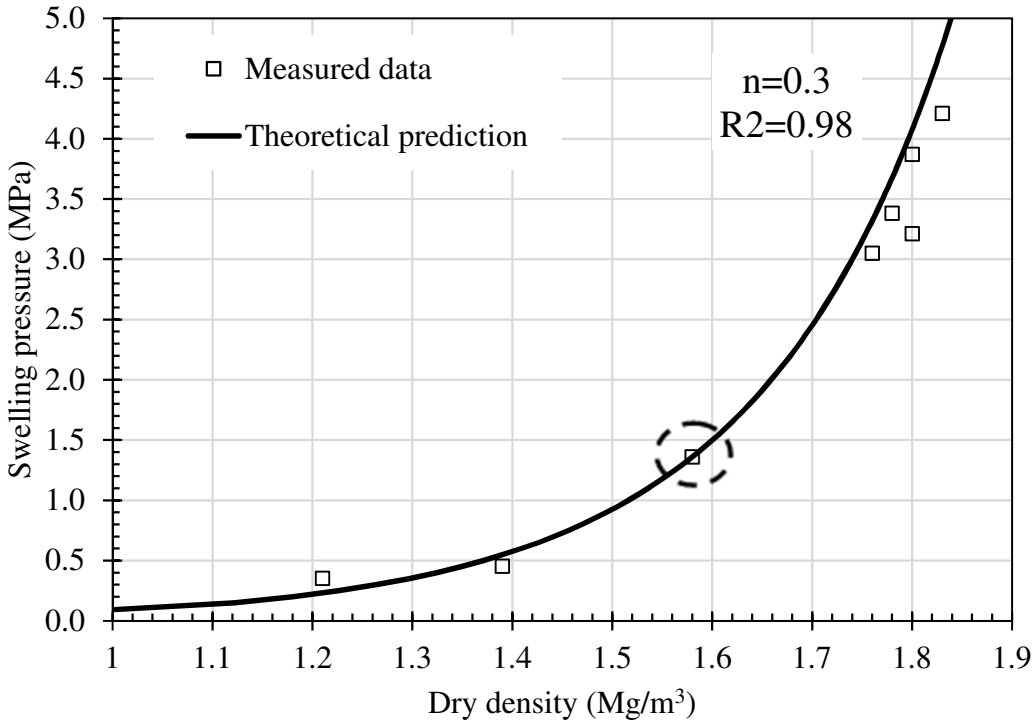

Figure 6.9b. Measured and predicted result of Kunigel-2 (K-2)

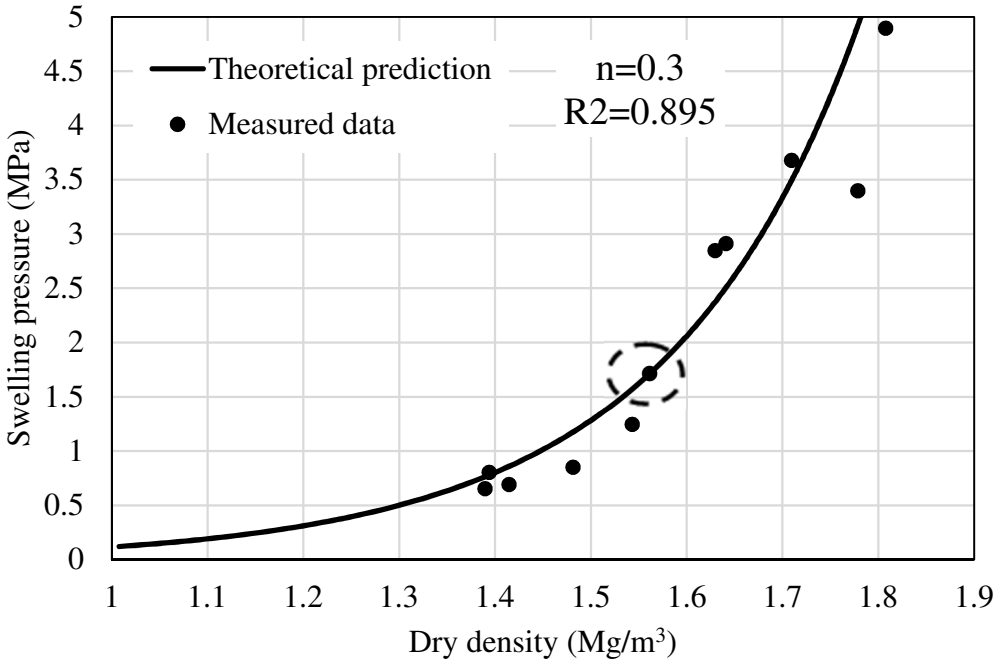

Figure 6.9c. Measured and predicted result of Volclay

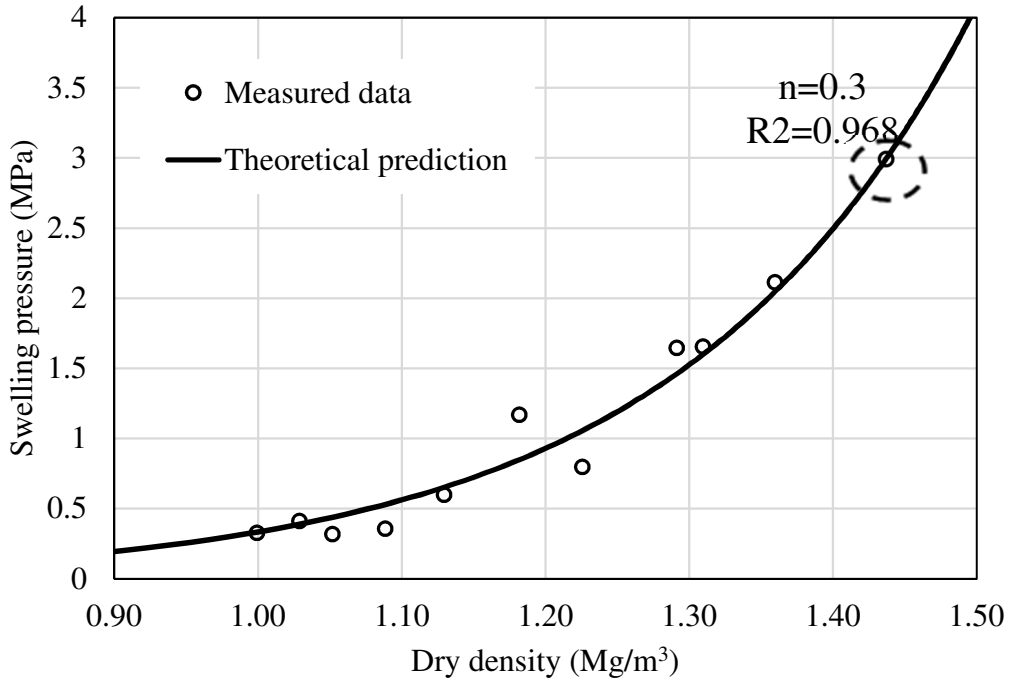

Figure 6.9d. Measured and predicted results of Kunibond

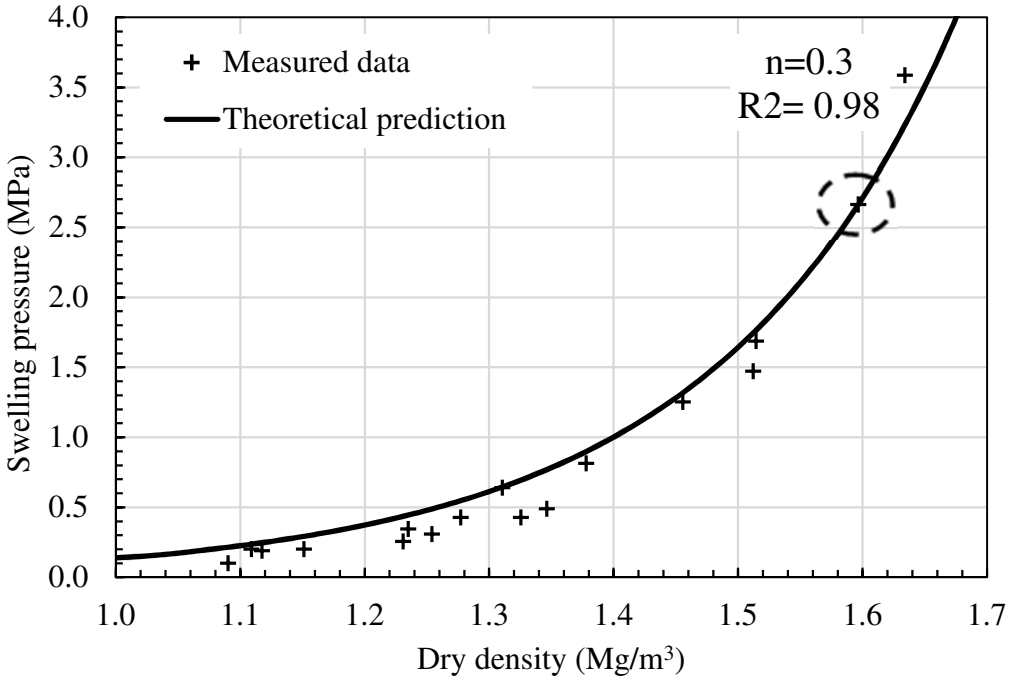

Figure 6.9e. Measured and predicted results of GMZ-Na bentonite

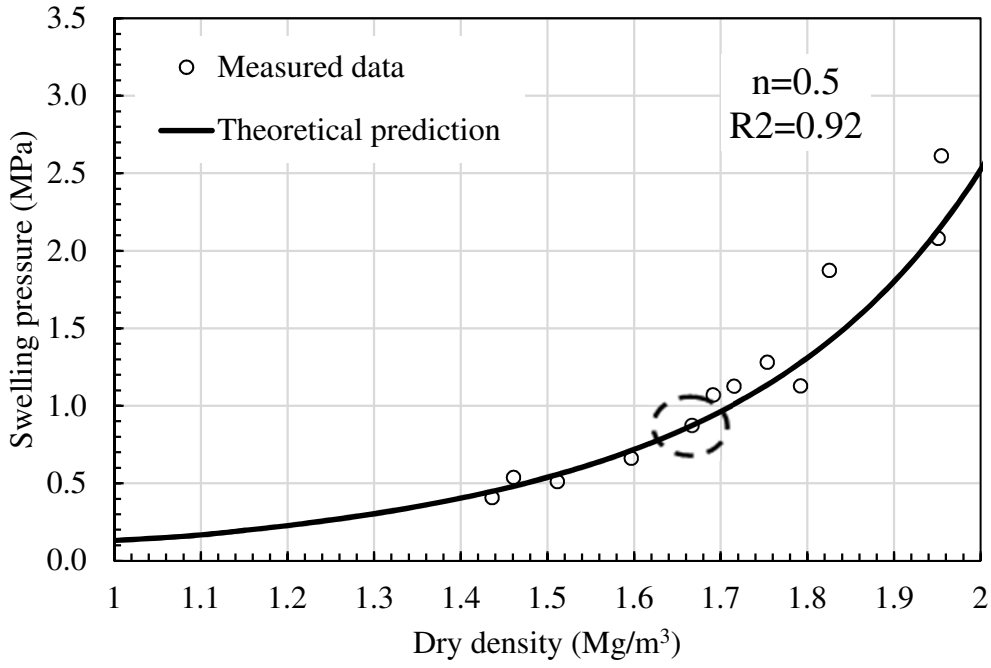

Figure 6.9f. Measured and predicted result of Kunigel-3 (K-3)

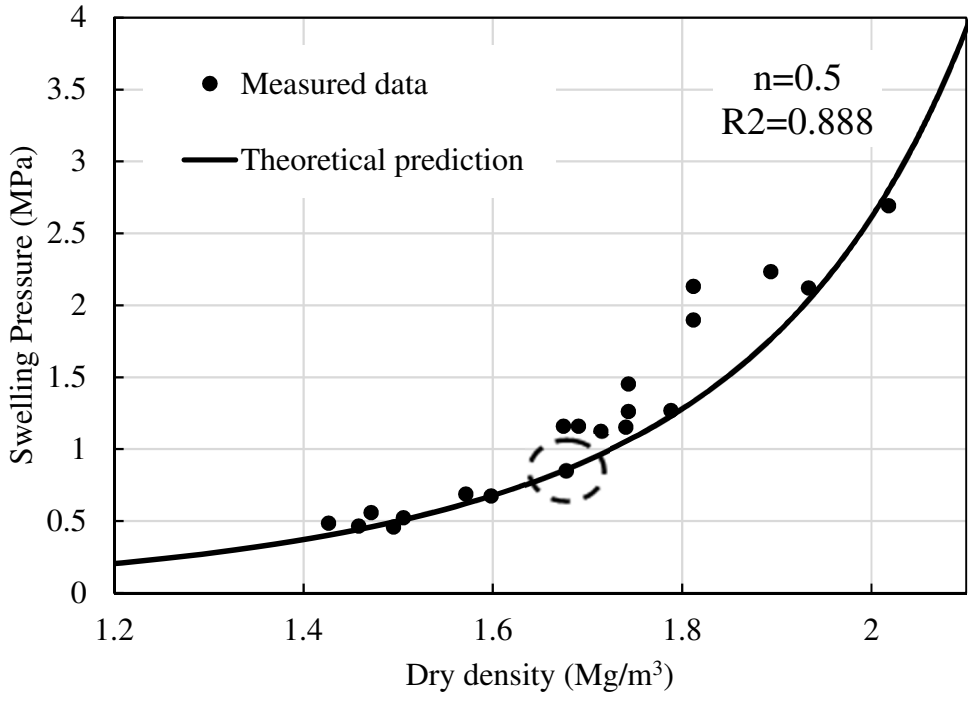

Figure 6.9g. Measured and predicted results of SB1 bentonite

Table 6.1: Coefficient of determination (R^2) values for the theoretical prediction on the experimental data

S. No.	Clay type	R^2
1	B1	0.98
2	B2	0.99
3	MX80	0.95
4	K-1	0.94
5	K-2	0.98
6	K-3	0.92
7	Montigel	0.95
8	Calcigel-2	0.92
9	GMZ-EXE	0.97
10	GMZ-1	0.98
11	Volclay	0.89
12	Kunibond	0.96
13	GMZ-Na	0.98
14	GMZ-Ca	0.98
15	SB1	0.88
16	SB2	0.82
17	SB3	0.94
18	SB4	0.80
19	SB5	0.94

CONCLUDING REMARKS

The measured swelling pressure–dry density data of the bentonites from the literature studies along with the Indian bentonites B1 and B2 were studied. Three zones were identified in the swelling pressure curve based on the development of swelling pressure. A new method based on linearization of the swelling pressure data was proposed for the prediction of swelling pressure characteristics. The proposed method is useful for the accurate estimation

of swelling pressures for different bentonites for the possible application in HNW repositories. The proposed model considered the influence of quality of clayey soil and associated mechanisms in the swelling pressure variation with density for the prediction. This method is also helpful in the quick estimation of approximate swelling pressure vs. dry density relationship of different bentonites based on the qualitative estimation of swelling pressures in zone – II based on the bentonite plasticity without undertaking the rigorous experimentation.

CHAPTER 7
EFFECTIVE STRESSES OF CLAYS OF DIFFERENT ACTIVITY UNDER DIFFERENT HYDRO-MECHANICAL LOADS

7.1 General

The effective stress variation in clays of different minerology/activity under hydro-mechanical loads was studied in this Chapter. Three series of suction-controlled tests were considered for understanding the effective stress development using the suction stress approach. In the first series of tests, the drying behavior of slurried kaolin and mixtures of

kaolin – B2 bentonite clays were considered. Two clay mixtures viz. MKB1 consists of 75% kaolin and 25% B2 bentonite, and MKB2 consists of 50% kaolin and 50% B2 bentonite, were used in these tests. The VSC and drying SWCC of initially slurried clays were established by conducting a series of volumetric shrinkage and suction controlled tests as described in **Chapter 3** for understanding the effective stress development due to drying using suction stress concept. The second series of experiments consisted of suction controlled swelling pressure and SWCC tests for ascertaining wetting SWCCs in isochoric conditions. The last series consisted of suction-controlled, wetting induced collapse tests on compacted kaolin under different inundation pressures. The suction stresses and effective stresses in kaolin, bentonite, and kaolin – bentonite mixtures were analyzed under the studied hydro-mechanical conditions.

7.2 Suction stress and effective stress of clays

The effective stress of the slurried clay and the compacted specimen was calculated using the concept of suction stress proposed by Lu et al. (2006). Suction stress refers to the net inter-particle force generated within the unsaturated soil matrix due to the combined effects of negative pore water pressure and surface tension. The relation between suction stress and volumetric water content is known as the suction stress characteristics curve (SSCC). Mathematically, suction stress (σ^S) is expressd as a product of effective degree of saturation (S_e) and matric suction.

$$\sigma' = (\sigma - u_a) - \sigma^S$$

$$\sigma^S = -\left[\frac{S - S_r}{1 - S_r}(u_a - u_w)\right]$$

$$= -S_e(u_a - u_w) \qquad (7.1)$$

where, u_a is the pore air pressure, w_u is the pore water pressure, and u_a-u_w is the matric suction.

7.2.1 Volumetric shrinkage curve

Figure 7.1 presents the volumetric shrinkage data of slurried kaolin, MKB1, and MKB2 from the shrinkage box tests. The VSC data of all the slurried clays were presented in terms of water content against total volume. It was observed that volume change due to drying increased with the increase in the bentonite percentage. The kaolin specimen reached shrinkage limit state earlier than the clay mixtures containing different percentages of

bentonite clay. The shrinkage limit was considered to be the water content at which the volume change was zero with a change in water content. The observed shrinkage limit water contents for kaolin, MKB1, and MKB2 were 28%, 20%, and 15%, respectively. The shrinkage limit of soil decreased with the increase in bentonite content. The shrinkage rate, however, was found to be similar for these three cases.

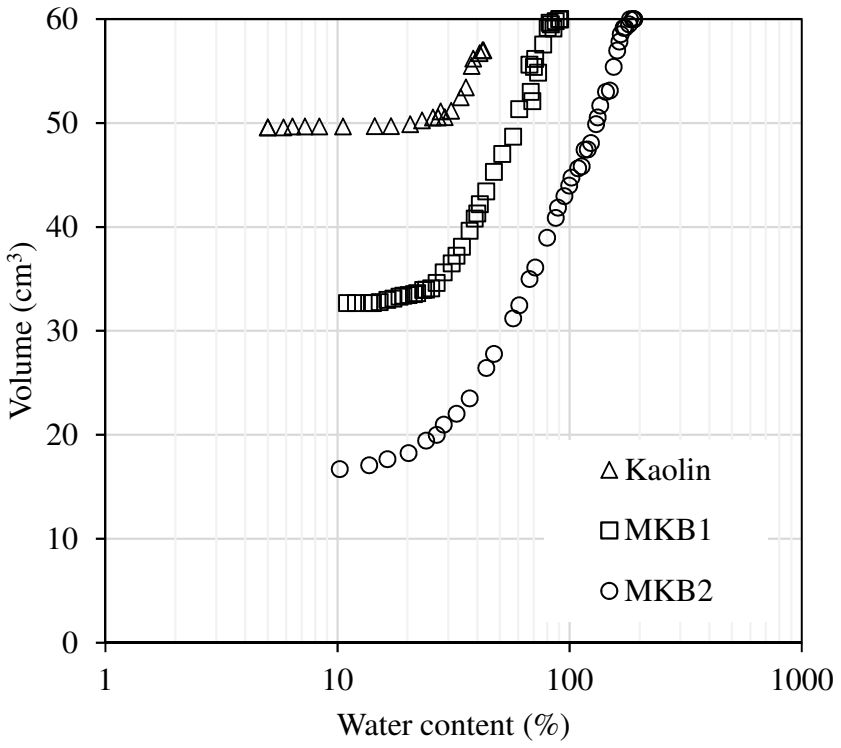

Fig. 7.1. VSC data of slurried clays

7.2.2. Suction stresses

The SWCC data in terms of degree of saturation vs. suction (ψ) were obtained for kaolin and clay mixtures in Fig. 7.2 using the SWCC data of θ vs. ψ and VSC data of Fig. 7.1. The suction value of a clay mixture at a given saturation increased significantly with the increasing bentonite content in the mixture. The air-entry value (AEV) of the mixture was also increased with increase in the bentonite content. Air-entry value of soil represents the suction corresponding to the air-entry into the largest pore of the soil. The increase in AEV indicates the increase in fineness of soil. The AEV of kaolin is around 0.6 MPa whereas for MKB2,

where 50% of the mixture contained B2, the value was 4 MPa. The residual zone was distinct for kaolin but was indistinct for mixtures containing bentonite. The SWCC response of mixtures was qualitatively similar to bentonites as shown elsewhere (Gapak and Bharat 2018). The drying SWCC data using degree of saturation vs. ψ representation (Fig. 7.2) were used to understand the development of effective stresses during the drying process by the suction stress approach for the clays from the initial slurry state. Figure 7.3 presents the SSCC of different clay mixtures based on the effective degree of saturation. A value of 0.094 was used for residual degree of saturation for kaolin and zero for the mixtures. A variation of 0.094 – 0.14 did not influence the SSCC behavior. The negative suctions stress ($-\sigma'$) is equal to the effective stress in this case due to zero external stress. The SSCCs of clays and clay mixtures of this study were qualitatively similar to SSCCs of sands, silts, Spergau kaolin and NX illite in the past studies by Lu et al (2010) and Baille et al (2014). The magnitude of suction stress induced in Indian kaolin due to drying was quantitatively comparable to Spergau kaolin and the induced stresses in MKB2 were smaller than NX illite (Baille et al. 2014). Suction stress decreased (i.e., negative values on x-axis) with increasing suction by following 1:1 line until the suction reached (a minimum value) slightly higher than the bubbling pressure (i.e., AEV) of the respective clay. The minimum values of suction stress increased (higher negative value) with the addition of percentage bentonite in the clay mixture. Further increase in the suction decreased the degree of saturation (Fig. 7.2) and simultaneously increased the suction stress (or decreased the effective stress) for all the clays. The characteristic increase-and-decrease behavior of the SSCC for the kaolin clay might have been due to the dominant influence of surface tension forces and forces arising from the negative pore water pressure at high suction values (Baille et al. 2014). However, the increase in percentage of bentonite in clay mixture did not influence the qualitative nature of the SSCC behavior suggesting insignificant local forces effect as opposed to the observed plastic characteristics of the kaolin – bentonite mixtures.

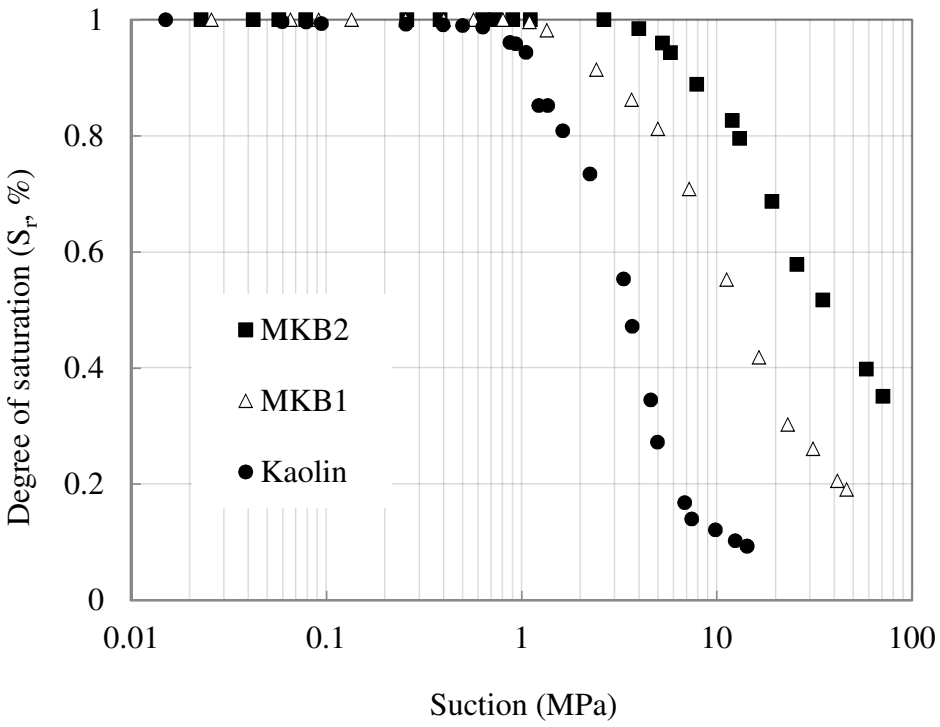

Fig. 7.2. Drying SWCCs of slurried clays

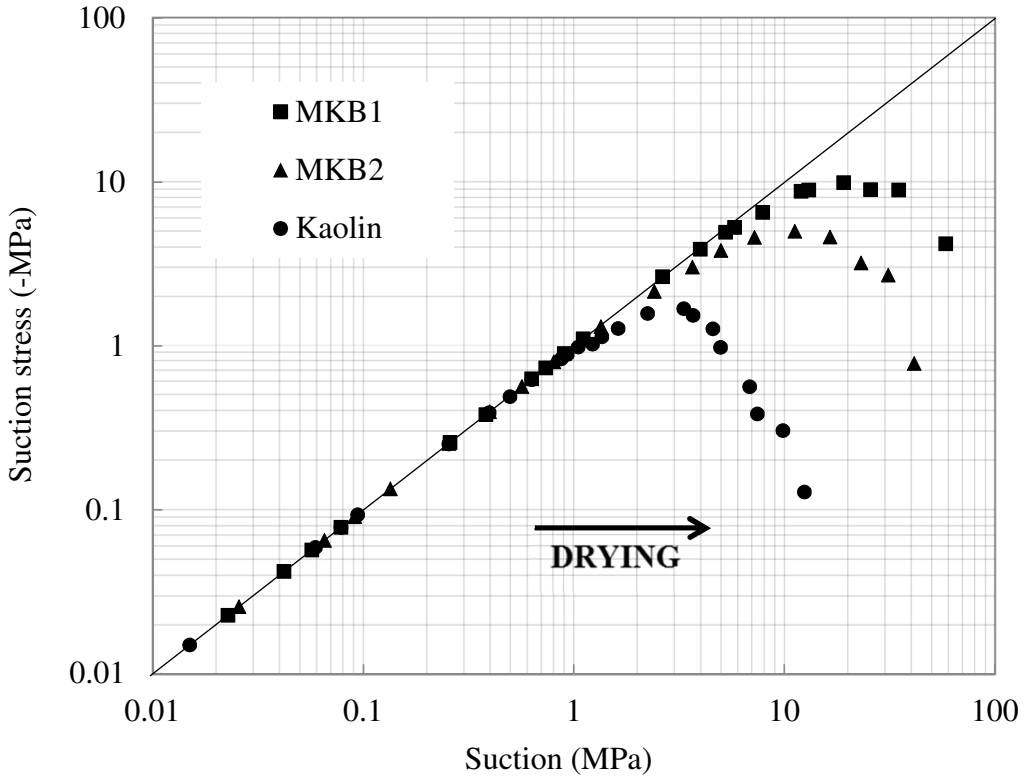

Fig. 7.3. Suction stress characteristic curves of clays during drying

7.3 Wetting induced effective stresses in compacted bentonite

The suction-controlled swelling pressure tests were conducted, for estimating the swelling pressure change with suction, by controlling the suction in the range of 90 – 5000 kPa. The swelling pressures evaluation with time under different controlled suctions for B1 bentonite at ρ_d = 1.45 Mg/m^3 were presented in Fig. 7.4. The swelling pressure evolution data with distilled water without suction control was also presented along with the other results for comparison. The swelling pressure evolution curves for different suctions followed independent paths due to the restriction on the water availability for larger pores whose suction values are smaller than the applied suction. The swelling pressure evolution with time for suction values $\psi \leq 296$ kPa showed a bimodal behavior similar to the case with distilled water as presented in **Chapter 5**. The development of swelling pressure was delayed with increase in the suction. A measurable swelling pressure was recorded only after ~6.5 hrs with suction value of 4391 kPa. The suction controlled tests were stopped after 14 days even though the swelling pressure data at higher suction values showed an increasing trend due to the limitations associated with the osmotic technique. The cellulose acetate membrane degrades due to microbial attack after 14 days (Tripathy et al. 2011).

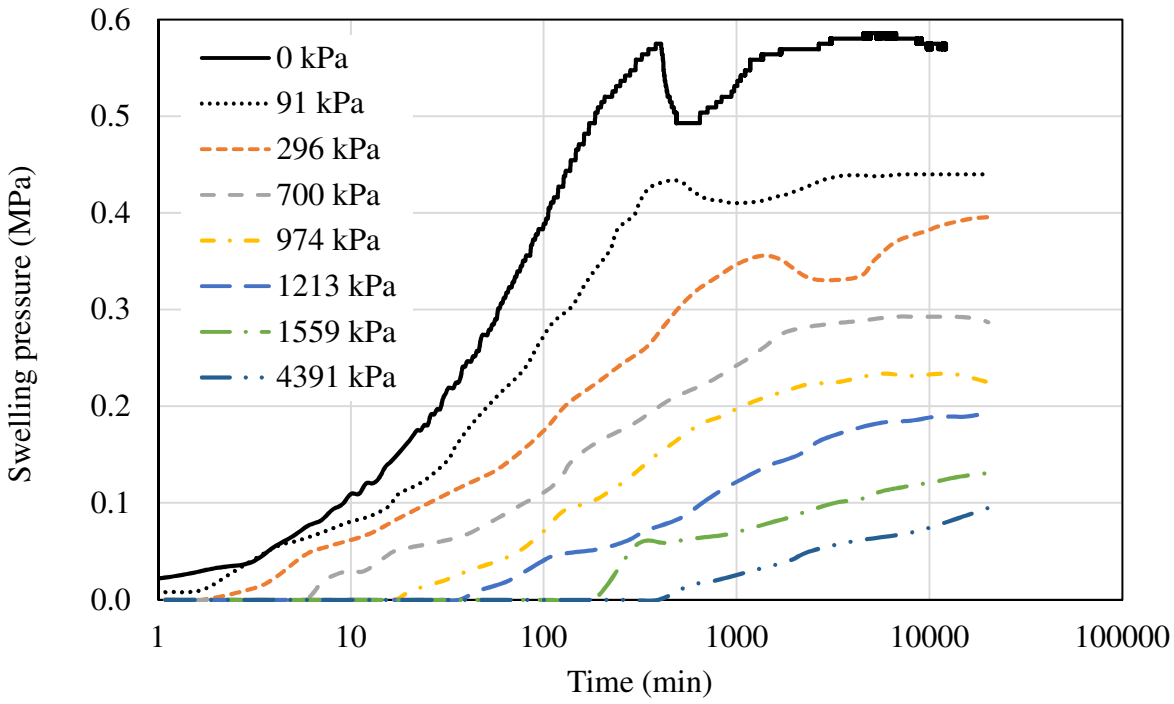

Fig. 7.4. Swelling pressure evolution with time for bentonite B1 at ρ_d = 1.45 Mg/m^3 at different suction values

The SWCCs in terms of suction vs. degree of saturation for B1 and B2 bentonites, compacted at two dry densities of 1.45 and 1.8 Mg/m^3, were shown in Fig. 7.5 – 7.6. The swelling pressure variations with suction from the suction-controlled osmotic tests for different bentonites and densities were also presented in the same figures utilizing the third axis. Degree of saturation for the bentonites compacted at 1.45 Mg/m^3 dry density, however, did not reach 100% saturation in the lower suction range, suggesting more amount of required time for reaching the hydraulic equilibrium, albeit swelling pressures reached an equilibrium value as shown in Fig. 7.4. The aging of cellulose acetate membranes (Tripathy et al. 2011) limited the suction-controlled swelling pressure tests to only 14 days. On the other hand, the computed degree of saturation of bentonites compacted at 1.8 Mg/m^3 based on the measured water contents for $\psi \leq$ 1000 kPa was more than 100%. The error in the computed degree of saturation arises from using a constant water density of 1 Mg/m^3. Several studies in the literature reported increasing the water density to a value between 1.4 and 1.872 Mg/m^3 (Martin 1960; Villar and Lloret 2008; Zhang and Lu 2018) depending on the soil compaction effort and bentonite plasticity. The degree of saturation values were thus adjusted to 100%

when the computed saturation values were higher than 100%. The swelling pressure continuously decreased with increasing suction similar to the degree of saturation for lower densities (Fig. 7.5a and 7.6a). On the other hand, the swelling pressure decreased with increasing suction while the clay remained saturated with degree of situation value of 100% (Fig. 7.5b and 7.6b).

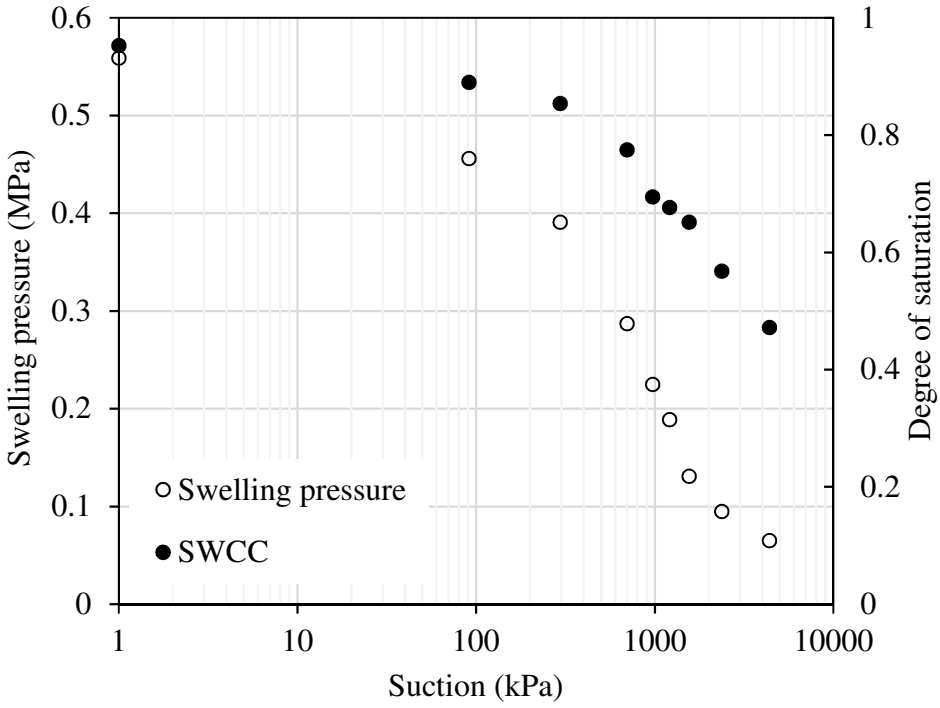

Fig. 7.5a. Swelling pressure and degree of saturation variation with suction for B1 at ρ_d= 1.45 Mg/m^3

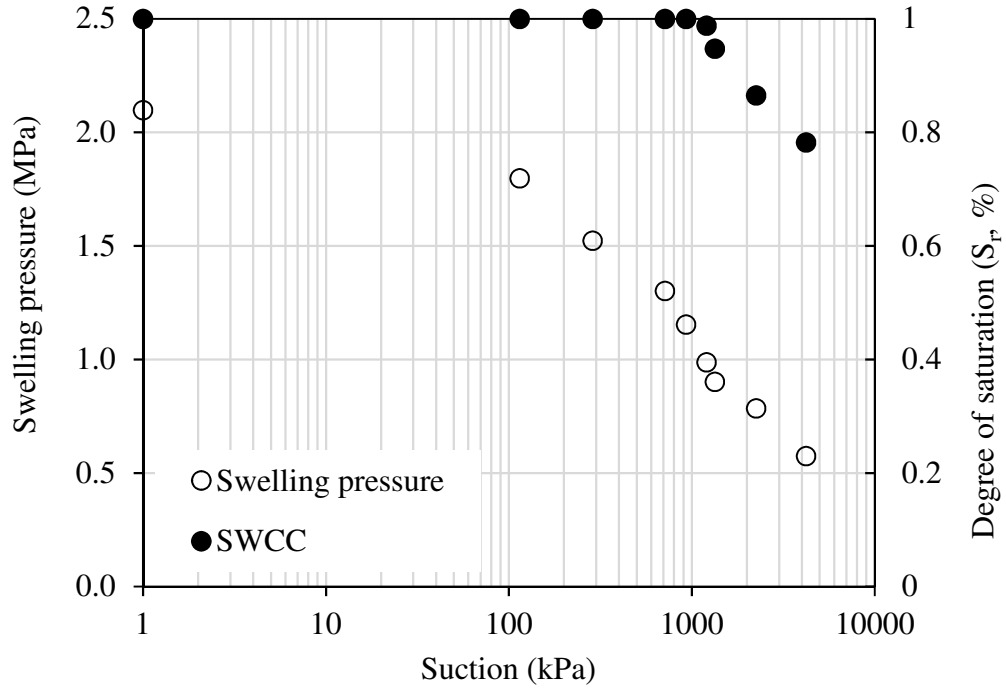

Fig. 7.5b. Swelling pressure and degree of saturation variation with suction for B1 at ρ_d= 1.8 Mg/m^3

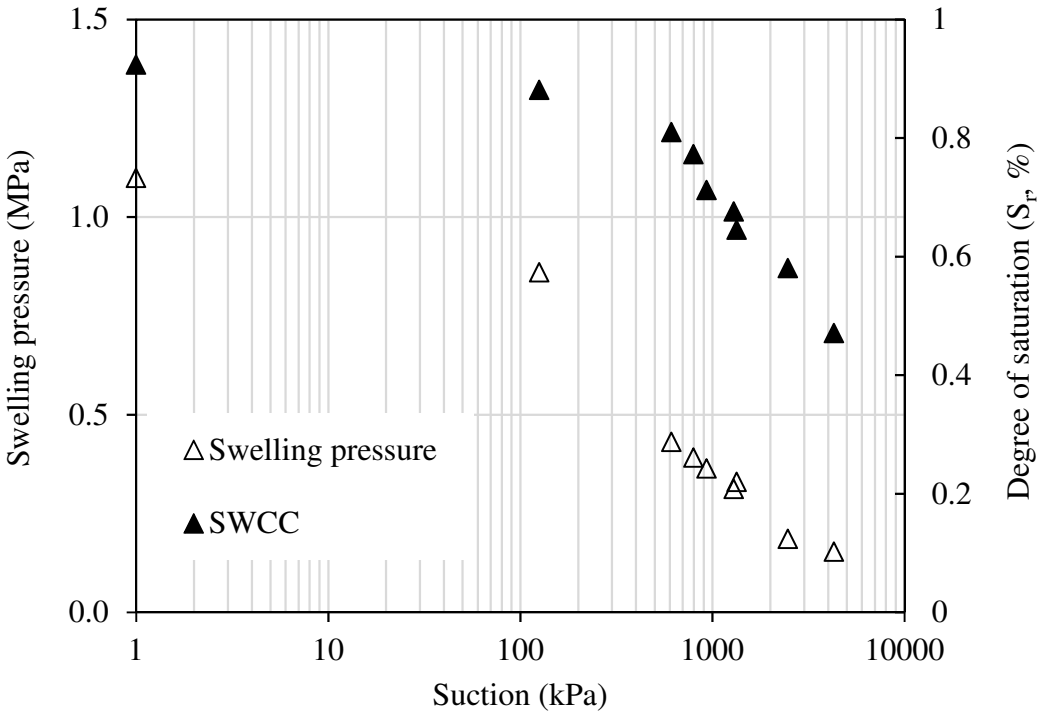

Fig. 7.6a. Swelling pressure and degree of saturation variation with suction for B2 at ρ_d= 1.45 Mg/m^3

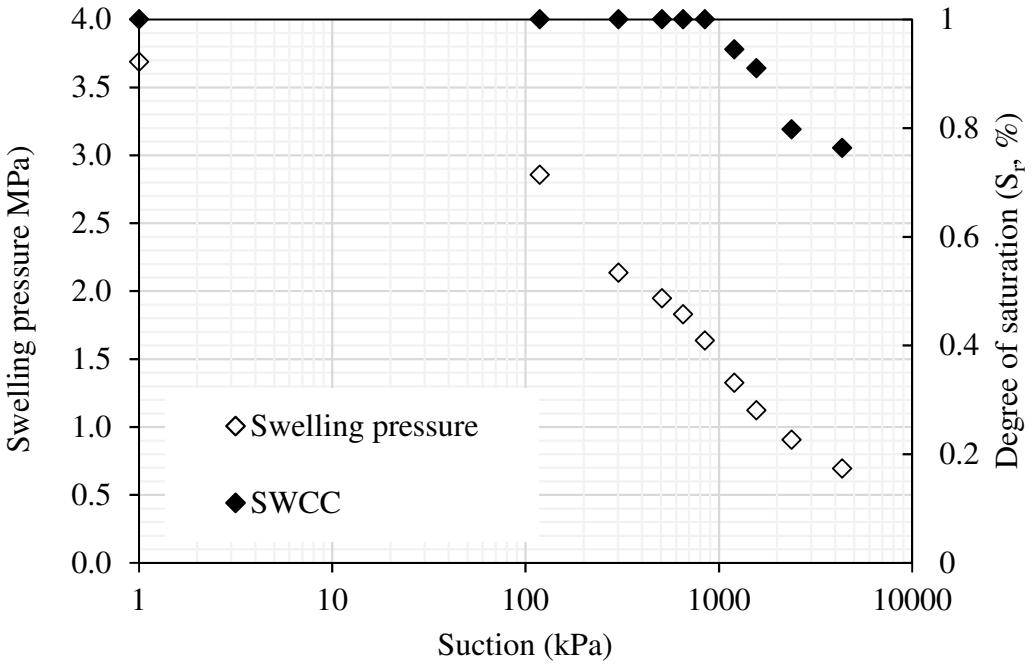

Fig. 7.6b. Swelling pressure and degree of saturation variation with suction for B2 at ρ_d= 1.8 Mg/m^3

Combined plots showing the influence of suction on the suction stress, effective stress, and swelling pressure were presented in Fig. 7.7 – 7.8 for the studied bentonites and two compaction densities. The suction stress decreased with increase in suction up to 2.5 MPa for bentonites compacted at lower densities, but increased with further increase in suction. The effective stress, on the other hand, increased with suction up to a maximum value of 560 kPa, but started decreasing beyond that suction albeit the swelling pressure decreased continuously (Fig. 7.7a and 7.8a). The results were distinctly different for bentonites compacted at higher density. The suction stress decreased with increase in suction linearly following 1:1 line up to 1.3 MPa, but showed decreasing trend at higher suctions also. The effective stress simultaneously increased with suction throughout (Fig. 7.7b and 7.8b). The results were distinctly different for bentonites compacted at higher density. The results for bentonites with

higher compaction density were consistent with Calcigel bentonite results from Baille et al. (2016).

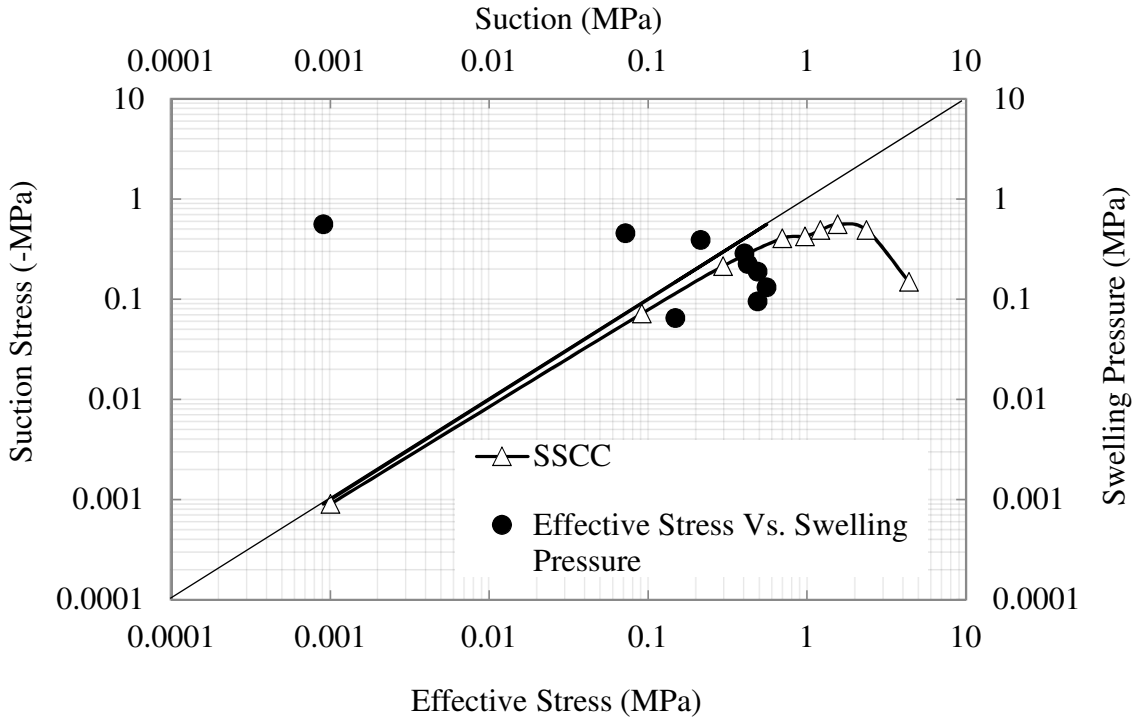

Fig. 7.7a. Variation of suction stress, effective stress, and swelling pressure with suction for B1 at ρ_d = 1.45 g/cm^3

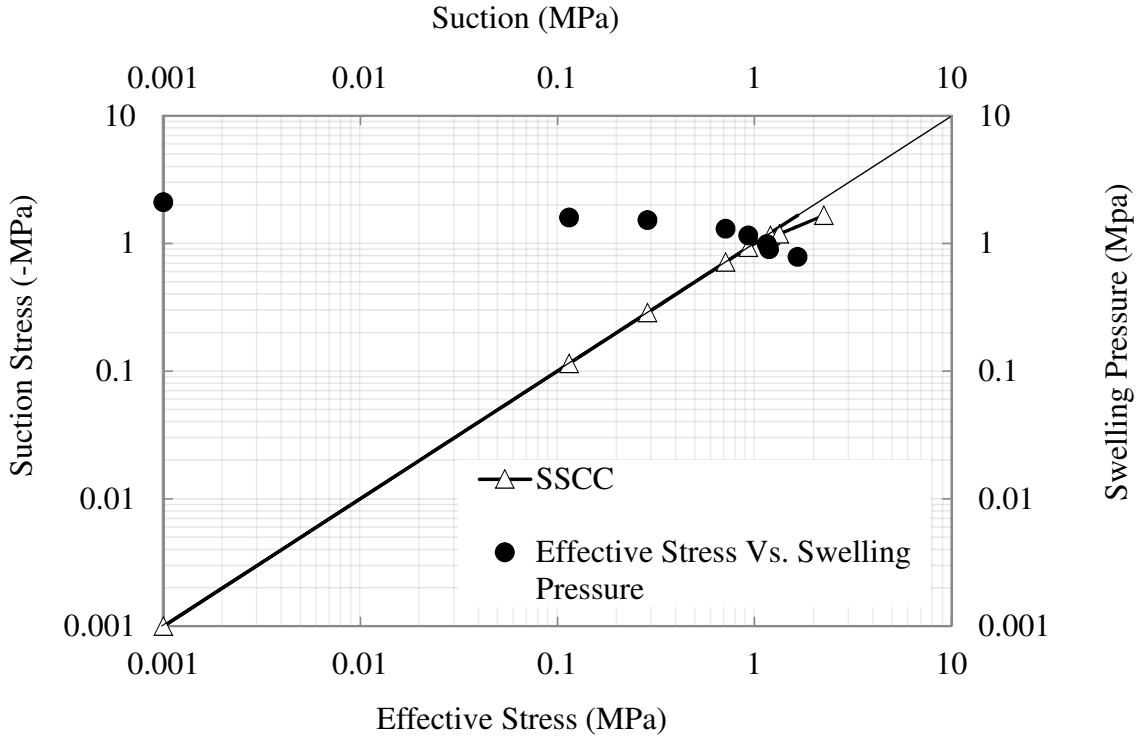

Fig. 7.7b. Variation of suction stress, effective stress, and swelling pressure with suction for B1 at $\rho_d = 1.8$ g/cm^3

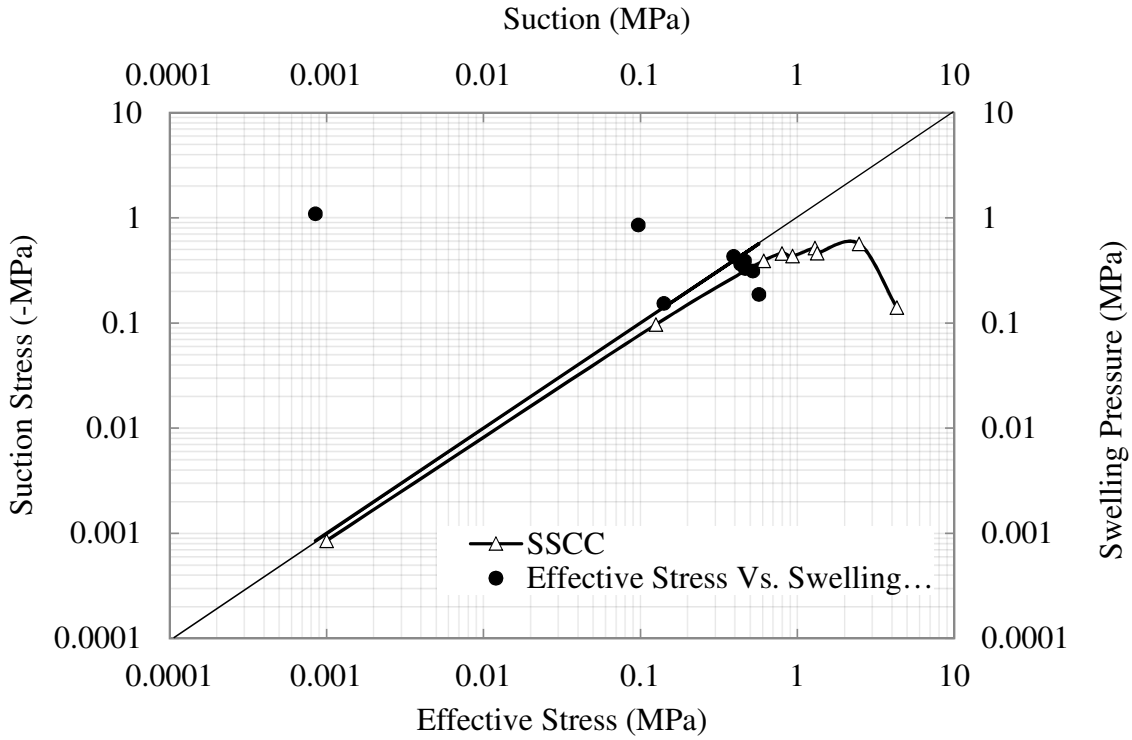

Fig. 7.8a. Variation of suction stress, effective stress, and swelling pressure with suction for B2 at ρ_d = 1.45 g/cm^3

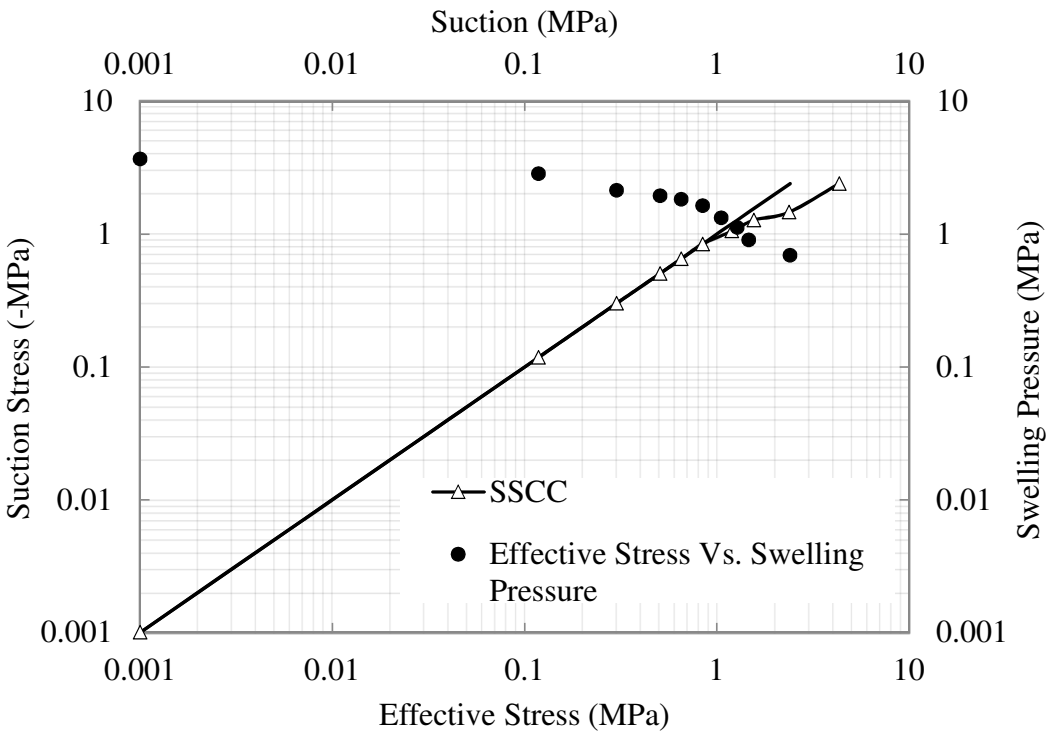

Fig. 7.8b. Variation of suction stress, effective stress, and swelling pressure with suction for B2 at ρ_d = 1.8 g/cm^3

7.4 Wetting induced effective stresses in compacted kaolin

The compacted kaolin exhibited volumetric collapse upon wetting under different inundation pressures as shown in **Chapter 4**. The wetting SWCCs of compacted kaolin under different inundation pressures were estimated using the osmotic suction controlled collapse tests for understanding the effective stress development through SSCC concept. The effective stress should increase in kaolin due to wetting due to decrease in volume. The collapse potential versus time under different controlled suctions for kaolin under 400 kPa inundation pressure were presented in Fig. 7.9. The collapse potential data with distilled water was also presented along with the other results for comparison. The collapse potential versus time for all the suction values showed typical s-curve similar to the case with distilled water as presented in **Chapter 4**. Figure 7.10 presented the wetting SWCCs of compacted kaolin under

different inundation pressure. Specimens attained hydraulic equilibrium within 7 days by completing the collapse. The AEVs of the wetting SWCCs under different inundation pressures were nearly same and was 0.37 MPa. The degree of saturation was higher for specimens with larger inundation pressure in the unsaturated zone of SWCC. The degree of saturation of the specimen at 1 MPa under 100 kPa inundation pressure was 52% whereas under 800 kPa inundation pressure was 73%. Figure 7.11 shows the collapse potential variation with suction for three inundation pressures. Collapse potential increased sharply with decreasing suction during the wetting up to AEV, but only an insignificant amount (~1%) of collapse was noticed beyond the AEV for all the studied cases. The collapse potential further increased with the inundation load for a given value of suction. The observed variation was was consistent with the results obtained in **Chapter 4** for wetting induced collapse without the suction control. The variation in the void ratio during collapse under controlled wetting conditions (i.e., variation in suction) was shown in Fig. 7.12. The initial void ratio of the specimen at air-dry state (before inundation) was also shown in the figure against a large suction value (~5 MPa) for all the inundation loads. The void ratio sharply decreased with decrease in suction during wetting up to the AEV and was nearly constant due to further wetting until full saturation. Therefore, it was expected in the wetting induced collapse tests that the effective stress increases due to wetting until the suction value is equal to the AEV and becomes constant. Figure 7.13 shows the computed effective stress variation with the suction for various inundation loads based on suction stress approach. In contrast to the above understanding based on the void ratio variation, the computed effective stress decreased (suction stress increased) during collapse due to wetting until AEV and nearly become constant after the AEV. The decrease in effective stress or increase in suction stress during the wetting induced collapse based on suction stress approach cannot be supported by the fundamental understanding of effective stress concept. The suction stress approach was thus not useful for understanding the volume change behavior.

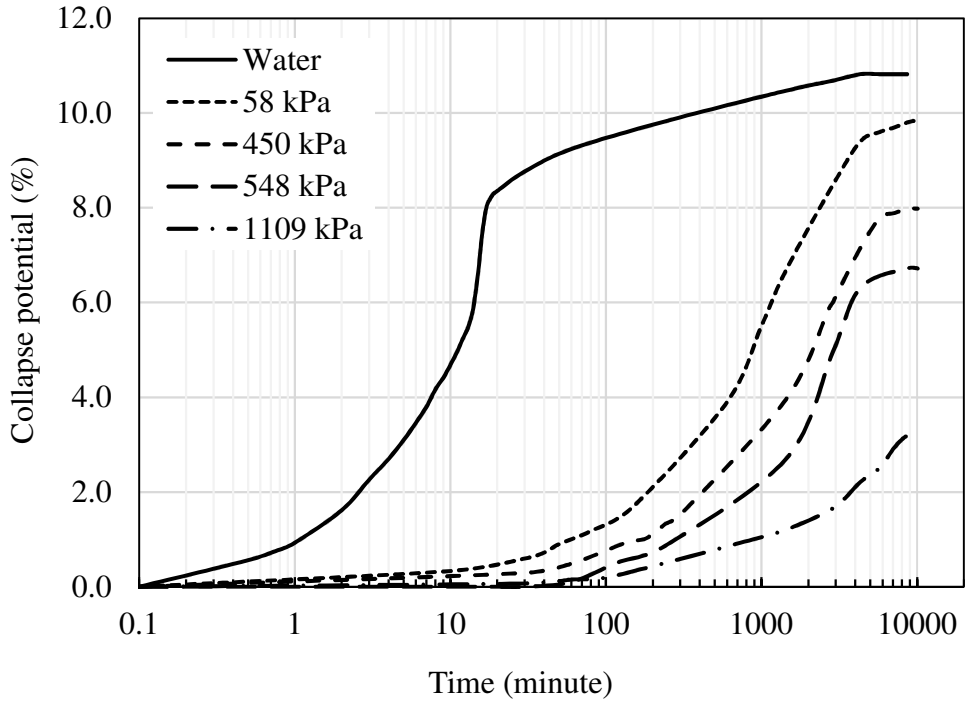

Fig. 7.9. Collapse potential with time for kaolin under 400 kPa inundation pressure at different suction values

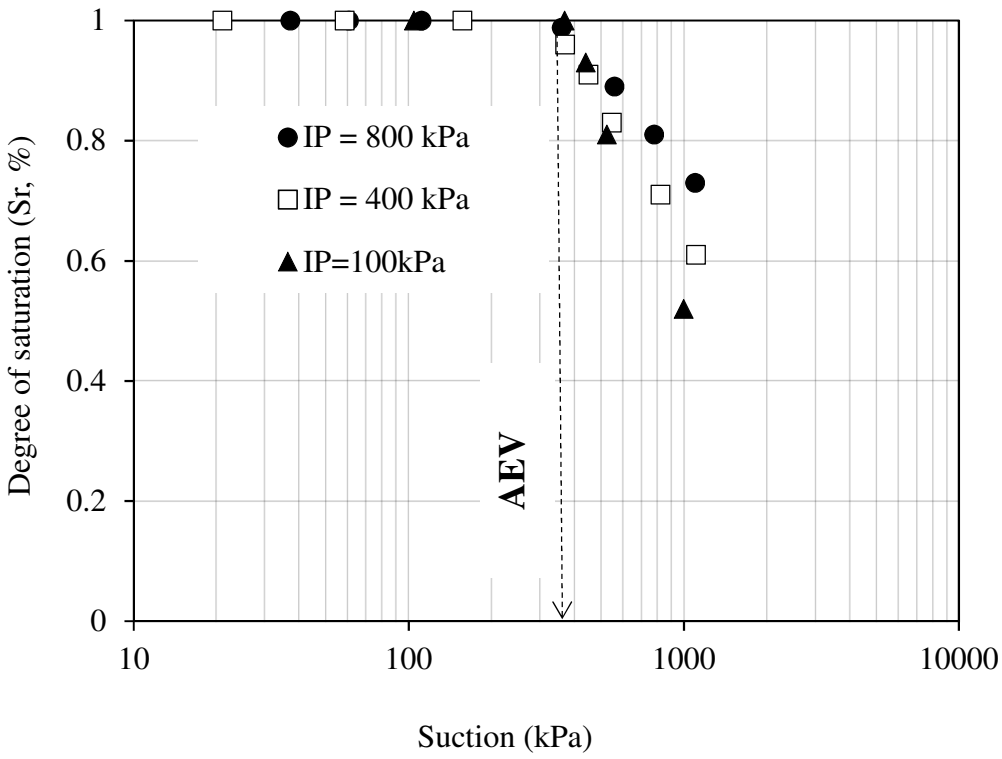

Fig. 7.10. Wetting SWCCs of compacted kaolin under different inundation loads

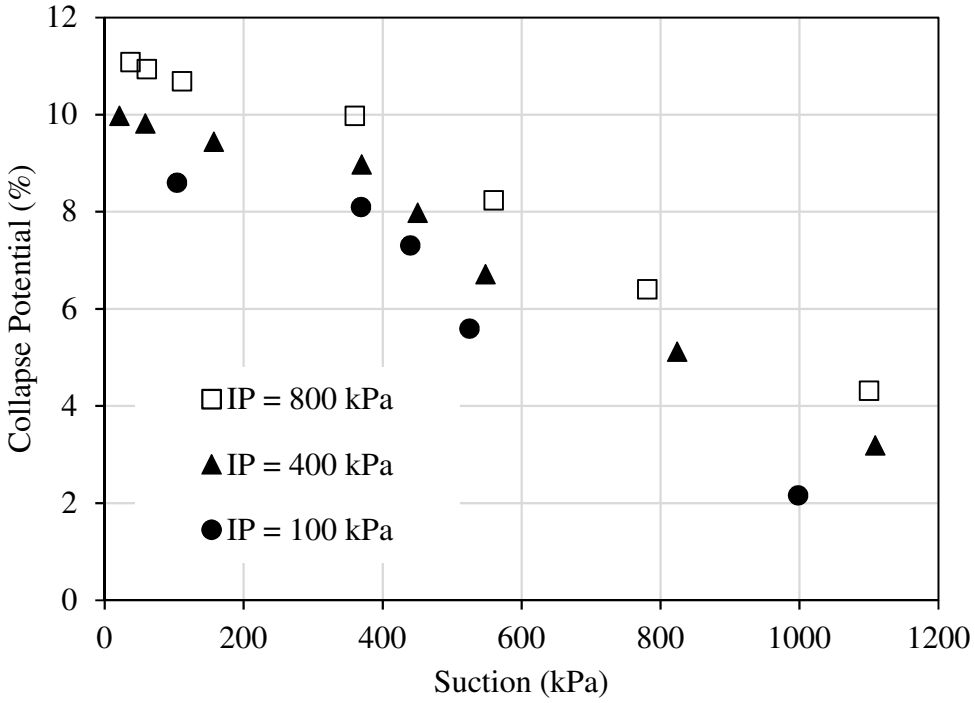

Fig. 7.11. Collapse potential variation with suction for compacted kaolin under different inundation loads

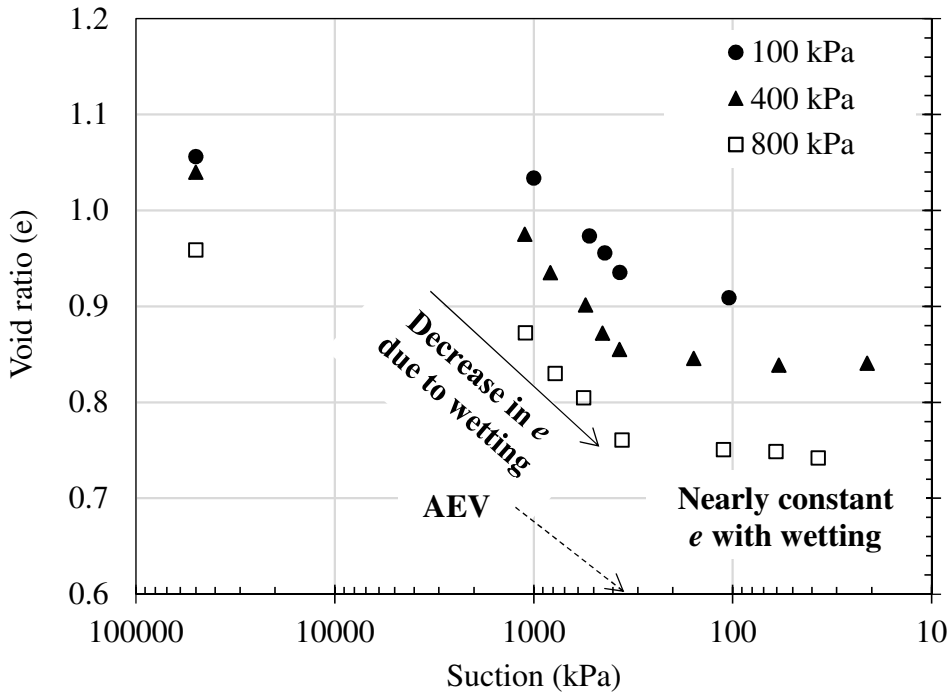

Fig. 7.12. Void ratio variation with suction for compacted kaolin under different inundation loads

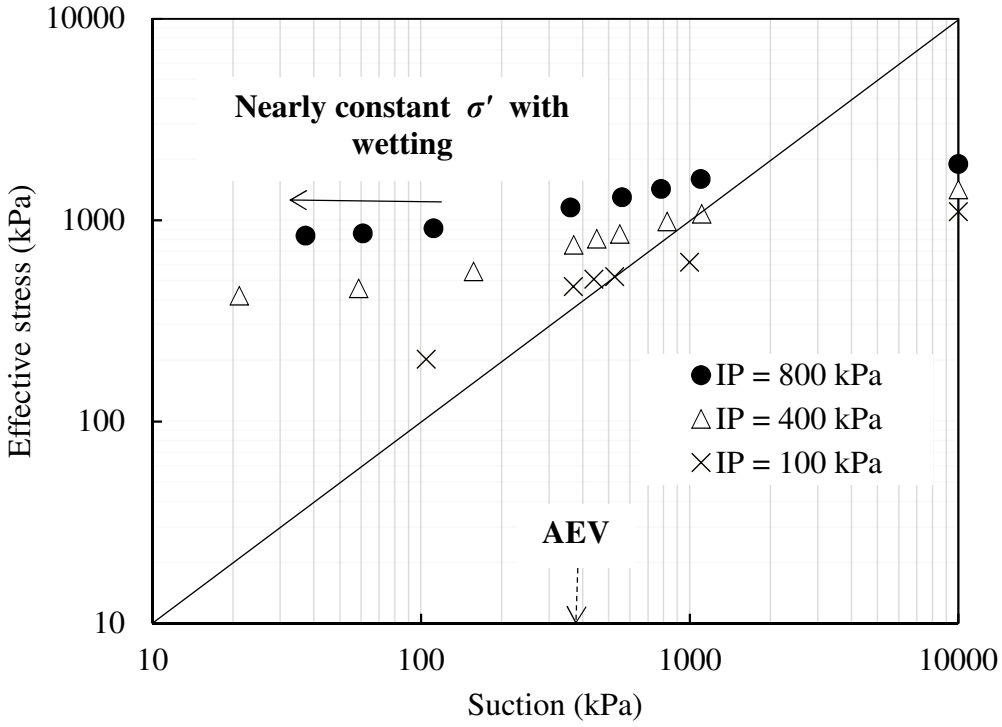

Fig. 7.13. Effective stress variation with suction for compacted kaolin under different inundation loads

CONCLUDING REMARKS

The variation of effective stresses in two clays of different activity due to wetting under hydro-mechanical loads was studied. The effective stress development was studied by using the suction stress approach. Three series of suction-controlled tests were conducted. In the first series of tests, the drying behavior of slurried kaolin, MKB1, and MKB2, were studied. In the second series of experiments, wetting SWCCs were established for bentonite by conducting suction controlled swelling pressure test in isochoric conditions. In the third series, suction-controlled collapse test was conducted on compacted kaolin under different inundation pressures. The suction stresses and effective stresses in kaolin, bentonite, and kaolin- bentonite mixtures were estimated under the studied hydro-mechanical conditions.

The SSCC of slurried kaolin was not influenced by the addition of bentonite during the drying process. In the suction controlled swelling pressure tests on bentonites, the decrease

in effective stress resulted in increase in the swelling pressures during the wetting process in isochoric at higher compactions densities. However, for bentonites compacted at lower densities, the effective stress increased with suction up to a maximum value but reduced beyond that suction although the swelling pressure decreased continuously. In the suction controlled collapse test, the effective stress decrease during the wetting induced collapse, which is opposite for a practical situation. The suction stress approach was thus not useful for understanding effective stress development due to hydro-mechanical loading.

Chapter 8

CONCLUSIONS

The key objective of this research work was to understand the hydro-mechanical behavior of clays of different mineralogy. An extensive laboratory testing program was undertaken on three commercially procured clays namely, kaolin and Indain bentonites (i.e., B1 and B2). The study focused on the collapse behavior of kaolin and swelling pressure development in compacted bentonite. The present study also emphasis on the development of effective stress due to hydro-mechanical load in the studied clays.

A detailed investigation was carried out on the collapse nature of kaolin. Wetting-induced collapse behavior of compacted kaolin under different inundation pressure was studied under the influence of pore-fluid chemistry. The effect of pH, salt concentration, and dielectric pore-fluid environment on the clay behavior was analyzed using sedimentation and collapse tests. The collapse test results were well verified with the sedimentation test data, SEM images of lyophilized specimens, and edge isoelectric point (IEP_{edge}). The influence of inundation fluid and inundation pressure on the fabric changes and collapse potential was explained in detail. The results were summarized in **Chapter 4**. Based on the study, the following salient conclusions were obtained.

Conclusions from Chapter 4: Wetting-induced collapse behavior of kaolin: influence of fabric and inundation pressure

1. The mode of particle association in kaolin was dispersed in the presence of distilled water as pH > IEPedge and EF in the presence of the solution with pH < IEPedge based on the sediment volume test data. The observed sediment volume increased five-fold due to the change in pH from 6.5 to 3.1, which changed the particle association from dispersed to EF. The particle association also changed to EF with the increase in salt concentration up to 0.1 mol/L. The increase in salt concentration beyond 0.1 mol/L NaCl did not increase the sediment volume as the particle association remained the same. The dielectric constant of the pore medium directly influenced the sediment volume as the mode of association in the medium dielectric constant fluids was “mixed” and in low dielectric constant fluids was EF. The sediment volume increased four-fold due to the decrease in the dielectric constant from 77.8 (distilled water) to 2.78 (kerosene).

2. The kaolin exhibited volumetric collapse behavior due to inundation with different pore fluids under mechanical loading. The collapse mechanism, however, was physicochemical in nature as observed from the particle associations. The magnitude of collapse potential was a function of the inundation fluid and inundation pressure. The particle association changed from EF to dispersed fabric due to the water inundation, which exhibited the highest collapse potential (14%). The soil exhibited insignificant collapse (0.6%) in the presence of kerosene as the particle association remained in EF mode even after inundation with the kerosene. The collapse potential of soil was directly proportional to the dielectric constant of the pore fluid as observed from the water-ethanol mixtures. The measured pH of the pore fluid was consistently >IEP_{edge} irrespective of the targeted pH values and the fabric was dispersed under the mechanical loading. The influence of pH on the collapse potential was therefore not obtainable. The collapse potential decreased consistently with the increase in electrolyte concentration from 0.01 to 0.1 mol/L NaCl under all inundation pressures. The collapse behavior of kaolin in the presence of different pore fluids was in accordance with the equilibrium sediment volume. The collapse potential was inversely proportional to the observed sediment volume.
3. The collapse potential increased with inundation pressure up to a pressure corresponding to a minimum equilibrium void ratio and then decreased further. The peak collapse potential was maximum with water, but the inundation pressure corresponding to the peak potential increased with low dielectric pore fluids and in the presence of electrolytes.
4. The results of the present work were qualitatively in agreement with the studies by Wang and Siu (2006*a*, 2006*b*) and Di Matteo et al. (2011) where the influence of fabric changes on compacted (very high) kaolin behavior was significant. The compacted kaolin specimen (at high solid/liquid ratio) exhibited irrecoverable collapse due to fabric changes.
5. The present study is useful in understanding the collapse behavior of kaolin due to wetting under foundation loading. The results are useful for developing accurate theoretical models for effective stress estimation using the analyses based on the soil suction stress characteristic curve (Lu et al. 2010) and critical state concept (Sivakumar et al. 2010) under the influence of different physicochemical factors. The influence of initial compaction density on the collapse potential under different physicochemical factors requires further study.

Swelling pressure evolution curve (SPEC) for different quality Indian bentonites was established under different compaction density. The effect of compaction density and bentonite quality on the pore-size distributions (PSDs) and clay fabric were analyzed for understanding the influence on SPEC behavior. The evolution of PSD and fabric during the water uptake process was analyzed for understanding the microstructural influence on the SPEC behavior. The results were presented in **Chapter 5**. The swelling pressure of bentonite is dependent on the initial compaction density and plasticity. A predictive model based on the linearization of the swelling pressure data using normalization dry density was proposed in **Chapter 6**. The model was validated with the literature data. The following conclusions were drawn out from **Chapter 5** and **Chapter 6**.

Conclusions from Chapter 5: Swelling pressure characteristics of bentonites in isochoric conditions by microstructural analysis

6. Different stages of swelling pressure development were noted on the swelling pressure evolution curve. The swelling behavior of bentonites exhibited either a bimodal behavior or monotonously increasing behavior depending on the bentonite quality and initial compaction density.
7. The drop in SPEC after the initial water uptake is due to the collapse of 10 – 100 μm pore size class present in the soil sample. The pore size class of 10 – 100 μm was insignificantly available in B2 specimen at the same compaction density which promotes the monotonously increasing swelling pressure without structural collapse. The SPEC followed monotonously increasing behavior for B2 due to the presence of insignificant amount of macro pore size class.
8. The volume contribution of macro pore-size class 10 – 100 μm at ρ_d = 1.45 Mg/m^3 maximum for B1 which is responsible for the maximum structural collapse at this density. Further increase in the compaction effort decreased the volume of macro pore size class to insignificant value which prompted the change in SPEC from bimodal to monotonously increasing behavior.
9. The increase in bentonite plasticity reduced the presence of macro pore size classes and altered the structural collapse behavior in SPEC. The volume of given smaller pore-size classes ($\leq$ 10 μm) was higher in high plastic clay compared to low plastic clay for any

given density. The inter-particle distance in high plastic clay is smaller compared to low plastic clay bentonite at the same compaction density. The FESEM diagrams of B1 at different compaction densities showed no noticeable variation, but for B2 showed unnoticeable pores and very smooth surfaces. The FESEM figure for B1 showed the aggregate formation with several pores of different pore size classes for as compacted while the FESEM figure for B2 showed the aggregate formation with relatively smaller pore size classes at same density.

Conclusions from Chapter 6: Swelling pressure prediction for compacted bentonites and bentonite-sand mixtures

10. The estimated swelling pressures based on the GC theory, at a given dry density, increased with the soil water density (ρ_w), to account for hydration forces during the bentonite wetting. The results are qualitatively in agreement with the measured swelling pressure data of different bentonites at different compaction densities, but the measured swelling pressure data are severely undermined, albeit at $\rho_w = 1.36$ Mg/m^3.
11. The variation of swelling pressure with dry density in the zone–II, where 1.45 Mg/m^3 < ρ_d < 1.7 Mg/m^3, represented different mechanisms, such as hydration and diffuse double layer formation, responsible for the swelling pressure development. The measured swelling pressure corresponds to any given dry density from zone – II is thus found to be the ideal normalization factor for establishing the entire swelling pressure – dry density relationship. Further, the swelling pressures of the different clayey soils are found to vary in the zone – II distinctly based on their plasticity.
12. The empirical parameter in the predictive equation for swelling pressure is related to the plasticity of the clayey soil. The parameter takes a value of 0.3 for high – moderate plastic bentonites and takes a value of 0.5 for low plastic bentonites and bentonite-sand mixtures. The plasticity of the clayey soils can be inferred based on the measured swelling pressure at a given density chosen from zone – II.
13. The proposed method is accurate and very simple in predicting the swelling pressures of clayey soils over a wide range of dry densities and plastic characteristics using a single, measured swelling pressure data point for the normalization. The method implicitly

considers all the factors that control the swelling pressure of the clay. This method is appreciably advantaged as it requires no knowledge of clay surface and pore–fluid characteristics, unlike the existing methods.

In the last chapter, the effective stress variation in clays of different mineralogy due to hydro-mechanical loads was studied. The suction stresses and effective stresses in kaolin, bentonite, and kaolin – bentonite mixtures were analyzed under hydro-mechanical conditions. The results were described in **Chapter 7**. Based on the study, the following salient conclusions were obtained.

Conclusions from Chapter 7: Effective stresses of clays of different activity under different hydro-mechanical loads

14. The characteristic increase-and-decrease behavior of the SSCC for the slurried kaolin during the drying process under no external stress was not influenced by the addition of bentonite.
15. The suction controlled swelling pressure tests on bentonites at higher compactions densities showed that the decrease in effective stress resulted in an increase in the swelling pressures during the wetting process in isochoric condition. These results were consistent with Calcigel bentonite results from Baille et al. (2016). The results were, however, distinctly different for bentonites compacted at lower densities. The effective stress increased with suction up to a maximum value but reduced beyond that suction albeit the swelling pressure decreased continuously.
16. Further, the decrease in effective stress during the wetting induced collapse based on suction stress approach cannot be supported by the fundamental understanding of the effective stress concept. The suction stress approach was thus not useful for understanding effective stress development due to hydro-mechanical loading.

LIMITATIONS AND FUTURE SCOPE

In this study, an attempt was made to understand the effective stress development in kaolin and bentonite clays due to hydro-mechanical loading. However, a few limitations of the work are noted and are highlighted below.

1. The kaolin behavior was studied in the natural state without any pretreatment. Few studies in the literature treat the kaolin with sodium chloride solution for the homoionization.

2. The temporal variation of swelling pressure of the bentonites with the addition of different percentages of sand provides insights into the pore-size distribution and swelling pressure characteristics.
3. The swelling pressure tests were terminated after noting a nearly constant value of pressure fore a couple of days. However, the degree of saturation was less than 100% for few cases indicating a very slow development of swelling pressure in densely compacted bentonites.

The scope for future work based on the aforementioned limitations is given below:

1. Measurement of collapse potential at different initial dry densities with different pore-fluids to develop complete knowledge on the kaolin.
2. Application of plasticity models for modeling the collapse behavior of kaolin.
3. Measurement of swelling pressure evolution with time using different sand-bentonite mixtures.
4. Development of a theoretical framework based on the measured data to explain the effective stress concept of collapsible and expansive clays.

REFERENCES

1. Agus, S.S., Schanz, T., 2008. A method for predicting swelling pressure of compacted bentonites. Acta Geotechnique, 3, 125-137.
2. Alonso, E. E., Gens, A., High, D.W., 1987. Special problem soils. General report. Proc. 9th European Conference on Soil Mechanics and Foundation Engineering, Dublin, 3, 1087-l 146.
3. Alonso, E.E., Gens, A., Josa, A., 1990. A constitutive model for partially saturated soils. Geotechnique, 40(3): 405-430.

4. Alonso, E.E., Vaunat, J., Gens, A., 1999. Modelling the mechanical behaviour of expansive clays. Engineering Geology, 54(1-2): 173-183.
5. Alonso, E. E., Pereira, J.M., Vaunat, J., Olivella, S., 2010. A microstructurally based effective stress for unsaturated soils. Geotechnique, 60(12): 913–925.
6. Anandarajah, A., Zhao, D., 2000. Triaxial behavior of kaolinite in different pore fluids. Journal of Geotechnical and Geoenvironmental Engineering, 126(2): 148–156. doi:10.1061/(ASCE)1090-0241(2000)126:2(148).
7. Arifin, Y.F., 2008. Thermo-hydro-mechanical behavior of compacted bentonite sand mixtures: An Experimental Study. PhD thesis. Weimar.ASTM D5890, 2003. Standard test method for swell index of clay mineral component of geosynthetic clay liners. American Society for Testing Materials, West Conshohocken, Pa. doi:10.1520/D5890-02.
8. ASTM D2216-10, 2010. Standard Test Methods for Laboratory Determination of Water (Moisture) Content of Soil and Rock by Mass. ASTM International, West Conshohocken, PA.
9. ASTM D422-63, 2007. Standard Test Method for Particle-size Analysis of Soils. ASTM International, West Conshohocken, PA, USA.
10. ASTM D4318, 2010. Standard Test Methods for Liquid Limit, Plastic Limit, and Plasticity Index of Soils. ASTM International, West Conshohocken, PA, USA.
11. ASTM D5333-03 2003. Standard test method for measurement of collapse potential of soils. Designation D 5333-03, American Society for Testing Materials, West Conshohocken, PA, USA.
12. ASTM D5890, 2003. Standard test method for swell index of clay mineral component of geosynthetic clay liners. American Society for Testing Materials, West Conshohocken, Pa. doi: 10.1520/D5890-02.
13. ASTM D854-92, 1994. Standard Test Method for Specific Gravity of Soils. ASTM International, West Conshohocken, PA, USA.
14. ASTM E104-02, 2012. Standard practice for maintaining constant relative humidity by means of aqueous solutions. West Conshohocken, PA, ASTM International.

15. ASTM D4546-14, 2014: Standard test methods for one-dimensional swell or collapse of soils. American Society for Testing Materials, West Conshohocken, Pa. doi: 10.1520/D4546.
16. ASTM D7928-17, 2017. Standard test method for particle-size distribution (gradation) of fine-grained soils using the sedimentation (hydrometer) analysis. American Society for Testing Materials, West Conshohocken, Pa. doi:10.1520/D7928-17.
17. Atabek, R.B., Felix, B., Robinet, J.C., Lahlou, R., 1991. Rheological behavior of saturated expansive clays materials. Workshop on Stress Partitioning in Engineered Clay Barriers, Duke University, Durham, NC.
18. Baille, W., Tripathy, S., Schanz, T., 2010. Swelling pressures and one-dimensional compressibility behaviour of bentonite at large pressures. Applied Clay Science, 48(3), 324-333.
19. Baille, W., Tripathy, S., Schanz, T., 2014. Effective stress in clays of various mineralogy Vadose Zone Journal, 13(5):1-10, doi:10.2136/vzj2013.06.0112.
20. Baille, W., Lang, L., Tripathy, S., Schanz, T., 2016. Influence of effective stress on swelling pressure of expansive soils. E3S Web of Conferences, 9, 14016. doi: 10.1051/e3sconf/20160914016Barden L., Madedor, A.O., Sides G.R., 1969. Volume change characteristics of unsaturated clay. Proceedings of American Society of Civil Engineers, 95:33-53.Barden L., Sides G.R., 1970. Engineering behavior and structure of compacted clay. Journal of the Soil Mechanics and Foundations Division, 96(4): 1171-1200.
21. Basma, A.A., Tuncer, E.R., 1992. Evaluation and control of collapsible soils. Journal of Geotechnical Engineering, 118(10):1491-504.
22. Bell, F.G., Culshaw, M.G., 2001. Problem soils: a review from a British perspective. Proceeding Symposium on Problematic Soils, Nottingham Trent University, I. Jefferson, E.J. Murray, E. Faragher, and P.R. Fleming, Edison, Thomas, Telford, London, 1-36.
23. Bharat, T. V., Das, D. S., 2017. Physicochemical approach for analyzing equilibrium volume of clay sediments in salt solutions. Applied Clay Science, 136, 164-175.

24. Bharat, T. V., Gapak, Y., 2018. Hydration kinetics of bentonite buffer material: Influence of vapor pressure, bentonite plasticity, and compaction density. Applied Clay Science, 157, 41-50.
25. Bharat, T. V., Sivapullaiah, P.V., Allam, M.M., 2013. Novel procedure for the estimation of swelling pressures of compacted bentonites based on diffuse double layer theory. Environmental Earth Sciences, 70, 303-314.
26. Bharat, T. V., Sridharan, A., 2015a. Prediction of compressibility data for highly plastic clays using diffuse double-layer theory. Clays and Clay Miner, 63, (1), 30-42.
27. Bharat, T. V., Sridharan, A., 2015b. A critical appraisal of Debye length in clay-electrolyte systems. Clays and Clay Miner, 63, (1), 43-50.
28. Bishop, A. W. 1959. The principle of effective stress. Tek. Ukeblad, 106(39), 859–863.
29. Bolt, G.H., 1956. Physico-chemical analysis of compressibility of pure clays. Geotechnique, 46, 291-311.
30. Bradbury, M.H., Baeyens, B., 2003. Porewater chemistry in compacted re-saturated MX-80 bentonite. Journal of Contaminant Hydrology, 61(1-4):329-38.
31. Brady, P.V., Cygan, R.T., Nagy, K.L., 1996. Molecular controls on kaolinite surface charge. Journal of Colloid and Interface Science, 183(2): 356–364. doi:10.1006/jcis.1996.0557. PMID: 8954678.
32. Brackley, I. J. A., 1973. Swell pressure and free swell in a compacted clay. Proceedings of the 3rd International Conference on Expansive Soils, 169–176, Academic, Jerusalem.
33. Braggs, B., Fornasiero, D., Ralston, J., and Smart, R.S., 1994. The effect of surface modification by an organosilane on the electrochemical properties of kaolinite. Clays and Clay Minerals, 42(2): 123–136.
34. Bucher, F., Mfiller-Vonmoos, M., 1989. Bentonite as a containment barrier for the disposal of' highly radioactive wastes. Applied Clay Science, 4: 157-177.Casagrande, 1932. The structure of clay and its importance in foundation engineering. Journal of Boston Society of Civil Engineering, 19:168-209.
35. Carty, W.M., 1999. The colloidal nature of kaolinite. American Ceramic Society Bulletin, 78(8): 72–76.

36. Celik, M.S., 2004. Electrokinetic behavior of clay surfaces. Interface Science Technology, 1: 57–89. doi:10.1016/S1573-4285(04)80037-1.
37. Cerato, A.B., Lutenegger, A.J., 2002. Determination of surface area of fine-grained soils by the ethylene glycol monoethyl ether (EGME) method. Geotech. Test. J. 25, 315–321.
38. Chen, Y.G., Dong, X.X., Zhang, X.D., Ye, W.M., Cui, Y.J., 2018. Combined thermal and saline effects on the swelling pressure of densely compacted GMZ bentonite. Applied Clay Science, 166:318-326.
39. Chapman, L.A., 1913. Contribution to the theory of electro capillarity. Philosophical Magazine, 25(6):475-481.
40. Chapman, H.D., 1965. Cation-exchange capacity. In Methods of soil analysis - chemical and microbiological properties. Edited by C.A. Black. Agronomy, 9:891–901.
41. Chen, J., and Anandarajah, A., 1998. Influence of pore fluid composition on volume of sediments in kaolinite suspensions. Clays and Clay Minerals, 46(2):145–152. doi:10.1346/CCMN.1998.0460204.
42. Chen, J., Anandarajah, A., Inyang, H., 2000. Pore fluid properties and compressibility of kaolinite. Journal of Geotechnical and Geoenvironmental Engineering, 126: 798–807. doi:10.1061/(ASCE)1090-0241(2000)126:9(798).
43. Chipera, S.J., Carey, J.W., Bish, D.L., 1997. Controlled-humidity XRD analyses: Application to the study of smectite expansion/contraction. In: Gilfrich J.V., et al. (Eds.). Advances in X-Ray Analysis, 39:13–721.
44. Choudhury, C., Bharat, T.V., 2018. Wetting-induced collapse behavior of kaolinite: influence of fabric and inundation pressure. Canadian geotechnical journal, 55:956-967.
45. Conley, R.F., and Althoff, A.C., 1971. Surface acidity in kaolinites. Journal of Colloid and Interface Science, 37(1): 186–195. doi:10.1016/0021-9797(71)90279□7.
46. Cui, Y.J., Loiseau, C., Delage, P., 2002. Microstructure changes of a confined swelling soil due to suction controlled hydration Unsaturated soils proceedings of the Third International Conference on Unsaturated Soils, Brazil, p. 593.

47. Cui, S.L., Zhang, H.Y., Zhang, M., 2012. Swelling characteristics of compacted GMZ bentonite-sand mixtures as a buffer/backfill material in China. Eng. Geol. 141-142(141), 65-70.
48. Delage, P., 2006. Some microstructure effects on the behaviour of compacted swelling clays used for engineered barriers. Chinese Journal of Rock Mechanics and Engineering, 25, Science Press (Beijing, 16 Donghuangchenggen North St, Beijing) 721-732.
49. Delage, P., Audiguier, M., Cui Y.J, Howat, M.D., 1996. Microstructure of a compacted silt. Canadian Geotechnical Journal, 33(1): 150-8.
50. Delage, P., Howat, M.D., Cui, Y.J., 1998. The relationship between suction and swelling properties in a heavily compacted unsaturated clay. Engineering Geology, 50, 31–48.
51. Derbyshire, E, Dijkstra, T & Smalley, I (editors), 1995. Genesis and properties of collapsible soils. Dordrecht: Kluwer. NATO ASI Series – Series C: Mathematical and Physical Sciences, 468.
52. Dhadapani, Y., Santhanam, M., 2017. Assessment of pore structure evolution in the limestone calcined clay cementitious system and its implications for performance. Cement and Concrete Composites, 84: 36-47.
53. Di Matteo, L., Bigotti, F., Ricco, R., 2011. Compressibility of kaolinitic clay contaminated by ethanol-gasoline blends. Journal of Geotechnical and Geoenvironmental Engineering, 137: 846–849. doi:10.1061/(ASCE)GT.1943-5606. 0000494.
54. Djedid, A., Quadah, N., 2012.Parameterized Study of the Swelling of Reconstituted Clay Soils. Parameterized Study of the Swelling of Reconstituted Clay Soils. Electronic Journal of Geotechnical Engineering, 17.
55. Dixon, D.A., Gray, M.N., 1985. The engineering properties of buffer material. Technical Report TR-350, Fuel Waste Technology Branch, Whiteshell Laboratories, Pinawa, Man.
56. Dudley, J. H., 1970. Review of Collapsing Soils. Journal of Soil Mechanics and Foundation Division, 96:925–947.

57. ENRESA, 2000. Full-scale engineered barriers experiment for a deep geological repository for high -level waste in crystalline host rock. Technical Publication 01/2000. Enresa, Madrid.
58. Estabragh, A.R., Javadi, A.A., Boot, J.C., 2004. Effect of compaction pressure on consolidation behavior of unsaturated silty soil. Canadian Geotechnical Journal, 41(3): 540-550.
59. Fredlund, D.G., Gan, J. K. M., 1995. The collapse mechanism of soil subjected to one-dimensional loading and wetting. In E Derbyshire et al (eds), Genesis and properties of collapsible soils. Dordrecht: Kluwer.
60. Gallipoli, D., Gens, A., Sharma, R., Vaunat, J., 20031. An elasto-plastic model for unsaturatedsoil incorporating the effects of suction and degree of saturation on mechanical behaviour. Géotechnique, 53(1):123–35.
61. Gapak Y., Das G., Yerramshetty, U., Bharat T V., 2017. Laboratory determination of volumetric shrinkage behavior of bentonites: A critical appraisal. Applied Clay Science 135, 554-566.
62. Gapak, Y., Bharat, T.V., 2018. Hysteretic water retention behaviour of bentonites. Journal of Hazardous, Toxic, and Radioactive Waste (ASCE), 22(3):
63. Gallipoli, D., Gens, A., Sharma, R. & Vaunat, J., 2003. An elasto-plastic model for unsaturated soil incorporating the effects of suction and degree of saturation on mechanical behavior. Geotechnique, 53(1): 123–135.
64. Garcia-Bengochea, I., Altschaeffl, A.G., Lovell, C.W., 1979. Pore Distribution and Permeability of Silty Clays. Journal of the Geotechnical Engineering Division, 1979, Vol. 105, Issue 7, Pg. 839-856.
65. Gens, A., Alonso, E.E., 1992. A framework for the behaviour of unsaturated expansive clays. Canadian Geotechnical Journal, 29: 1013-1032.
66. Gens A., Guimaraes L., do N., Garcia-Molina A., Alonso E.E., 2002. Factors controlling rock–clay buffer interaction in a radioactive waste repository. Engineering Geology, 64: 297-308.
67. Grabowska-olszewsla, 1988. Engineering geological problems of loess in Poland Eng. Geol., 25 (2–4): 177-199.

68. Gray, M.N., Cheung, S.C.H., Dixon, D.A., 1984. The influence of sand content on swelling pressures and structure developed in statically compacted Na-bentonite. Report 7825, Atomic Energy of Canada Limited, Mississauga, Ont, 1□24.
69. Grindrod P., Peletier, M., Takase, H., 1999. Mechanical interaction between swelling compacted clay and fractured rock, and the leaching of clay colloids. Engineering Geology, 54(1-2): 159-165.
70. Gouy, G., 1910. Sur la constitution de la charge e´ lectrique a` la surface d'un e´ lectrolyte. Journal de Physique, Theorique et Appliquee, 4: 457-468 (in French).
71. Gupta, V., 2011. Surface charge features of kaolinite particles and their interactions. The University of Utah, ProQuest Dissertations Publishing, 3443628.
72. Handy, R.L., 1973. Collapse loess in Iowa. Proceedings of the Soil Science Society of America, 37: 281-284.
73. Haase, H., Schanz, T., 2016. Compressibility and saturated hydraulic permeability of clay-polymer composites-experimental and theoretical analysis. Applied Clay Science, 130: 62-75.
74. He, Y., Ye, W.M., Chen, Y.G., Cui, Y.J., 2019. Effects of K^+ solutions on swelling behavior of compacted GMZ bentonite. Engineering Geology, https://doi.org/10.1016/j.enggeo.2018.12.020.
75. Herbert, H.J., Moog, H.C., 2002. Untersuchungen zur Quellung von Bentonit in hochsalinaren Lösungen. Report GRS-179, Gesellschaft für Anlagen und Reaktorsicherheit (GRS) mbH, Berlin.
76. Houston, W.N., Mahmoud, H.H., Houston, S.L., 1993. A laboratory procedure for partial wetting collapse determination. Geotechnical Special Publication, ASCE, 39: 54–63.
77. Houston, S.L., Houston, W.N., Spadola, D.J., 1988. Prediction of field collapse of soils due to wetting. Journal of Geotechnical Engineering, 114(1): 40□58.
78. Houston, W., Mahmoud, H., Houston, S., 1993. A Laboratory Procedure for Partial-Wetting Collapse Determination. Unsaturated Soils, Special Geotechnical Publication No. 39: 54 – 63.
79. Imbert, C., Villar, M.V., 2006. Hydro-mechanical response of a bentonite pellets-powder mixture upon infiltration. Applied Clay Science, 32(3-4): 197-209.

80. IS. 2720-40: 1977. Methods of test for soils, Part 40: Determination of free swell index of soils. CED 43: Soil and Foundation Engineering, Bureau of Indian Standards (IS).
81. IS. 2720-5: 1985Methods of test for soils, Part 5: Determination of liquid and plastic limit. CED 43: Soil and Foundation Engineering, Bureau of Indian Standards (IS).
82. Japan Nuclear Cycle Development Institute, 1999. H12: project to establish the scientific and technical basis for HLW disposal in Japan: supporting report 2 (respiratory design and engineering Technology). Japan Nuclear Cycle Development Institute, Tokyo.
83. Jenning, E.B., Burland, J.B., 1962. Limitation to the use of effective stress in partially saturated soils. Geotechnique, 2: 125-144.
84. Jennings, J.E. Knight, K., 1957. The additional settlement of foundations due to a collapse of structure of sandy subsoils on wetting. Proceedings of the 4th International Congress on Soil Mechanics and Foundation Engineering, London, 1: 316-319.
85. Jennings, J.E., Knight, K., 1975. A guide to construction on or with materials exhibiting additional settlement due to collapse of grain structure. Proceedings of the 6th Regional Conference for Africa on Soil Mechanics and Foundation Engineering, Durban, South Africa, 1: 99-105.
86. Juang, C.H., Holtz, R.D., 1986. Fabric, Pore Size Distribution, and Permeability of Sandy Soils. Journal of Geotechnical Engineering, 112(9).
87. Kim, S.H., 2008. Polyacrylamide-treated kaolinite clay: a fabric study. M.Sc. thesis, Pennsylvania State University, USA.
88. Kanno, T., Wakamatsu, H., 1992. Water uptake and swelling properties of unsaturated bentonite buffer materials. Canadian Geotechnical Journal, 29: 1102-1107.
89. Karnland, O., 1998. Bentonite Swelling Pressure in Strong NaCl solutions. Correlation of model calculations to experimentally determined data (No. POSIVA-98-01).
90. Khalili, N & Geiser, F & E. Blight, G. (2004). Effective Stress in Unsaturated Soils: Review with New Evidence. International Journal of Geomechanics, ASCE, 4:(2):1532-3641.
91. Komine, H., Ogata, N., 1994. Experimental study on swelling characteristics of compacted bentonite. Canadian Geotechnical Journal 31: 478-490.

92. Komine, H., Ogata, N., 1996. Prediction for swelling characteristics of compacted bentonite. Canadian Geotechnical Journal, 33: 11-22.
93. Komine, H., Ogata, N., 1999. Experimental study on swelling characteristics of sand–bentonite mixture for nuclear waste disposal. Canadian Geotechnical Journal, 1994, 31(4): 478-490, https://doi.org/10.1139/t94-057.
94. Komine, H., Ogata, N., 2003. New equations for swelling characteristics of bentonite-based buffer materials. Canadian Geotechnical Journal, 40: 460-475, 10.1139/T02-115.
95. Laloui, L., Mathieu Nuth, M., 2009. Reply to Discussion on ‘‘On the use of generalised effective stress in the constitutivemodelling of unsaturated soils.” Computers and Geotechnics, 36 :1362–1363.
96. Lambe, T.W., 1958. The Structure of Compacted Clay. Journal of the Soil Mechanical and Foundation Division, ASCE, 84: 1-35.
97. Lawton, E.C., Fragaszy, R.J., Hardcastle, J.H., 1989. Collapse of compacted clayey sand. Journal of Geotechnical Engineering, 115(9): 1252–1267. doi:10.1061/(ASCE)0733-9410(1989)115:9(1252).
98. Lawton, E.C., Fragaszy, R.J., and Hetherington, M.D., 1992. Review of wettinginduced collapse in compacted soil. Journal of Geotechnical Engineering, 118(9): 1376–1394.
99. Lee, J.O., Lim, J.G., Kang, I.M., Kwon, S., 2012. Swelling pressures of compacted Ca–bentonite. Eng. Geol., 129–130: 20-26.
100. Lefebvre, G. and Ben Belfadhel, M. 1989. Collapse at Permeation for a Compacted Non-Plastic Till. 12th. ICSMFE, Rio de Janeiro, 619-622.
101. Lefebvre, G., 1994. Collapse mechanisms and design considerations for some partly saturated and saturated soils. In E Derbyshire et al (eds), Genesis and properties of collapsible soils. Dordrecht: Kluwer.
102. Li, P., Vanapalli, S., and Li, T., 2016. Review of collapse triggering mechanism of collapsible soils due to wetting. Journal of Rock Mechanics and Geotechnical Engineering, 8(2): 256–274. doi:10.1016/j.jrmge.2015.12.002.

103. Likos, W., 2004. Measurement of Crystalline Swelling in Expansive Clay. Geotechnical Testing Journal, 27(6):540-546, https://doi.org/10.1520/GTJ11857. ISSN 0149-6115.

104. Liu, J., Miller, J.D., Yin, X., Gupta, V., Wang, X., 2014. Influence of ionic strength on the surface charge and interaction of layered silicate particles. Journal of Colloid and Interface Science, 432: 270–277.

105. Liu, Z., Liu, F., Ma, F., Wang, M., Bai, X., Zheng, Y., Yin, H., and Zhang, G., 2016. Collapsibility, composition, and microstructure of loess in China. Canadian Geotechnical Journal, 53(4): 673–686. doi:10.1139/cgj-2015-0285.

106. Lloret, A., Villar, M.V., Sanchez, M., Gens, A., Pintado, X., Alonso, E.E., 2003. Mechanical behaviour of heavily compacted bentonite under high suction changes. Geotechnique, 53 (1): 27–40.

107. Lu, N., Godt, J.W., Wu, D.T., 2010. A closed-form equation for effective stress in unsaturated soil. Water Resources Research, 46(5): 1–14. doi:10.1029/2009WR008646.

108. Lu, N., Likos, W.J., 2006. Suction stress characteristic curve for unsaturated soil. J. Geotech. Geoenviron. Eng., ASCE, 132(2): 131-142.

109. Lyklema, J., 1995. Fundamentals of interface and colloid science. Vol. II: Solidliquid interfaces. Academic Press, New York.

110. Ma, C., Eggleton, R.A., 1999. Cation exchange capacity of kaolinite. Clays and Clay Minerals, 47(2): 174–180.

111. Ma, K., Pierre, A.C., 1999. Clay sediment-structure formation in aqueous kaolinite suspensions. Clays and Clay Minerals, 47(4): 522–526.

112. Massat, L., Cuisinier, O., Bihannic, I., Claret, F., Pelletier, M., Masrouri, F., Gaboreau, S., 2016. Swelling pressure development and inter-aggregate porosity evolution upon hydration of a compacted swelling clay. Applied Clay Science, 124–125:197-210.

113. Matyas, E.L., Radhakrishna, M.S., 1968. Volume change characteristics of partially saturated soils. Géotechnique, 18(4): 432-448.

114. Medero, G.M., Schnaid, F., Gehling, W.Y.Y., Gallipoli, D., 2003. Analysis of the mechanical response of an artificial collapsible soil. In Proceedings, From

Experimental Evidence towards Numerical Modelling of Unsaturated Soils, Springer, Berlin, pp. 135–145.

115. Melloul, A.J., Goldenberg, L.C., 1997. Monitoring of seawater intrusion in coastal aquifers: basics and local concerns. Journal of Environmental Management, 51: 73–86. doi:10.1006/jema.1997.0136.
116. Michaels, A.S., Bolger, J.C., 1962. Settling rates and sediment volumes of flocculated kaolin suspensions. Industrial & Engineering Chemistry Fundamentals, 1: 24–33. doi:10.1021/i160001a004.
117. Miller, J.D., Nalaskowski, J., Abdul, B., Du, H., 2007. Surface characteristics of kaolinite and other selected two layer silicate minerals. The Canadian Journal of Chemical Engineering, 85(5): 617–624. doi:10.1002/cjce.5450850508.
118. Mitchell, J. K., Soga, K., (2005). Fundamentals of soil behavior, John Wiley and Sons, Hoboken, N.J.
119. Mosser-Ruck, R., Devineau, K., Charpentier, D., Cathelineau, M., 2005. Effects of ethylene glycol saturation protocols on XRD patterns: a critical review and discussion. Clay Clay Miner, 53 (6), 631–638.
120. Mooney, R.W., Keenan, A.G., Wood, L.A., 1952a. Adsorption of water vapor by montmorillonite, I. Heat of desorption and application of BET theory : J. Amer. Chem. Sec., 74: 1367-1371.
121. Muller-Vonmoos, M., Kahr, G., 1982. Bereitstellung von Bentonit für Laboruntersuchungen. Nagra Technischer Bericht, 82-04.
122. Nalezny, C. L. Li, Mo. Co., 1967. Effect of soil structure and thixotropic hardening on the swelling behavior of compacted clay soils: Highway Res. Rec. No. 209: 1-20.
123. Nicol, S.K., Hunter, R.J., 1970. Some rheological and electrokinetic properties of kaolinite suspensions. Australian Journal of Chemistry, 23(11): 2177–2186.
124. Noorany, I., 1992. Discussion: stress ratio effects on collapse of compacted clayey sand. Journal of Geotechnical Engineering, ASCE, 188: 1472-1473.
125. Nuth, M., Laloui, P., 2008. Effective stress concept in unsaturated soils: Clarification and validation of a unified framework. International journal for numerical and analytical methods in geomechanics, 32: 771–801.

126. Ohtsubo, M., Egashira, K., Tanaka, H., and Mishima, O., 2002. Clay minerals and geotechnical index properties of marine clays in East Asia. Marine Georesources & Geotechnology, 20(4): 223–235. doi:10.1080/03608860290051921.
127. Palomino, A.M., and Santamarina, J.C., 2005. Fabric map of kaolinite: Effects of pH and ionic concentration on behavior. Clays and Clay Minerals, 53(3): 209–222. doi:10.1346/CCMN.2005.0530302.
128. Palomino, A.M., Burns, S.E., Santamarina, J.C., 2008. Mixtures of fine-grained minerals - kaolinite and carbonate grains. Clays and Clay Minerals, 56(6): 599–611(13). doi:10.1346/CCMN.2008.0560601.
129. Peck, R.B., Hanson, W.E., and Thornburn, T.H., 1974. Foundation Engineering, 2nd ed., John Wiley and Sons, New York, NY.
130. Pereira, J., and Fredlund, D., 2000. Volume change behavior of collapsible compacted gneiss soil. Journal of Geotechnical and Geoenvironmental Engineering, 126(10): 907–916.
131. Peron, H., Hueckel, T., Laloui, L., Hu, L., 2009. Fundamentals of desiccation cracking of finegrained soils: experimental characterisation and mechanisms identification. Canadian Geotechnical Journal, 46: 1177–1201.
132. Puppala, A. J., Pedarla, A., Pino, A., Hoyos, L. R., 2017. Diffused double-layer swell prediction model to better characterize natural expansive clays. Journal of Engineering Mechanics, 143(9), 04017069.
133. Pusch, R., 1982. Mineral–water interactions and their influence on the physical behaviour of highly compacted Na bentonite. Canadian Geotechnical Journal, 19: 381-387.
134. Pusch, R., 2001b. The microstructure of MX-80 clay with respect to its bulk physical properties under different environmental conditions SKBF/KBS technical report. No.TR01-08.
135. Pusch, R., Yong, R., 2006. Microstructure of Smectite Clays and Engineering Performance. Taylor and Francis, New York.
136. Pusch, R., Moreno, L., 2001. Saturation and permeation of buffer clay Proceedings of the 6th International Workshop on Key Issues in Waste Isolation Research, Ecole Nationale des Ponts et Chaussees, Paris, 71-81.

137. Rand, B., Melton, I.E., 1977. Particle interactions in aqueous kaolinite suspensions: I. Effect of pH and electrolyte upon the mode of particle interaction in homoionic sodium kaolinite suspensions. Journal of Colloid and Interface Science, 60: 308–320. doi:10.1016/0021-9797(77)90290-9.

138. Rao, S.M., Revanasiddappa, K., 2002. Collapse behavior of a residual soil. Geotechnique, 52(4): 259-268.

139. Rao, S.M., Sridharan, A., 1985. Mechanism controlling the volume change behaviour of kaolinite. Clays and Clay Minerals, 33(4): 323-328. doi:10.1346/CCMN.1985.0330407.

140. Ranganatham, B.V., Satyanarayan, B., 1965. A rational method of predicting swelling potential for compacted expansive clays: Proc. 6th Inter. Conf. Soil Mechanics Foundation Engineering, 1: 92-96.

141. Reddi, L.N., Inyang, H.I., 2001. Geo-Environmental Engineering Principles and Applications, Marcel Decker Inc., New York.

142. Romero, E., Gens, A., Lloret, A., 1999. Water permeability, water retention and microstructure of unsaturated compacted Boom clay. Engineering Geology, 54 (1–2): 117-127.

143. Ross, D., 1995. Recommended soil tests for determining soil cation exchange capacity J.T. Sims, A. Wolf (Eds.), Recommended Soil Testing Procedures for the Northeastern United States, Northeast Regional Bull. 493, Agric. Exp. Stn., Univ. of Delaware, Newark, DE, 62-69.

144. Sanchez, M., Gens, A., Guimaraes, L.N., Olivella, S., 2005. A double structure generalized plasticity model for expansive materials. International Journal for Numerical and Analytical Methods in Geomechanics, 29 (8): 751–787.

145. Santamarina, J.C., Klein, K.A., Palomino, A.M., Guimaraes, M.S., 2002. Microscale aspects of chemical mechanical coupling-interparticle forces and fabric. In Proceedings of the Workshop "Chemo-Mechanical Coupling in Clays:From Nano-scale to Engineering". Edited by C. Di Maio, T. Hueckel, and B. Loret. Balkema, 47–64.

146. Santamarina, J.C., Klein, K.A., Wang, Y.H., Prencke, E., 2002. Specific surface: determination and relevance. Canadian Geotechnical Journal, 39: 233-241.

147. Savage, D., 2005. The Effects of High Salinity Groundwater on the Performance of Clay Barriers. SKI Report 54.
148. Saiyouri, N., Hicher, P.Y., Tessier, D., 2000. Microstructural approach and transfer water modelling in highly compacted unsaturated swelling clays. Mech. Cohes. – Frict. Mater., 5, 41–60.
149. Saiyouri, N., Tessier, D., Hicher, P.Y., 2004. Experimental study of swelling in unsaturated compacted clays. Clay Minerals, 39: 469-479.
150. Saleh-Mbemba, F., Aubertin,M., Mbonimpa,M., Li, L., 2016. Experimental characterization of the shrinkage and water retention behaviour of tailings from hard rock mines. Geotechnical Geological Engineering, 34, 251–266.
151. Schanz, T., Tripathy, S., 2009. Swelling pressure of a divalent-rich bentonite: Diffuse double-layer theory revisited. Water Resources Research, 45(W00C12), doi:10.1029/2007WR006495.
152. Schofield, R.K., Samson, H.R., 1954. Flocculation of kaolinite due to the attraction of oppositely charged crystal faces. Discussions of the Faraday Society, 18: 135–145. doi:10.1039/df9541800135.
153. Schroth, B.K., Sposito, G., 1997. Surface charge properties of kaolinite. Clays and Clay Minerals, 45(1): 85–91. doi:10.1346/CCMN.1997.0450110.
154. Seed, H. B. C., Chan, K., 1959. Structure and Strength Characteristics of Compacted Clays. Journal of the Soil Mechanics and Foundations Division, 85(5):87-128.
155. Seed, H. B., Woodward, R. J., Jr. Lundgren, R., 1962. Prediction of swelling potential for compacted clays: J. ASCE, Soil Mechanics and Foundation Division, 88(SM-3, Part I): 53-87.
156. Sivakumar, V., Sivakumar, R., Murray, E.J., MacKinnon, P., and Boyd, J., 2010. Mechanical behaviour of unsaturated kaolin (with isotropic and anisotropic stress history). Part 1: wetting and compression behaviour. Geotechnique, 60(8): 581–594. doi:10.1680/geot.8.P.007.
157. Sivapullaiah, P.V., Sitharam, T.G., Rao, K.S.S., 1987. Modified free swell index for clays. Geotechnical Testing Journal, 10(2): 80–85. doi:10.1520/GTJ10936J.

158. Skempton, A. W., 1960. Significance of Terzaghi's concept of effective stress. From theory to practice in soil mechanics, L. Bjerrum, A. Casagrande, R. B. Peck, and A. W. Skempton, eds., Wiley, New York.
159. Sloane, R.L., Kell, T.R., 2013. The fabric of mechanically compacted kaolin. In Clays and Clay Minerals: Proceedings of the Fourteenth National Conference, Berkeley, California, Elsevier p. 289.
160. Sowers, G.F., Kennedy, C.M., 1967. High volume change clays of the South-Eastern coastal plain: Proc.3rd Pan Am. Conf. Soil Mechanics Foundation Engineering, Caracas, Venezuela, 99–120.
161. Sridharan, A., Choudhury, D., 2002. Swelling pressure of sodium montmorillonites. Geotechnique, 52, 459-462.
162. Sridharan, A., Rao, V.G. 1977. Mechanisms controlling volume change of saturated clays and the role of the effective stress concept. Geotechnique, 23(3), 359–382.
163. Sridharan, A., Rao, S.M., Murthy, N.S., 1985. Free swell index of soils: a need for redefinition. Indian Geotechnical Journal, 15(2): 94–99.
164. Sridharan, A., Rao, S.M., Murthy, N.S., 1988. Liquid limit of kaolinitic soils. Geotechnique, 38(2): 191–198. doi:10.1680/geot.1988.38.2.191.
165. Sridharan, A., Rao, S.M, Sivapullaiah, P.V., 1986. Swelling pressure of clays. Geotechnical testing journal, ASTM, 9 (1): 24–33.
166. Sridharan, A., M.S., Jayadeva, 1982. Double layer theory and compressibility of clays. Geotechnique, 32(2), 133-144.
167. Sridharan, A., Rao, S.M., Murthy, N.S., 1986. Compressibility behavior of homoionized bentonites. Geotechnique, 36, 551-564.
168. Sridharan, A., Rao, S.M., and Murthy, N.S. 1988. Liquid limit of kaolinitic soils. Geotechnique, 38(2): 191–198. doi:10.1680/geot.1988.38.2.191.
169. Sridharan, A., Choudhury, D., 2008. Computation of hydraulic conductivity of montmorillonitic clays by diffuse double layer theory. International Journal of Geotechnical Engineering, 2, 1-10.
170. Sultan, H.A., 1969. Collapseing Soils. Proceedings Seventh Inter-national Conference on Soil Mechanics and Foundation Engineering. Specialty Session No. 5, Mexico City.

171. Sun, D.A., Cui, H., Sun, W., 2009. Swelling of compacted sand-bentonite mixtures. Applied Clay Science, 43, 485-492.
172. Sun, D.A., Sheng, D., Xu, Y., 2007. Collapse behaviour of unsaturated compacted soil with different initial densities. Canadian Geotechnical Journal, 44(6): 673–686. doi:10.1139/t07-023.
173. Swedish Nuclear Fuel and Waste Management Company, 1983. Final storage of spent nuclear fuel-KBS-3, III barriers. Swedish Nuclear Fuel Supply Company, Division KBS Technical Report, 9:1-16:12.
174. Tang, A.M., Cui, Y.J., 2009. Modelling the thermo-mechanical behavior of compacted expansive clays. Geotechnique, 59 (3): 185–195.
175. Tang, C.S., Tang, A.M., Cui, Y.J., Delage, P., Schroeder, C., Shi, B., 2011. A study of the hydro-mechanical behaviour of compacted crushed argillite. Engineering Geology, 118: 93–103.
176. Tang, C.S., Tang, A.M., Cui, Y.J., Delage, P., Schroeder, C., De Laure, E., 2011b. Investigating the swelling pressure of compacted crushed-Callovo-Oxfordian claystone. Physics and Chemistry of the Earth, doi:10.1016/j.pce.2011.10.001.
177. Terzaghi, K., 1936. The shearing resistance of saturated soils. Proceedings 1st International Conference on Soil Mechanics, Cambridge, Mass (1): 54–56.
178. Torrance, J., and Ohtsubo, M., 1995. Ariake Bay quick clays: A comparison with the general model. Soils and Foundations, 35(1): 11–19. doi:10.3208/sandf1972.35.11.
179. Tripathy, S., Sridharan, A., Schanz, T., 2004. Swelling pressures of compacted bentonites from diffuse double layer theory. Canadian Geotechnical Journal, 41: 437-450, doi: 10.1139/t03-096.
180. van Olphen, H., 1963. An introduction to clay colloid chemistry: for clay technologists, geologists and soil scientists. Interscience, New York.
181. van Olphen, H., 1977. An Introduction to Clay Colloid Chemistry: For Clay Technologists. Geologists and Soil Scientists, John Wiley and Sons, New York.
182. Van Olphen, H., 1991. Clay Colloid Chemistry, 2nd ed., Krieger.
183. Verwey, E. J. W., J. T. G., Overbeek, 1948. Theory of the Stability of Lyophobic Colloids. Elsevier, Amsterdam.

184. Villar, M.V., Lloret, A., 2008. Influence of dry density and water content on the swelling of a compacted bentonite. Applied Clay Science, 39: 38-49.

185. Wang, Y.-H., Siu, W.K., 2006a. Structure characteristics and mechanical properties of kaolinite soils. I. Surface charges and structural characterizations. Canadian Geotechnical Journal, 43(6): 587–600. doi:10.1139/t06-026.

186. Wang, Y.-H., Siu, W.K., 2006b. Structure characteristics and mechanical properties of kaolinite soils. II. Effects of structure on mechanical properties. Canadian Geotechnical Journal, 43(6): 601–617. doi:10.1139/t06-027.

187. Wang Q., Tang A. M., Cui Y.J., Delage P., Gatmiri B., 2012. Experimental study on the swelling behaviour of bentonite/claystone mixture. Engineering Geology, Elsevier, 124: 59–66.

188. Wheeler, S.J., and Sivakumar, V., 1995. An elasto-plastic critical state framework for unsaturated soil. Géotechnique, 45(1): 35–53. doi:10.1680/geot.1995.45.1.35.

189. Wieland, E., and Stumm, W., 1992. Dissolution kinetics of kaolinite in acidic aqueous solutions at 25°C. Geochimica et. Cosmochimica Acta, 56: 3339–3355. doi:10.1016/0016-7037(92)90382-S.

190. Xu, Y.F., Matsuokab, H., Sun, D.A., 2003. Swelling characteristics of fractal-textured bentonite and its mixtures. Applied Clay Science, 22: 197-209.

191. Ye, W.M., Chen, Y.G., Wang, B. Q., Wang, J., 2010. Advances on the knowledge of the buffer/backfill properties of heavily compacted GMZ bentonite Engineering Geology, 116:12-20.

192. Ye, W.M., Wan, M., Chen B., Chen Y.G., Cui Y.J., Wang J., 2012. Temperature Effects on the Unsaturated Permeability of the Densely Compacted GMZ01 Bentonite under Confined Condition. Engineering Geology, Elsevier, 126: 1-7.

193. Yong, R.N., 1999. Soil suction and soil–water potentials in swelling clays in engineered clay barriers. Eng. Geol. 54: 3–13.

194. Yong, R., Taylor, L.O., Warkentin, B.P., 1962. Swelling pressure of sodium montmorillonite at depres- sed temperature: Clays and Clay Minerals 11: 268-281.

195. Zbik, M., Smart, St. C., 1998. Nanomorphology of kaolinites: Comparative SEM and AFM studies. Clays and Clay Minerals, 46(2): 153–160. doi:10.1346/CCMN.1998.0460205.

196. Zhang, H., Cui, S.L., Zhang, M., Jia, L., 2010. Swelling behaviors of GMZ bentonite–sand mixtures inundated in NaCl–Na 2SO 4 solutions. Nuclear Engineering and Design, 242 DOI: 10.1016/j.nucengdes.2011.10.042.
197. Zhang, F., Ye, W. M., Wang, Q., Chen, Y. G., Chen, B., 2019. An insight into the swelling pressure of GMZ01 bentonite with consideration of salt solution effects. Engineering Geology, https://doi.org/10.1016/j.enggeo.2019.02.016.
198. Zhang, C., Lu, N., 2018. What is the range of soil water density? Critical reviews with a unified model. Reviews of Geophysics, 56(3): 532-562.
199. Zheng, L., Samper J., Montenegro L., 2011. A coupled THC model of the FEBEX in situ test with bentonite swelling and chemical and thermal osmosis. J. Contam Hydrol, 126(1-2): 45-60.
200. Zhou, Z.H., Gunter, W.D., 1992. The nature of the surface charge of kaolinite. Clays and Clay Minerals, 40(3): 365–368. doi:10.1346/CCMN.1992.0400320.
201. Zhu, C.M., Ye, W.M., Chen, Y.G., Chen, B., Cui, Y.J., 2013. Influence of salt solutions on the swelling pressure and hydraulic conductivity of compacted GMZ01 bentonite Eng. Geol., 166: 74-80.
202. Zourmpakis, A., Boardman, D.I., Rogers, C.D.F., 2005. Creation of artificialloess soils. In Unsaturated soils: Experimental studies. Springer Proceedings in Physics, Vol. 93. Edited by T. Schanz. Springer, Berlin, Heidelberg, 123–134. doi:10.1007/3-540-26736-0_10.

PUBLICATIONS

JOURNALS

1. Choudhury C. and Bharat T.V. (2018). "Wetting-induced collapse behavior of kaolinite: influence of fabric and inundation pressure." **Canadian Geotechnical Journal**, 55: 956-967.
2. Choudhury C. and Bharat T.V. (-). Prediction of swelling pressure characteristics of compacted bentonites in isochoric conditions. Applied Clay Science, Under review.
3. Bharat T.V., Choudhury C., and Das DS "Effect of fabric on swelling pressure development of compacted bentonites in isochoric condition." Geotechnique, Under review.
4. Bharat T.V. and Choudhury C. "Effective stress variation in collapsible and swelling clays based on suction stress approach", Manuscript under preparation.
5. Choudhury C. and Bharat T.V. "Wetting-induced collapse behavior of kaolinite using single and double oedometer tests.", Manuscript under preparation.

CONFERENCES

1. Choudhury, C., and Bharat, T.V. (2014). "Soil-water characteristic curve models for clays." Indian Geotechnical Conference, Kakinada.
2. Choudhury, C., and Bharat, T.V. (2015). "Collapse behavior of clay soil under one-dimensional (1d) compression condition." Indian Geotechnical Conference, Pune.
3. Choudhury, C., and Bharat, T. V. (2018). "Effect of suction on swelling pressure of compacted bentonite." Second International Conference on Advances in Concrete, Structural & Geotechnical Engineering, Bits Pilani.